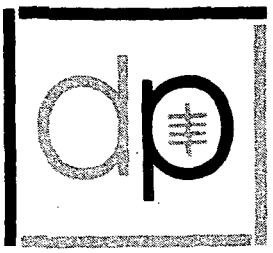

COLUMBIA UNIVERSITY

DEPARTMENT OF PHYSICS

PROGRESS REPORT No. 21

JULY 1, 1970 THROUGH JUNE 30, 1971

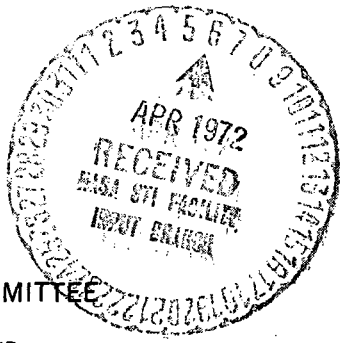

To:

THE JOINT SERVICES TECHNICAL ADVISORY COMMITTEE

REPRESENTING: THE U. S. ARMY ELECTRONICS COMMAND
THE U. S. ARMY RESEARCH OFFICE
THE OFFICE OF NAVAL RESEARCH
THE AIR FORCE OFFICE OF SCIENTIFIC RESEARCH

COLUMBIA RADIATION LABORATORY NEW YORK, NEW YORK 10027

JUNE 30, 1971

The research reported in this document was made possible through support extended the Columbia Radiation Laboratory, Columbia University, by the Joint Services Electronics Program (U. S. Army Electronics Command and U. S. Army Research Office, Office of Naval Research, and the Air Force Office of Scientific Research) under Contract DAABO7-69-C-0383.

Portions of this work were also supported by:

U. S. Army Research Office (Durham)

Contract DA-31-124-ARO-D-341 and
Grant DA-ARO-D-31-124-G-972

Air Force Office of Scientific Research

Grant AFOSR-68-1454

National Aeronautics and Space Administration

Grant NGR 33-008-012: Scope F

National Science Foundation

Grants NSF-GP 14243 and NSF-GP 16029

The support of these agencies is acknowledged in footnotes in the text.

Security Classification

AD-728 826

DOCUMENT CONTROL DATA · R&D

(Security classification of title, body of abstract and indexing annotation must be entered when the overall report is classified)

1. ORIGINATING ACTIVITY (Corporate author)	2a. REPORT SECURITY CLASSIFICATION
COLUMBIA UNIVERSITY, Dep't of Physics Columbia Radiation Laboratory New York, New York 10027	Unclassified
	2b. GROUP

3. REPORT TITLE

RESEARCH INVESTIGATION DIRECTED TOWARD EXTENDING THE USEFUL RANGE OF THE ELECTROMAGNETIC SPECTRUM

4. DESCRIPTIVE NOTES (Type of report and inclusive dates)

Progress Report, 1 July 1970 - 30 June 1971

5. AUTHOR(S) (Last name, first name, initial)

Hartmann, Sven R.: Director, CRL

6. REPORT DATE	7a. TOTAL NO. OF PAGES	7b. NO. OF REFS
30 June 1971	xii + 105	67

8a. CONTRACT OR GRANT NO.	9a. ORIGINATOR'S REPORT NUMBER(S)
DAAB07-69-C-0383	Progress Report No. 21
b. PROJECT NO. DA 200 61102 B31F	
c.	9b. OTHER REPORT NO(S) (Any other numbers that may be assigned this report)
d.	CU-6-71 C-0383 Physics

10. AVAILABILITY/LIMITATION NOTICES

This document has been approved for public release and sale; its distribution is unlimited.

11. SUPPLEMENTARY NOTES	12. SPONSORING MILITARY ACTIVITY
	Joint Services Electronics Program through (Administering Service -Office of Naval Research, Air Force Office of Scientific Research, or U.S. Army Electronics Command)

13. ABSTRACT

We have completed the determination of the lifetimes and fine structure of He^- using time-of-flight techniques and quenching by a static axial magnetic field.

Using the techniques of level-crossing spectroscopy, we have measured the hyperfine constants A (magnetic dipole) and B (electric quadrupole), and the lifetime τ of the $3\ ^2P_{3/2}$ state of lithium 7. The results were obtained by using a computer to curve-fit the experimental data taken by a signal averager, $A = -0.98 \pm 0.01$ MHz, $B = -0.092 \pm 0.005$ MHz, and $\tau = 212 \pm 4$ nsec. We have also created a polarization of the rubidium 7S level as a first step in determining the hyperfine structure of the alkali excited S state.

We have studied the parametric interaction between light and microwaves in optically pumped Rb^{87} vapor, and the results are in excellent qualitative agreement with theory.

Measurements and analyses of the $1_{10} \rightarrow 1_{11}$ transitions in formaldehyde (H_2CO) and its isotopic species HDCO, $H_2{}^{13}CO$, and $H_2C^{18}O$, and in the lowest two excited vibrational states of H_2CO have been completed. Also, we have begun measurements on transitions in furan

DD FORM 1 JAN 64 1473

Unclassified

Security Classification

14. KEY WORDS	LINK A		LINK B		LINK C	
	ROLE	WT	ROLE	WT	ROLE	WT
Metastable atoms and ions						
Metastable autoionizing atoms						
Level-crossing spectroscopy						
Optical double-resonance spectroscopy						
Collision phenomena						
Electron-impact excitation of atoms						
Atomic frequency standards						
Intensity modulation of light						
Molecular spectroscopy						
Photon-echo resonance						
Echo behavior in ruby						
Raman echoes						
Nonlinear propagational effects						
Surface physics						
Two-photon radiation						
Frequency shifts						

INSTRUCTIONS

1. ORIGINATING ACTIVITY: Enter the name and address of the contractor, subcontractor, grantee, Department of Defense activity or other organization *(corporate author)* issuing the report.

2*a*. REPORT SECURITY CLASSIFICATION: Enter the overall security classification of the report. Indicate whether "Restricted Data" is included. Marking is to be in accordance with appropriate security regulations.

2*b*. GROUP: Automatic downgrading is specified in DoD Directive 5200.10 and Armed Forces Industrial Manual. Enter the group number. Also, when applicable, show that optional markings have been used for Group 3 and Group 4 as authorized.

3. REPORT TITLE: Enter the complete report title in all capital letters. Titles in all cases should be unclassified. If a meaningful title cannot be selected without classification, show title classification in all capitals in parenthesis immediately following the title.

4. DESCRIPTIVE NOTES: If appropriate, enter the type of report, e.g., interim, progress, summary, annual, or final. Give the inclusive dates when a specific reporting period is covered.

5. AUTHOR(S): Enter the name(s) of author(s) as shown on or in the report. Enter last name, first name, middle initial. If military, show rank and branch of service. The name of the principal author is an absolute minimum requirement.

6. REPORT DATE: Enter the date of the report as day, month, year; or month, year. If more than one date appears on the report, use date of publication.

7*a*. TOTAL NUMBER OF PAGES: The total page count should follow normal pagination procedures, i.e., enter the number of pages containing information.

7*b*. NUMBER OF REFERENCES: Enter the total number of references cited in the report.

8*a*. CONTRACT OR GRANT NUMBER: If appropriate, enter the applicable number of the contract or grant under which the report was written.

8*b*, 8*c*, & 8*d*. PROJECT NUMBER: Enter the appropriate military department identification, such as project number, subproject number, system numbers, task number, etc.

9*a*. ORIGINATOR'S REPORT NUMBER(S): Enter the official report number by which the document will be identified and controlled by the originating activity. This number must be unique to this report.

9*b*. OTHER REPORT NUMBER(S): If the report has been assigned any other report numbers *(either by the originator or by the sponsor)*, also enter this number(s).

10. AVAILABILITY/LIMITATION NOTICES: Enter any limitations on further dissemination of the report, other than those imposed by security classification, using standard statements such as:

(1) "Qualified requesters may obtain copies of this report from DDC."

(2) "Foreign announcement and dissemination of this report by DDC is not authorized."

(3) "U. S. Government agencies may obtain copies of this report directly from DDC. Other qualified DDC users shall request through _____."

(4) "U. S. military agencies may obtain copies of this report directly from DDC. Other qualified users shall request through _____."

(5) "All distribution of this report is controlled. Qualified DDC users shall request through _____."

If the report has been furnished to the Office of Technical Services, Department of Commerce, for sale to the public, indicate this fact and enter the price, if known.

11. SUPPLEMENTARY NOTES: Use for additional explanatory notes.

12. SPONSORING MILITARY ACTIVITY: Enter the name of the departmental project office or laboratory sponsoring *(paying for)* the research and development. Include address.

13. ABSTRACT: Enter an abstract giving a brief and factual summary of the document indicative of the report, even though it may also appear elsewhere in the body of the technical report. If additional space is required, a continuation sheet shall be attached.

It is highly desirable that the abstract of classified reports be unclassified. Each paragraph of the abstract shall end with an indication of the military security classification of the information in the paragraph, represented as *(TS)*, *(S)*, *(C)*, or *(U)*.

There is no limitation on the length of the abstract. However, the suggested length is from 150 to 225 words.

14. KEY WORDS: Key words are technically meaningful terms or short phrases that characterize a report and may be used as index entries for cataloging the report. Key words must be selected so that no security classification is required. Identifiers, such as equipment model designation, trade name, military project code name, geographic location, may be used as key words but will be followed by an indication of technical context. The assignment of links, rules, and weights is optional.

13. ABSTRACT (cont'd)

(C_4H_4O), pyrrole (C_4H_5N), formic acid (H_2CO_2), and cyanoacetylene (HC_3N).

We have continued our study of the Hanle effect in the NO molecule and have developed rf-power oscillators with flat, wideband output to observe excited-state hyperfine transitions at zero field predicted by detailed calculations based on the theory of optical-rf double resonance.

A substantial amount of data has been generated on the time-dependent behavior of photon echoes in ruby, and we are currently attempting to develop theories which will explain the observed behavior in terms of electron-electron and electron-nucleus-spin interactions in the ground state of ruby. We have constructed a microwave spectrometer to observe electron-spin echoes in the $\bar{E}(^2E)$ excited state of ruby at 16.24 GHz and 9.31 GHz. The parameters of a least-squares fit of our data are in essential agreement with ENDOR results; but if used to predict positions at which ENDOR lines should have been observed, they do not agree with published experimental data.

We have produced interesting results in our investigation of stimulated Raman scattering in atomic thallium vapor. Preliminary results on the dependence of Stokes scattering at 1.513 μ on the polarization of the exciting ruby laser are in agreement with theory. Our interrogation dye laser is now tunable in the $^2P_{3/2} \rightarrow {}^2S_{1/2}$ resonance region at 5350 Å, thereby giving stronger signals and enhancing echo detectability.

We have built a Q-switched, temperature-tuned ruby laser that operates between 6934 Å and 6938 Å. We have obtained pulses with a peak greater than 2 MW and a 15-nsec width. We have observed the 5846.68-Å, $9D_{5/2} \rightarrow 6P_{3/2}$ fluorescent decay following absorption of two 6935.76-Å laser photons in the transition $6S_{1/2} \rightarrow {}^9D_{5/2}$.

We have calculated the frequency shift due to resonant interaction between identical radiating atoms and have shown that in some cases the shift exceeds 1/10 of the pressure-broadened width. We will attempt to measure the shift in cesium vapor using high resolution Fabry-Perot interferometers.

We propose to measure the superfluid density ρ_s of helium II as a function of the velocity v_s of the superfluid relative to the normal fluid. Our apparatus should resolve changes in ρ_s/ρ of $\sim 10^{-5}$ by sensing changes in the resonant frequency of a high-Q torsion pendulum whose moment of inertia is partly determined by ρ_s.

COLUMBIA RADIATION LABORATORY

RESEARCH INVESTIGATION DIRECTED TOWARD
EXTENDING THE USEFUL RANGE OF THE
ELECTROMAGNETIC SPECTRUM

Progress Report No. 21

July 1, 1970 through June 30, 1971

Contract DAAB07-69-C-0383
[Continuation of Contract DA 28-043 AMC-00099(E)]

CU-6-71 C-0383 Physics

Object of the research:

Physical research in fields in which microwave frequency techniques are employed; the development of microwave electronic and circuit devices.

The research reported in this document was made possible through support extended the Columbia Radiation Laboratory, Columbia University, by the Joint Services Electronics Program (U. S. Army Electronics Command and U. S. Army Research Office, Office of Naval Research, and the Air Force Office of Scientific Research) under Contract DAAB07-69-C-0383.

Submitted by: S. R. HARTMANN, Director

Coordinated by: A. Owen, Editor

COLUMBIA UNIVERSITY

Division of Government Aided Research

New York, N. Y. 10027

June 30, 1971

TABLE OF CONTENTS

The names of the authors are arranged alphabetically.

PUBLICATIONS AND REPORTS

Publications

M. D. Crisp,[1] "Propagations of Small-Area Pulses of Coherent Light through a Resonant Medium," Phys. Rev. A 1, 1604 (1970).

L. M. Blau,[2] R. Novick, and D. Weinflash, "Lifetimes of the $(1s2s2p)\,^4P_J$ States of the Helium Negative Ion," Phys. Rev. Letters 24, 1268 (1970).

D. Grischkowsky[3] and S. R. Hartmann, "Behavior of Electron-Spin Echoes and Photon Echoes in High Fields," Phys. Rev. B 2, 60 (1970).

K. D. Tucker, G. R. Tomasevich, and P. Thaddeus, "Precise Laboratory Measurement of the 4830-MHz Formaldehyde Rotational Transition," Astrophys. J. 161, L153 (1970).

W. A. Stern and R. Novick, "A Field-Independent Optically Pumped ^{85}Rb Maser Oscillator," Appl. Phys. Letters 17, 216 (1970).

B. S. Mathur,[4] H. Y. Tang, and W. Happer, "Light Propagation in Optically Pumped Alkali Vapors," Phys. Rev. A 2, 648 (1970).

Robert W. Schmieder,[5] Allen Lurio,[6] W. Happer, and A. Khadjavi,[7] "Level-Crossing Measurement of Lifetime and hfs Constants of the $^2P_{3/2}$ States of the Stable Alkali Atoms," Phys. Rev. A 2, 1216 (1970).

---

1. Present Address: Owens-Illinois Technical Center, Toledo, Ohio 43601.
2. Present Address: Hospital for Special Surgery, New York, New York 10021.
3. Present Address: IBM Watson Research Center, Yorktown Heights, New York 10598.
4. Present Address: Owens-Illinois Technical Center, Toledo, Ohio 43601.
5. Present Address: Lawrence Radiation Laboratory, University of California, Berkeley, California 94720.
6. Present Address: IBM Watson Research Center, Yorktown Heights, New York 10598.
7. Present Address: IBM Watson Research Center, Yorktown Heights, New York 10598.

R. Friedberg and S. R. Hartmann, "Pulse-Induced Radiation in the Linear Regime," Opt. Comm. 2, 301 (1970).

M. Levitt, R. Novick, and P. D. Feldman,[8] "Determination of Energies and Lifetimes of the Metastable Auto-Ionizing $(1s2s2p)\,^4P$ States of Li^6 and Li^7 by a Zeeman-Quenching Technique," Phys. Rev. A 3, 130 (1971).

R. W. Schmieder,[5] Allen Lurio,[6] and W. Happer, "Quadratic Stark Effect in the $^2P_{3/2}$ States of the Alkali Atoms," Phys. Rev. A 3, 1209 (1971).

K. R. German,[9] R. N. Zare, and D. R. Crosley,[10] "Reinvestigation of the Hanle Effect for the NO A $^2\Sigma^+$ State," J. Chem Phys. 54, 4039 (1971).

Papers by CRL Staff Members Presented at Scientific Meetings

R. Novick and D. Weinflash, "Precision Measurement of the Fine Structure and Lifetimes of the $(1s2s2p)\,^4P_J$ States of He^- and Li*," International Conference on Precision Measurements and Fundamental Constants, sponsored by the National Bureau of Standards, Gaithersburg, Maryland, 3-7 August 1970.

R. W. Guernsey, "Quantized Rotation of Superfluid Helium," Twelfth International Conference on Low Temperature Physics, Kyoto, Japan, 4-10 September 1970.

American Physical Society Meeting, Seattle, Washington, 23-25 November 1970.

R. Gupta, S. P. Chang, and W. Happer, "Electronic Polarization of the Rubidium $7S_{1/2}$ State," Bull. Am. Phys. Soc. II, 15, 1508 (1970).

P. Thaddeus, "Interstellar Molecules," Invited Paper, Fifth Texas Symposium on Relativistic Astrophysics, Austin, Texas, 18 December 1970.

---

8. Present Address: The Johns Hopkins University, Baltimore, Maryland 21218.
9. Present Address: Bell Telephone Laboratories, Holmdel, New Jersey 07733.
10. Present Adress: Department of Chemistry, University of Wisconsin, Madison, Wisconsin 53706.

Annual Meeting of the American Physical Society, New York, New York, 1-4 February 1971.

R. A. Weingarten, L. A. Levin, and S. R. Hartmann, "Stimulated Raman Scattering in Thallium Vapor," Bull. Am. Phys. Soc. II, 16, 41 (1971).

P. F. Liao and S. R. Hartmann, "Redetermination of Aluminum Hyperfine Parameters in Ruby from Electron Spin-Echo Behavior," Bull. Am. Phys. Soc. II, 16, 70 (1971).

American Physical Society Meeting, Cleveland, Ohio, 29 March-1 April 1971.

W. Happer, A. Lurio,[6] and W. Nagourney, "Low-Field Level-Crossing Measurements of Lithium[7] Hyperfine Structures and Lifetimes in the First and Second Excited P States," Bull. Am. Phys. Soc. II, 16, 310 (1971).

R. N. Zare, "Laser-Induced Fluorescence of Alkali Dimer Molecules," Invited Paper, Bull. Am. Phys. Soc. II, 16, 347 (1971).

K. D. Tucker, G. R. Tomasevich, and P. Thaddeus, "Molecular Beam-Maser Studies of the $1_{10} \rightarrow 1_{11}$ Transition of Several Formaldehyde Isotopes," Twenty-Sixth Symposium on Molecular Structure and Spectroscopy," Columbus, Ohio, 14-18 June 1971.

Radiation Laboratory Seminars

Meetings are held weekly at Columbia University, New York, N.Y., during the academic year and are open to all members of the Physics Department. Guest speakers are invited to discuss work in the general area of the research in the Columbia Radiation Laboratory.

D. Grischkowsky, IBM Watson Laboratories, "Self-Focusing of Light by Potassium Vapor," October 9, 1970.

R. Friedberg, Columbia University, "Frequency Shifts in Resonant Systems," October 16, 1970 (Joint Seminar with the Department of Theoretical Physics).

R. D. Deslattes, National Bureau of Standards,"Yet Another Approach to the Fine Structure Constant - Via X Rays," October 23, 1970.

C. K. N. Patel, Bell Telephone Laboratories, Inc., "Spin-Flip Raman Laser," November 6, 1970.

C. C. Costain, National Research Council, Ottawa, Canada, "High Resolution Lamb-Dip Spectroscopy in the Centimeter Region," November 13, 1970.

T. H. Bergeman, Columbia Radiation Laboratory, "Double Resonance and Other Measurements on Carbon Monosulfide," November 20, 1970.

M. Dakss, IBM Watson Laboratories, "Excitation and Deflection of Optical Guided Waves in Thin Films," December 4, 1970.

F. Franz, University of Indiana, "Optical Pumping Studies of Collisional Interactions," December 11, 1970.

R. Alfano and S. Shapiro, General Telephone and Electronics Laboratories, Inc., "Interaction of Picosecond Laser Pulses with Matter," December 18, 1970.

N. Shiren, IBM Watson Laboratories, "Self-Induced Transparency in Acoustic Paramagnetic Resonance," January 8, 1971.

J. Vanier, Université Laval, Québec, Canada, "Nuclear Magnetic Resonance Thermometry," January 15, 1971.

M. M. Hessel, Fordham University, "Experimental Observation of a New Alkali Molecule (NaLi) by Laser Techniques," January 22, 1971.

H. Bleich, Columbia University, "Nuclear Triple Resonance in Solids," February 12, 1971.

C. Fabjan, Harvard University, "A New Approach to Measurement of the Lamb Shift," February 19, 1971.

G. Flynn, Columbia University, "Laser-Induced-Fluorescence Studies of Energy Transfer and Transport in SF_6," March 5, 1971.

J. Waugh, Massachusetts Institute of Technology, "Time Reversal Experiments and Spin Temperature in Solids," March 12, 1971.

J. Eberly, University of Rochester, "Superradiance," March 26, 1971.

W. W. Smith, University of Connecticut, "Electron-Emission Spectroscopy of Autoionizing States of Lithium-Like Fluorine and Oxygen Ions," April 9, 1971.

G. Agarwal, University of Rochester, "Superradiance: A Problem in Nonequilibrium Statistical Mechanics," April 16, 1971.

H. Danielmeyer, Bell Telephone Laboratories, Inc., "Kinetics of Excited Laser States," April 23, 1971.

W. Mims, Bell Telephone Laboratories, Inc., "Experiments on Phonon Avalanche," April 30, 1971.

S. Abbi, Cornell University, "Subdivision into Small-Scale Filaments of a Laser Beam in a Nonlinear Medium," May 7, 1971.

H. Y. Tang, Columbia Radiation Laboratory, "Parametric Frequency Conversion in Optically Pumped Atomic Vapors," May 14, 1971.

H. Boehm, Owens-Illinois Technical Center, "Electrical Conductivity of Vitreous GeO_2," May 21, 1971.

Lectures

R. Friedberg, "Frequency Shifts in Resonant Systems," Joint Seminar, Department of Theoretical Physics and Columbia Radiation Laboratory, October 16, 1970; "Frequency Shifts in Resonant Systems: The Truth about the Cooperative Lamb Shift," Colloquium, Institute for Advanced Study, Princeton, New Jersey, April 23, 1971.

R. W. Guernsey, "Quantized Rotation of Superfluid Helium," Department of Physics, Rutgers University, New Brunswick, New Jersey, October 13, 1970; id., Department of Physics, Wesleyan University, Middletown, Connecticut, December 14, 1970; id., Cryogenics Center, Stevens Institute of Technology, Hoboken, New Jersey, December 16, 1970; "Macroscopic Quantum Effects in Liquid Helium," Colloquium, Department of Physics, Columbia University, October 23, 1970.

S. Hameed, "Calculation of Atomic Polarizabilities," Seminar, Department of Physics, New York University, October 14, 1970; "Many-Electron Effects in Atoms," Theoretical Physics Seminar, Columbia University, March 1, 1971.

W. Happer, "Lamb Shifts," Colloquium, Department of Physics and Astronomy, University of Toledo, Toledo, Ohio, April 15, 1971.

S. R. Hartmann, "Frequency Shifts in Resonant Systems: The Cooperative Lamb Shift," Seminar, L'Université Libre de Bruxelles, November 5, 1970; id., Colloquium, Physikalischen Kolloquium Stuttgart, December 8, 1970; id., Seminar, Technische Hochschule, Munich, December 11, 1970; id., Colloquium Ehrenfestti, Kamerlingh Onnes Laboratorium, Der Rijksuniversiteit te Leiden, December 16, 1970; Seminar, Laboratoire d'Optique Quantique, Université de Paris, Faculté de Sciences d'Orsay, December 21, 1970; id., Colloquium, University of Rome, January 19, 1971; id., Colloquium, IBM Research Laboratories, Zurich, January 25, 1971; id., Seminar, Laboratoire de Physique de l'Ecole Normale Superieure, Paris, January 29, 1971; id., Seminar, Solid State Physics Laboratory, General Electric Company, Schenectady, New York, April 6, 1971; id., Colloquium, Department of Physics, Fordham University, Bronx, New York, April 13, 1971; id., Colloquium, Department of Physics and Astronomy, University of Toledo, Toledo, Ohio, May 20, 1971.

L. A. Levin, "Stimulated Raman Scattering in Atomic Thallium Vapor," Colloquium, Department of Physics, Fordham University, Bronx, New York, March 30, 1971; id., Seminar, Avco Everett Research Laboratory, Everett, Massachusetts, May 18, 1971; id., Seminar, RCA-David Sarnoff Research Center, Princeton, New Jersey, May 19, 1971; id., Colloquium, Department of Physics, University of Toledo and Owens-Illinois Technical Center, Toledo, Ohio, May 25, 1971.

D. Raskin, "Interaction between Neutral Polar Molecules and Conducting Surfaces," Atomic Physics Seminar, National Bureau of Standards, Gaithersburg, Maryland, January 6, 1971; id., Department of Physics, Fordham University, Bronx, New York, February 9, 1971; id., Atomic Physics Seminar, City College, New York, New York, February 18, 1971; id., Atomic Physics Seminar, New York University, New York, New York, March 4, 1971.

P. Thaddeus, "Millimeter-Wavelength Observations of Interstellar Molecules," Astronomy Colloquium, State University of New York at Stony Brook, Stony Brook, Long Island, January 21, 1971; "Interstellar Formaldehyde - A Cosmic Refrigerator," Colloquium, Department of Physics, University of California, Berkeley, California, February 17, 1971; "The Short Wavelength Spectrum of the Universal Radiation," Seminar of the Plasma Physics Laboratory, Stanford University, Stanford, California, February 18, 1971; "Interstellar Organic Chemistry," Colloquium, Department of Physics, Columbia University, March 5, 1971.

R. N. Zare, "Our Beams are Brighter," Colloquium, Department of Chemistry, Columbia University, February 18, 1971; "Laser-Induced Molecular Fluorescence," Colloquium, Department of Chemistry, Pennsylvania State University, University Station, Pennsylvania, March 11, 1971; "Crossed-Beam Pyrotechnics," "Stop, Look, and Listen at the Molecular Level Crossing," and "Have Laser, Will Travel," Arthur D. Little Lectureship, Department of Chemistry, Massachusetts Institute of Technology, Cambridge, Massachusetts, April 12-16, 1971.

ABSTRACT

We have completed the determination of the lifetimes and fine structure of He^- using time-of-flight techniques and quenching by a static axial magnetic field.

Using the techniques of level-crossing spectroscopy, we have measured the hyperfine constants A (magnetic dipole) and B (electric quadrupole), and the lifetime τ of the $3\ ^2P_{3/2}$ state of lithium 7. The results were obtained by using a computer to curve-fit the experimental data taken by a signal averager, $A = -0.98 \pm 0.01$ MHz, $B = -0.092 \pm 0.005$ MHz, and $\tau = 212 \pm 4$ nsec. We have also created a polarization of the rubidium 7S level as a first step in determining the hyperfine structure of the alkali excited S state.

We have studied the parametric interaction between light and microwaves in optically pumped Rb^{87} vapor, and the results are in excellent qualitative agreement with theory.

Measurements and analyses of the $1_{10} \rightarrow 1_{11}$ transitions in formaldehyde (H_2CO) and its isotopic species HDCO, $H_2{}^{13}CO$, and $H_2C^{18}O$, and in the lowest two excited vibrational states of H_2CO have been completed. Also, we have begun measurements on transitions in furan (C_4H_4O), pyrrole (C_4H_5N), formic acid (H_2CO_2), and cyanoacetylene (HC_3N).

We have continued our study of the Hanle effect in the NO molecule and have developed rf-power oscillators with flat, wide-band output to observe excited-state hyperfine transitions at zero field predicted by detailed calculations based on the theory of optical-rf double resonance.

A substantial amount of data has been generated on the time-dependent behavior of photon echoes in ruby, and we are currently attempting to develop theories which will explain the observed behavior in terms of electron-electron and electron-nucleus spin interactions in the ground state of ruby. The parameters of a least-squares fit of our data from electron-spin echoes in the ground state are in essential agreement with ENDOR results; but if used to predict positions at which ENDOR lines should have been observed, they do not agree with published experimental data. We have constructed a microwave spectrometer to observe electron-spin echoes in the $\bar{E}(^2E)$ excited state of ruby at 16.24 GHz.

We have produced interesting results in our investigation of stimulated Raman scattering in atomic thallium vapor. Preliminary results on the dependence of Stokes scattering at 1.513 μ on the polarization of the exciting ruby laser are in agreement with theory. Our interrogation dye laser is now tunable in the $^2P_{3/2} \rightarrow {}^2S_{1/2}$ resonance region at 5350 Å, thereby giving stronger signals and enhancing echo detectability.

We have built a Q-switched, temperature-tuned ruby laser that operates between 6934 Å and 6938 Å. We have obtained pulses with a peak power greater than 2 MW and a 15-nsec width. We have observed the 5846.68-Å, $9D_{5/2} \rightarrow 6P_{3/2}$ fluorescent decay following absorption of two 6935.76-Å laser photons in the transition $6S_{1/2} \rightarrow 9D_{5/2}$.

We have calculated the frequency shift due to resonant interaction between identical radiating atoms and have shown that in some cases the shift exceeds 1/10 of the pressure-broadened width. We will attempt to measure the shift in cesium vapor using high resolution Fabry-Perot interferometers.

We propose to measure the superfluid density ρ_s of helium II as a function of the velocity v_s of the superfluid relative to the normal fluid. Our apparatus should resolve changes in ρ_s/ρ of $\sim 10^{-5}$ by sensing changes in the resonant frequency of a high-Q torsion pendulum whose moment of inertia is partly determined by ρ_s.

I. ATOMIC PHYSICS

A. METASTABLE AUTOIONIZING ATOMS

1. Rf Spectroscopy of Metastable Alkali Atoms
(T. Lucatorto, R. Novick, G. Sprott)

Research on this project has been completed, and the results are now being prepared for publication.

---

2. Rf Spectroscopy of Metastable Lithium Atoms
(M. R. Levitt, R. Novick, S. Skwire)

This project has been transferred to the Columbia Astrophysics Laboratory.

---

3. He^- Ion
(R. Novick, D. Weinflash)

During this period, we concluded the study by a time-of-flight technique of the metastable, autoionizing $(1s2s2p)\,^4P_J$ states of the helium negative ion. Important new data was obtained for Zeeman quenching of the metastable He^- beam. Zeeman quenching causes the increase in the decay rate produced by application of a magnetic field. The new data (Fig. 1) provide the basis for a more rigorous analysis of previous observations. The results of the new analysis, described in some detail below, are lifetimes for all three ^4P_J states of He^-, as well as for the 5/2 - 3/2 fine structure interval Δ_{53}.

The He^- metastable current varies with the distance of the detector from the source, the magnetic field, the beam velocity, and the residual pressure. The dependence of the decay on these variables is analyzed to obtain the lifetimes and fine structure of the $(1s2s2p)\,^4P_J$ states of He^-. By the hypothesis of differential metastability, we conclude that the graph of the He^- current versus the distance from the source should be a sum of a large number of exponential components arising from the various Zeeman substates in the beam.

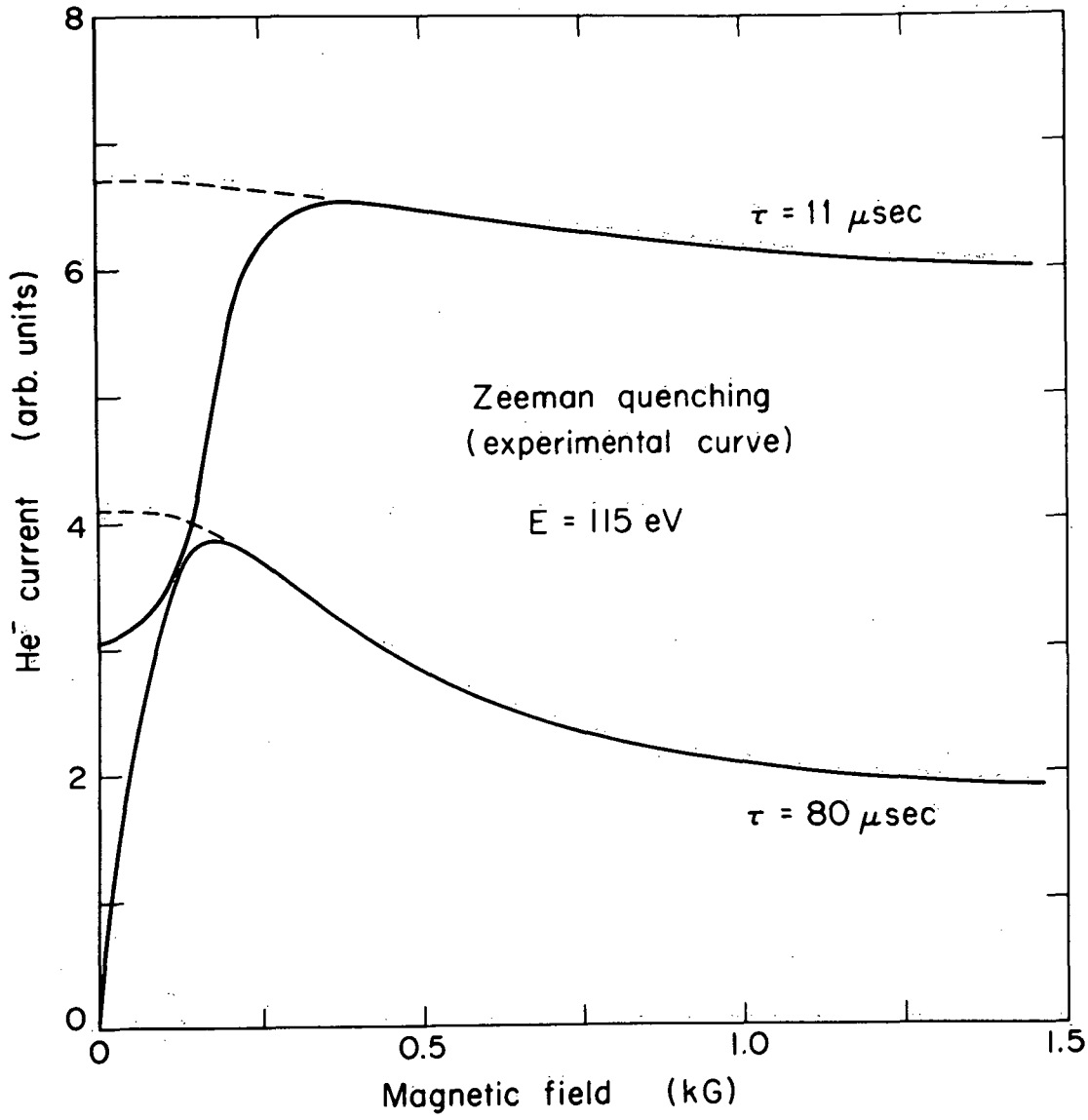

Fig. 1. He^- metastable current received by the Faraday cup as a function of axial magnetic field with the detector stationary at positions corresponding to flight times of 11 μsec and 80 μsec. The data were recorded continuously on an x-y recorder as the field was raised.

However, the observed decay curves can be fitted within experimental error with just <u>two</u> exponential components. It is assumed that each of these two exponential components is itself a sum of unresolved exponentials. The longer-lived component is identified with the net current from the $^4P_{5/2}$ Zeeman substates, while the shorter-lived component is assumed to be the sum of the $^4P_{3/2}$ and $^4P_{1/2}$ currents. The decay rate of the shorter-lived component γ_S is essentially independent of the magnetic field, the beam velocity, and the residual pressure. The decay rate of the longer-lived component γ_L increases with all three of these variables and must be extrapolated to zero pressure and zero magnetic field to obtain the decay rate of the $^4P_{5/2}$ state, $\gamma_{5/2}$.

The gas-quenching rate is assumed to be of the form $P\sigma_p v$, and γ_L for H = 400 G is extrapolated to zero pressure by varying the pressure and velocity independently. The two methods of pressure extrapolation agree within experimental error.

The zero-pressure decay rates of the two components at 400 G are:

$$\gamma_L = (5.2 \pm 0.3) \times 10^3 \text{ sec}^{-1} \text{ and}$$
$$\gamma_S = (71 \pm 12) \times 10^3 \text{ sec}^{-1}.$$

The corresponding lifetimes at 400 G are:

$$\tau_L = 190 \pm 20 \text{ } \mu\text{sec and}$$
$$\tau_S = 13 \pm 2 \text{ } \mu\text{sec}.$$

The extrapolation of γ_L to zero magnetic field is accomplished by analyzing the Zeeman-quenching curve, i.e. the curve of the metastable current as a function of magnetic field, with the detector stationary. Figure 1 shows experimental Zeeman-quenching curves for two flight times. The influence of the J = 1/2 state is ignored, as can be theoretically justified for the magnetic fields used in this work. In this approximation, the 5/2 - 1/2 fine structure interval, Δ_{53}, and the differential decay rate, $(\gamma_{3/2} - \gamma_{5/2})$, can be determined from the Zeeman-

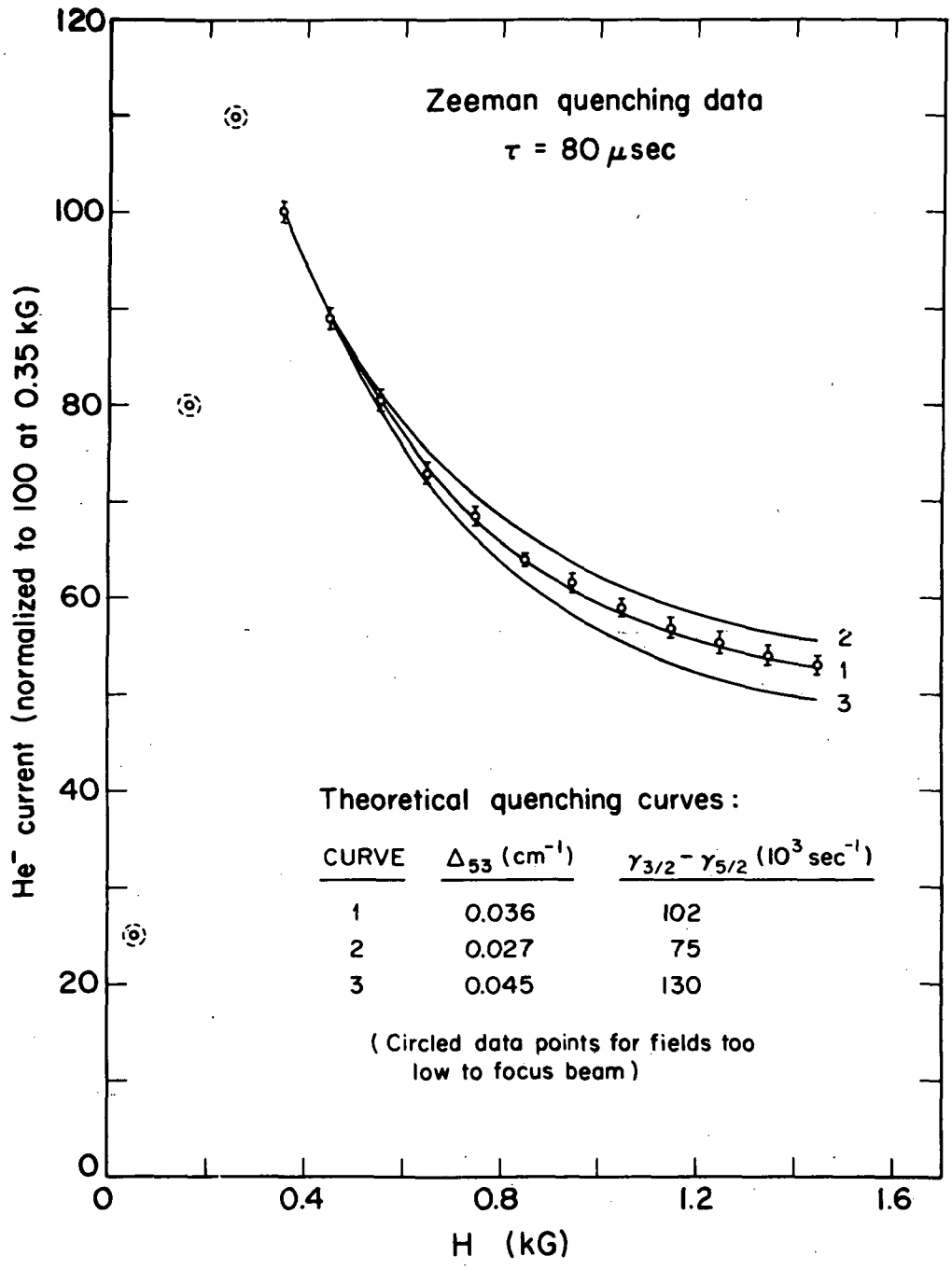

Fig. 2. Comparison of theoretical curves and experimental data points for Zeeman quenching of the He^- beam. The three curves correspond to different choices for the fine structure interval, Δ_{53}, and for the differential decay rate, $(\gamma_{53} - \gamma_{5/2})$. At the flight time of 80 μsec, only $^4P_{5/2}$ substates are still present in the beam.

quenching data alone. Figure 2 shows three theoretical quenching curves that agree with the data between 350 and 450 G. Only one of these theoretical curves gives the observed quenching at higher magnetic fields. The results for the fine structure interval and the differential decay rate are:

$$\Delta_{53} = 0.036 \pm 0.009 \text{ cm}^{-1} \text{ and}$$
$$(\gamma_{3/2} - \gamma_{5/2}) = (100 \pm 20) \times 10^3 \text{ sec}^{-1}.$$

These two atomic parameters are sufficient for us to calculate the decay rate of the $^4P_{5/2}$ state, $\gamma_{5/2}$, from the experimental zero-pressure value of γ_L at 400 G. We find the value $\gamma_{5/2} = (2.0 \pm 0.5) \times 10^3 \text{ sec}^{-1}$ ($\tau_{5/2} = 500 \pm 200$ μsec).

With the decay rates of the J = 5/2 and J = 3/2 states now determined, the decay rate of the J = 1/2 state can be estimated by returning to the time-of-flight data, which previously was fit using two exponential components. The decay rate of the shorter-lived component γ_S was assumed to be an average of the J = 3/2 and J = 1/2 decay rates. With $\gamma_{3/2}$ now known independently, one can determine $\gamma_{1/2}$. The J = 1/2 current was obtained graphically from the total metastable current by subtracting the current arising from the J = 5/2 and J = 3/2 states. The result is a fit of the decay data with three components, as shown in Fig. 3.

The relative weights w_J of the three components, when extrapolated back to the source, are in proportion to their statistical weights. The value of the ratio $w_{3/2}/w_{5/2} = 0.667$ must be assumed to calculate the J = 3/2 current. However, the value of the ratio $w_{1/2}/w_{5/2} = 0.33 \pm 0.09$, which is a consequence of the analysis, is an independent check of the validity of the three-component fit.

As a result of this analysis, values for the zero-field lifetimes of all three ^4P_J states of He^- have been obtained, as well as the value of the 5/2 - 3/2 fine structure interval Δ_{53}. Only the 5/2 - 1/2 fine structure interval Δ_{51} remains inaccessible using the present experimental technique.

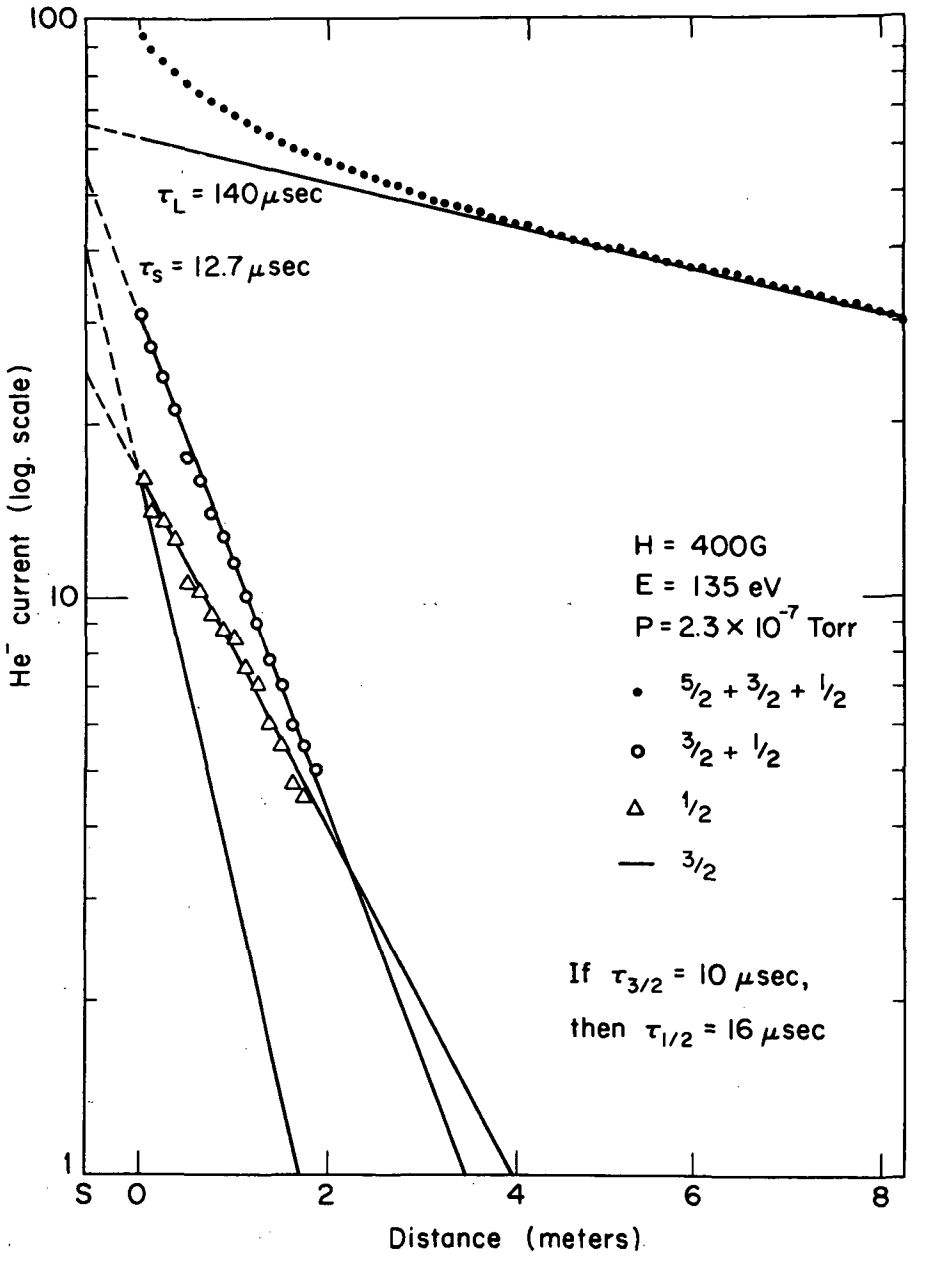

Fig. 3. He^- time-of-flight data fitted with two and then three exponential components. The two-component fit (circles and dots) is based on these data alone. The three-component fit uses $\tau_{3/2}$ from the Zeeman-quenching data to determine $\tau_{1/2}$ (triangles). The relative strengths of the three components extrapolated back to the source at S agree with the statistical weights of the assigned J states.

Conclusions: The values obtained for the zero-field decay rates are:

$$\gamma_{5/2} = (2.0 \pm 0.5) \times 10^3 \text{ sec}^{-1},$$
$$\gamma_{3/2} = (100 \pm 20) \times 10^3 \text{ sec}^{-1}, \text{ and}$$
$$\gamma_{1/2} = (60 \pm 10) \times 10^3 \text{ sec}^{-1}.$$

The corresponding lifetimes are:

$$\tau_{5/2} = 500 \pm 200 \ \mu\text{sec},$$
$$\tau_{3/2} = 10 \pm 2 \ \mu\text{sec}, \text{ and}$$
$$\tau_{1/2} = 16 \pm 4 \ \mu\text{sec}.$$

The value of the 5/2 - 1/2 fine structure interval, as determined from the Zeeman-quenching data, is

$$\Delta_{53} = 0.036 \pm 0.009 \text{ cm}^{-1}.$$

Program for the next interval: The study of the helium negative ion by rf spectroscopy is being continued at the Columbia Astrophysics Laboratory under NSF Grant GP 13479.

B. LEVEL-CROSSING AND OPTICAL DOUBLE-RESONANCE SPECTROSCOPY

1. Hyperfine Structure of 2P and 3P States of Lithium*
(W. Happer, A. Lurio, W. Nagourney)

We have completed our measurements of the hyperfine constants A and B and the lifetime for the $3P_{3/2}$ state of Li^7. As with the $2P_{3/2}$ state measurement,[1] we used the technique of level-crossing spectroscopy. There were two main differences between the methods used in making the $3P_{3/2}$ state measurements and those used for the $2P_{3/2}$ state. First, a stronger source of resonance radiation was needed for this state than for the $2P_{3/2}$ state. The hollow cathode lamp used for the $2P_{3/2}$ state was tried but was not strong enough. We found a modified flow lamp to be satisfactory. The second difference was our choice of polarizations. As we mentioned in the previous Progress Report,[2] the best lifetime data and good data for the hyperfine constant A were obtained with both source and detector polarizations aligned along the direction of the magnetic field. We chose this alignment

by examining sets of computer-generated theoretical curves for the various possible choices of polarization. When this was done with $3P_{3/2}$ state curves, it was evident that the best data for the lifetime and the constant A would be obtained with both polarizations at right angles to the magnetic field.

Several small problems which did not appear in the first state were encountered in the $3P_{3/2}$ measurements. First, to obtain an adequate signal for the second state, we needed a greater beam density, and hence oven temperature, than we used for the first state. This required a modest revision in the design of the beam oven, the main change in which being the incorporation of about twice as many nichrome heaters as were used previously. Secondly, since the Hanle width was much narrower, and the experiment was performed over a much smaller sweep range (-2.5 to +2.5 G), the requirements for magnetic field calibration were much more stringent. This problem was never completely solved, although the estimated magnetic field-calibration error was reduced to about 30 mG. A third problem was the uncertainty in the orientations of the polarizers. In order to take this source of error into account, several runs were taken without any polarizers. Although the signal-to-noise ratio for these runs was much worse than for the others, the results were in fairly good agreement with the results of the runs that used polarizers.

Our preliminary results for the second state are as follows:

$A = -0.098 \pm 0.01$ MHz;

$\tau = 212 \pm 4$ nsec;

$B = -0.092 \pm 0.005$ MHz.

Program for the next interval: We have only recently begun the double-resonance experiment, the purpose of which is to measure the constant A for the $3P_{1/2}$ state. The experiment is being performed at zero field, using the level-crossing apparatus. We are not yet certain that we have seen the

resonance; the main problem is an inadequate signal-to-noise ratio, since the fractional signal for the double resonance in the $P_{1/2}$ state is about 60 times smaller than that of the $P_{3/2}$ state Hanle effect. We are now searching for ways of increasing the amount of scattered signal so that the signal-to-noise ratios may be improved.

*This research was also supported by the Air Force Office of Scientific Research under Grant AFOSR-68-1454.

(1) CRL Progress Report, June 30, 1970, p. 10.

(2) Ibid., p. 10.

---

2. Electric-Quadrupole Hyperfine Structure in Lithium (H. M. Foley, S. Hameed)

The effect of the core on quadrupole hyperfine structure has traditionally been estimated by calculating the quadrupole moment induced in the core by the nucleus and evaluating its interaction with the valence electron. In terms of perturbation theory of many-electron terms in the Hamiltonian, this corresponds to a first order correction beyond a single-particle approximation to the atomic wavefunction. Recently, two calculations have been reported which include higher order correlation effects. One of these[1] uses the Brueckner-Goldstone perturbation formalism and results in a slight modification of the first order result. The other[2] employs variational procedures to obtain solutions to atomic Bethe-Goldstone equations and reports that the higher order effects nearly cancel out the first order correction. Thus the importance of correlation effects in the determination of quadrupole hfs is not clear at present.

To investigate this question we have undertaken a perturbation calculation with a restricted Hartree-Fock wavefunction as the starting point. The first order correction, which can be calculated by obtaining the first order correction to the wavefunction with respect to the quadrupole interaction, is found to be nearly 10% of the zeroth order effect. The second order correction is

$$\langle \psi^{(1)} | \sum_i \frac{e^2 Q \ (3\cos^2\theta_i - 1)}{\gamma_i^3} | \psi^{(1)} \rangle$$

$$+ 2\mathrm{Re} \langle \psi^{(0)} | \sum_i \frac{e^2 Q \ (3\cos^2\theta_i - 1)}{\gamma_i^3} | \psi^{(2)} \rangle .$$

It is found that the second term can be expressed in terms of $\psi^{(1)}$, and the evaluation of the second order correlated wavefunction $\psi^{(2)}$ is not necessary. The first order function $\psi^{(1)}$ is taken to be a linear combination of 45 singly and doubly excited configurations:

$$\psi^{(1)} = \sum_k c_k \psi_k .$$

Each ψ_k is a determinant of Slater-type orbitals. The coefficients c_k are determined by calculating $E^{(2)}$ variationally:

$$E^{(2)} = \langle \psi^{(1)} | H^{(0)} - E^{(0)} | \psi^{(1)} \rangle + 2\mathrm{Re} \langle \psi^{(0)} | H^{(1)} - E^{(1)} | \psi^{(1)} \rangle .$$

The amount of correlation energy given by $E^{(2)}$ would be a criterion of the adequacy of $\psi^{(1)}$ obtained by this procedure. Thus, starting from the Hartree-Fock approximation to calculate the first and second order corrections in an accurate manner, we should be able to determine the importance of correlation effects in quadrupole hyperfine structure.

---

3. Fine Structure of Singly Ionized Lithium
(T. Lucatorto, R. Novick, G. Sprott)

Research on this project has been discontinued because of changes in personnel.

4. Hyperfine Structures of Excited $^2S_{1/2}$ States of Alkali Atoms*

(S. Chang, R. Gupta, W. Happer)

We have continued our work on the experiment to measure the hyperfine structure of the excited S state of alkali atoms. Using electron excitation in a discharge, we have created an electronic polarization of the 7S level of rubidium. A second method of obtaining orientation is being tested.

Figure 4 shows the resonance curves obtained using the apparatus described in the previous Progress Report.[1] The radio-frequency field, which destroys the ground-state polarization, is frequency modulated, and the signal is detected on a lock-in amplifier. Curve A indicates the intensity of the transmitted 7947-Å pumping light, which is a measure of the ground-state polarization. Curve B shows the intensity of circularly polarized 7408-Å fluorescent light, which is a measure of the excited-state polarization. Changing the sense of polarization of the lamp light changes the sign of curve B while leaving curve A unchanged. The light pipe shown in the previous Report has been removed, because with the light pipe in place the solid angle of the incident light exceeded the tolerance of the interference filter.

We are now investigating an alternative way to produce orientation in the excited state. Unpolarized ground-state atoms are excited with circularly polarized radiation to a P level that is energetically higher than the 7S state (see Fig. 5). Some of the P-state atoms decay to the 7S state, and a portion of the polarization of the P state is carried over to the 7S state. The advantage of this method is that the buffer gas and discharge can be eliminated. The discharge has been difficult to regulate. Since the resonance cell contains no buffer gas, we should be able to avoid an accidental discharge when large rf fields are applied.

Figure 6 shows the present apparatus. A 4 in x 4 in, 7408-Å interference filter allows a large solid angle of

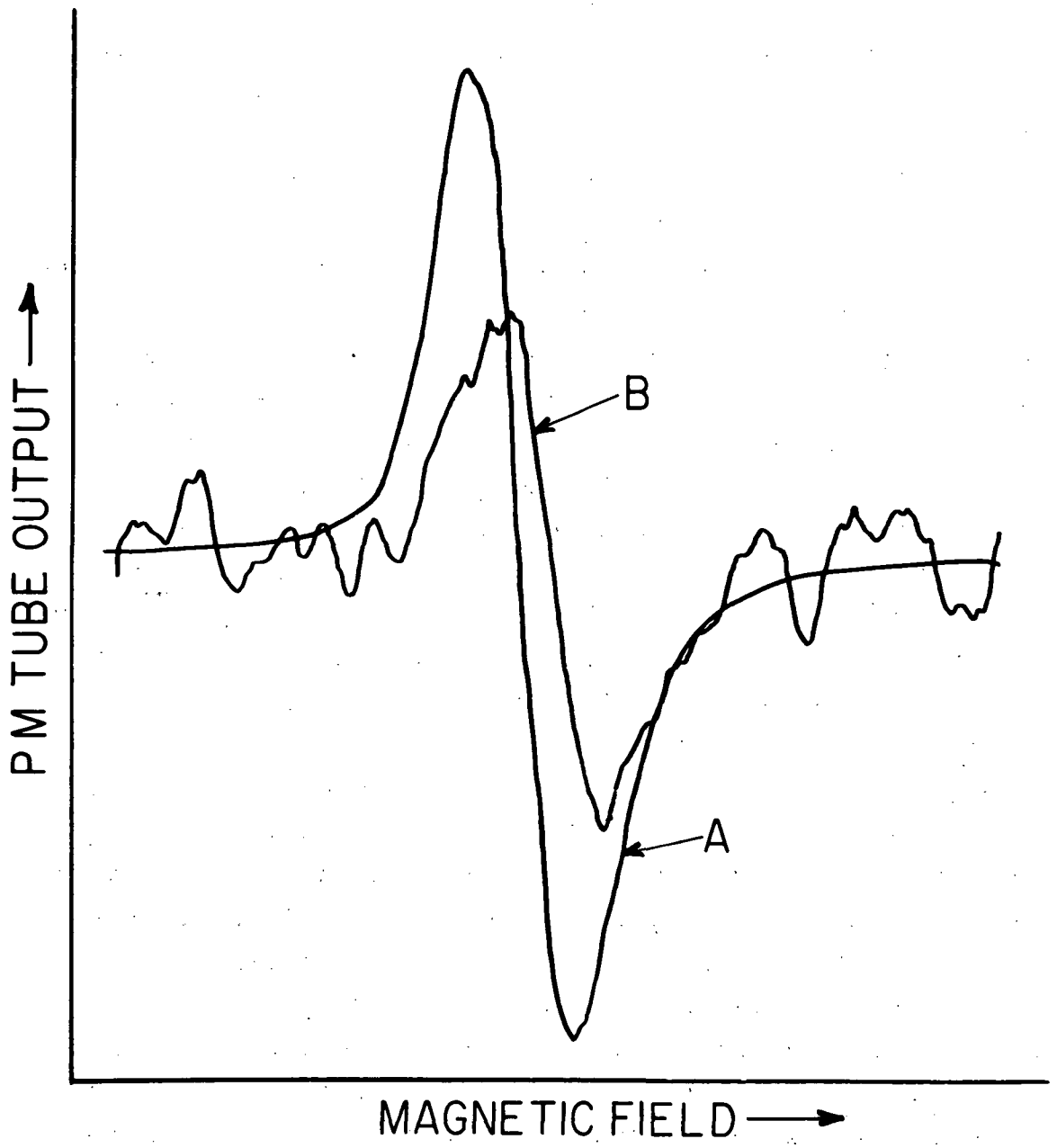

Fig. 4. Graph of the photomultiplier-tube output versus the magnetic field. The letter A indicates the rubidium ground-state resonance signal, while B shows the rubidium $^{7}S_{1/2}$ polarization signal.

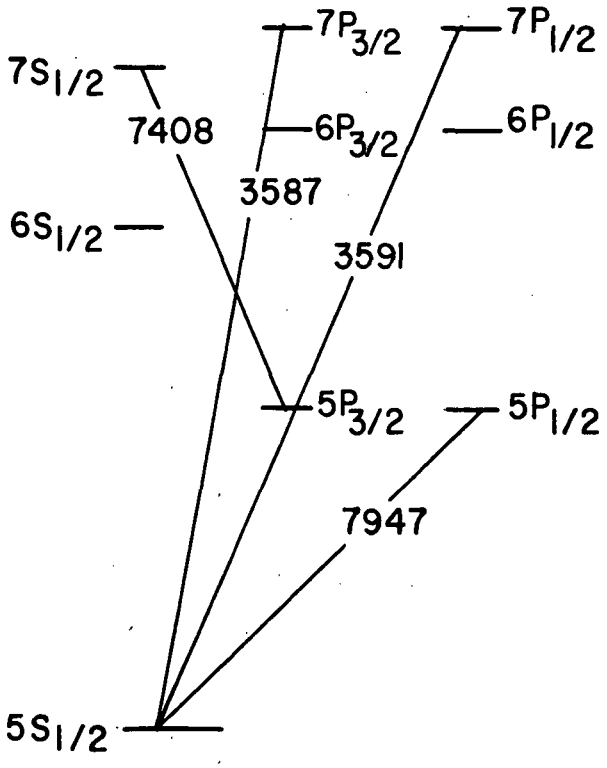

Fig. 5. Energy levels of rubidium.

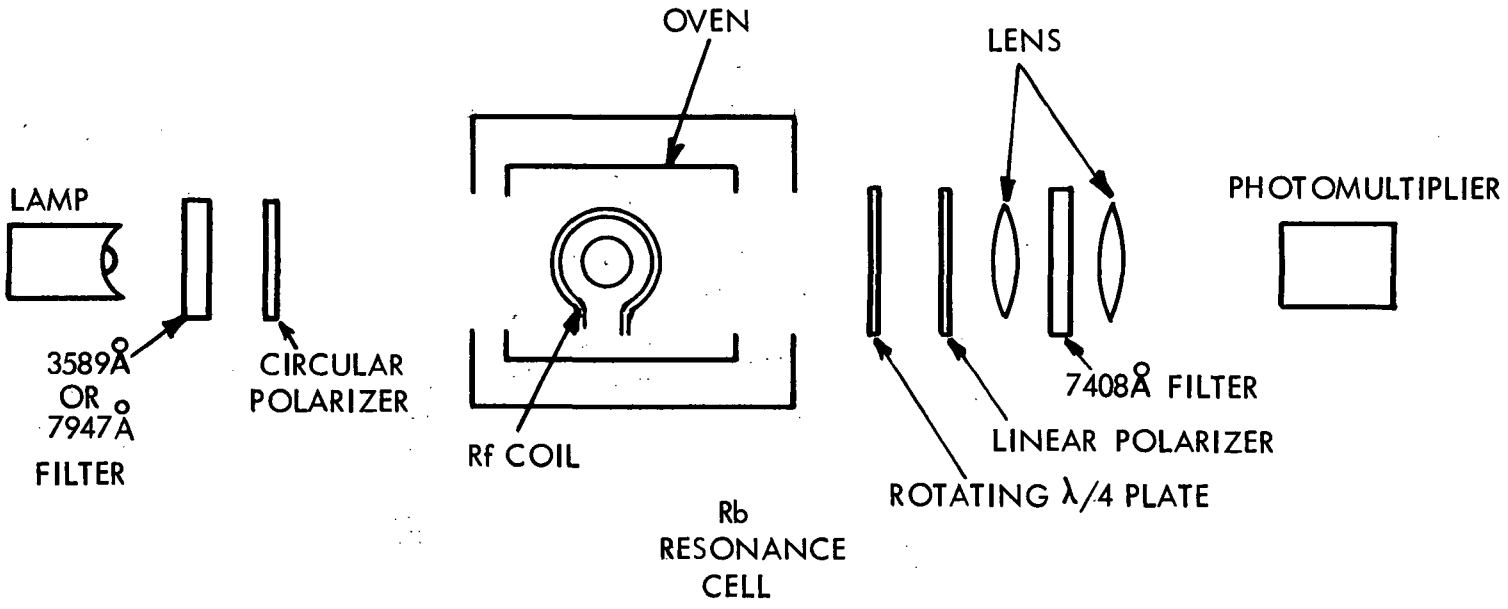

Fig. 6. Apparatus.

detection. A rotating quarter-wave plate modulates any 7408-Å circular polarization for phase-sensitive detection. We are now trying to improve the rubidium spectral lamp.

Program for the next interval: We will continue our investigation of the 7S magnetic sublevels.

*This research was supported by the Air Force Office of Scientific Research under Grant AFOSR-68-1454.

(1) CRL Progress Report, June 30, 1970, p. 15.

C. COLLISION PHENOMENA

1. Relaxation of Excited Atoms*
(B. R. Bulos, W. Happer)

The study of the collision-induced quenching of excited alkali atoms has continued. Cross sections for quenching of rubidium by nitrogen, hydrogen, deuterium, methane, ethane, and ethylene have been measured. The experimental procedure employed to determine these cross sections has been perfected and is now being applied to the quenching of cesium.

In the previous Progress Report,[1] filter leakage and its effects on the experiment were discussed. Interference filters are designed for rays normal to their surfaces, and this requires that nearly parallel light beams be used for excitation and detection. This restriction reduces the amount of light flux that can be used, and a compromise must be reached. In the present apparatus, the solid angles subtended by the excitation lamp and detectors at the cell have been reduced to the point where unwanted resonance lines have been effectively eliminated. This decreases the signal-to-noise ratio of the two-channel outputs; however, the ratio is still adequate for accurate measurements.

The procedure we have developed to measure the four quenching rates of a gas requires that four experimental runs be made: The first employs a D_1 filter in the excitation path and D_1 filters for both detection channels, while the second uses a D_1 filter in the excitation path, a D_1 filter in the transmitted channel, and no filter in the fluorescent channel.

The third uses a D_2 filter in the excitation path and D_2 filters for both detection channels, and the fourth has a D_2 filter in the excitation path, a D_2 filter in the transmitted channel, and no filter in the fluorescent channel. The four ratios obtained for transmitted-to-fluorescent differential signals are denoted by

$$\frac{A_1}{B_1}, \quad \frac{A_1}{B_1 + B_2}, \quad \frac{A_2}{B_2}, \text{ and } \quad \frac{A_2}{B_1 + B_2}.$$

These ratios can be calculated in terms of the four quenching rates γ_{10}, γ_{20}, γ_{21} by solving the rate equations for the $^2P_{1/2}$ and $^2P_{3/2}$ levels of an alkali. The pressure dependence of quenching rates is linear, since binary collisions are assumed. Thus, if we define

$$k_{ij}p = \gamma_{ik}/\Gamma,$$

where Γ is the natural decay rate, γ_{ij} is the quenching rate from level i to j, and p is the pressure of the quenching in torr; and we then define

$$k_{10} + k_{12} = k_1 \text{ and}$$

$$k_{20} + k_{21} = k_2,$$

we can write the intensity ratios for the four cases mentioned as

$$\frac{A_1}{B_1} = \frac{a_1}{b_1}\left[\frac{(k_1k_2 - k_{12}k_{21})p^2 + (k_1 + k_2)p + 1}{1 + k_2p}\right];$$

$$\frac{A_1}{B_1 + B_2} = \frac{a_1}{b_{12}}\left[\frac{(k_1k_2 - k_{12}k_{21})p^2 + (k_1 + k_2)p + 1}{1 + (k_2 + k_{12})p}\right];$$

$$\frac{A_2}{B_2} = \frac{a_2}{b_2}\left[\frac{(k_1k_2 - k_{12}k_{21})p^2 + (k_1 + k_2)p + 1}{1 + k_1p}\right];$$

$$\frac{A_2}{B_1 + B_2} = \frac{a_2}{b_{12}}\left[\frac{(k_1k_2 - k_{12}k_{21})p^2 + (k_1 + k_2)p + 1}{1 + (k_1 + k_{21})p}\right].$$

As we said above, for each gas we conduct four experimental runs which yield four curves relating the ratio of the transmitted channel-differential signal to the fluorescent channel differential signal. The above four functions are then simultaneously fitted to the four experimental curves with a least-squares computer program employing the four rates k_1, k_2, k_{12}, and k_{21} as free parameters. The program yields the best values for these parameters.

For illustration, we show the four curves obtained for the quenching of rubidium by hydrogen (see Fig. 7). The points are the experimentally-determined values, and the solid curves are the computer-fitted functions.

We have included a table of our results for the quenching of rubidium.

The ratio of the quenching rates γ_{12}/γ_{21} is predicted by the principle of detailed balance, which gives the ratio as

$$\frac{\gamma_{12}}{\gamma_{21}} = \frac{2J_2 + 1}{2J_1 + 1} \exp\left(-\frac{\Delta E}{kT}\right) .$$

For rubidium at 20°C, this yields

$$\frac{\gamma_{12}}{\gamma_{21}} = 0.62$$

Comparing this value to those obtained from the experimental results, one sees good agreement.

Upon studying the results, one notices large differences in the quenching ability of the gases studied. The unsaturated hydrocarbons CH_4 and C_2H_6 are poor direct quenching agents and good cross quenching agents, while the unsaturated hydrocarbon C_2H_4 is a very good agent for both types of quenching.

There are no existing theoretical calculations to account for these large differences. The process is probably a very complicated chemical interaction, which makes it a difficult problem to solve.

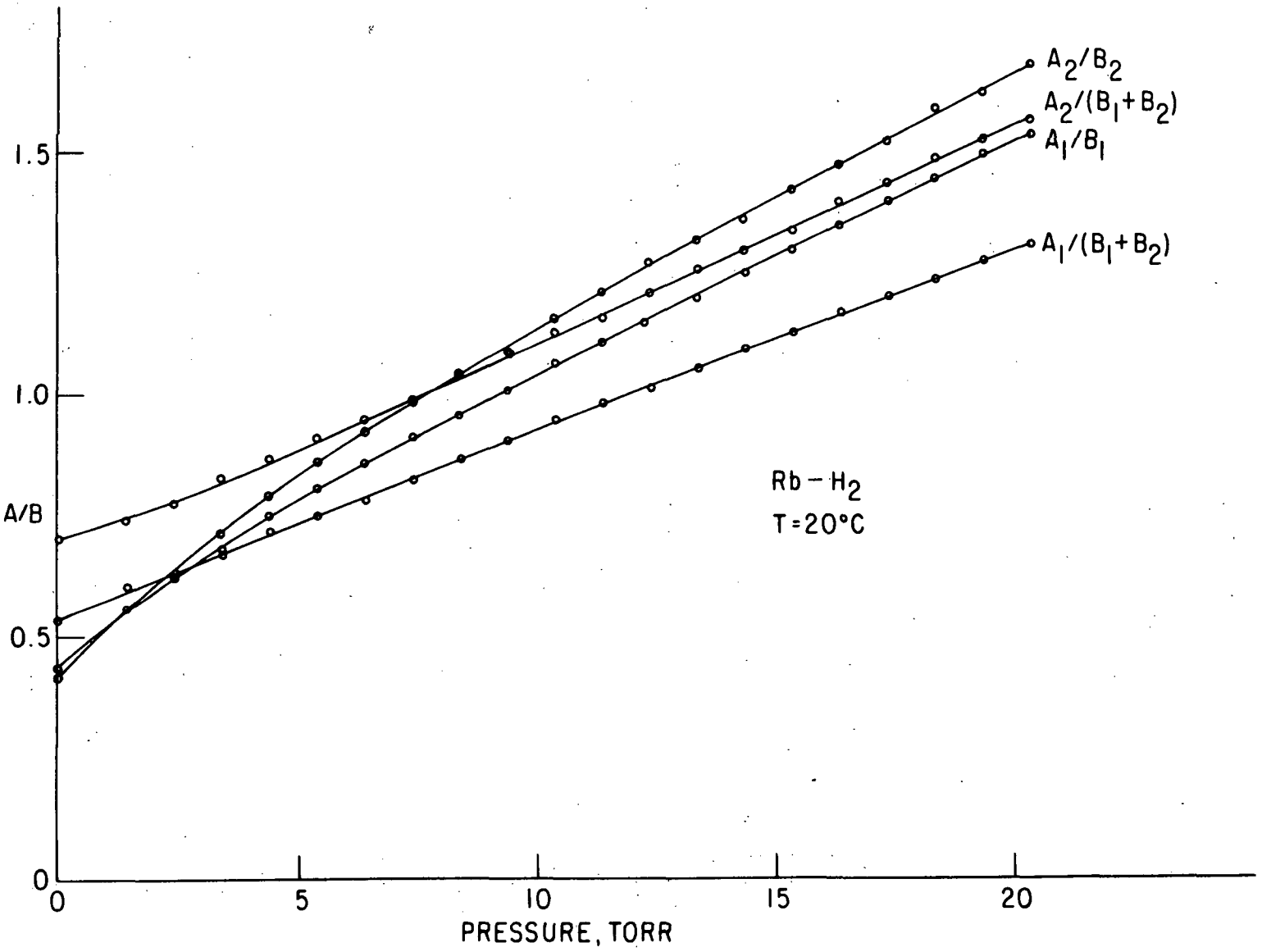

Fig. 7. Graph showing the dependence of the four ratios on hydrogen-gas pressure. Circles are measured data, while the solid lines are the computer fits.

TABLE I. Results obtained for the quenching of rubidium.

Gas-Metal	σ_{10} Å^2	σ_{20} Å^2	σ_{12} Å^2	σ_{21} Å^2	σ_{12}/σ_{21}
N_2 - Rb	57.8	42.2	14.1	23.6	0.60
H_2 - Rb	5.7	2.5	9.09	14.9	0.61
D_2 - Rb	1.3	2.2	19.6	28.6	0.68
CH_4 - Rb	0.0	3.5	31.6	52.7	0.60
C_2H_4 - Rb	174	112	11.9	18.7	0.64
C_2H_6 - Rb	0.0	4.5	56.5	86.0	0.65

The experimental work we have been performing dealt with quenching, which is one phenomenon resulting from collisions with atoms in the excited state. Another effect of the collision is depolarization of the state. Extensive work has been done in the past to study this important phenomenon.

A basic assumption common to all theories about depolarization caused by collisions is that the nucleus remains unaffected during the collision process. This is true because the collision duration ($\sim 10^{-12}$ sec) is much shorter than that of a nuclear period ($\sim 10^{-9}$ sec). This has been shown to hold for depolarization in the ground state of alkalis,[2] and there are no theoretical reasons to expect it to be otherwise for the excited states. It was previously assumed that, because the nucleus remained inert during the collision, the nuclear spin had no effect on the depolarization process. However, we now know that the nuclear spin greatly increases the effective depolarization time. This occurs because the polarization of the electrons is transferred to the nucleus as a result of the hyperfine interaction. Since the nucleus then becomes polarized, it can again recouple to the electron, thereby causing it to repolarize after a collision. This effect, which increases with increasing nuclear spin, should be taken into account when measuring depolarization lifetimes.

We have performed an experiment to measure the depolarization rate of the $^2P_{1/2}$ state of rubidium. It is the standard Hanle-type experiment of zero-field crossing,[3] that has been extensively employed in the past to measure lifetimes, depolarization rates, and other atomic parameters.

Circularly polarized D_1 rubidium resonance radiation is incident on a cell containing rubidium metal and a foreign gas. A static magnetic field is applied in a direction orthogonal to the light path. A photomultiplier monitors the fluorescence in an orthogonal direction to both input excitations and magnetic field through a circular analyzer. The circular polarizer in the excitation path is rotated at a frequency ω which switches the sense of polarization from positive to negative at 2ω, and the

2ω component of the photomultiplier-tube output is detected with a phase-sensitive amplifier whose output drives a chart recorder.

The experimental procedure determines the value of the magnetic field at which the Hanle signal becomes maximum for a given foreign gas pressure. This is repeated for different gas pressures and for the two rubidium isotopes. The results are shown in the following graph, where helium was used as the depolarizing gas.

As we said above, the nuclear spin plays an important role in the depolarization process using the hyperfine interaction. We have calculated the functional dependence of the Hanle signal on magnetic field and foreign gas electron-randomization time, and we have obtained the following equation:

$$S = \frac{R}{3(2I+1)^2} \frac{\omega\left[\frac{3}{2}(2I+1) + \frac{2\Gamma(4I^2+4I+3)}{T(2I+1)} + \frac{6}{T^2(2I+1)} + \frac{3}{2}(2I+1)\omega^2\right]}{\left\{\left[\Gamma + \frac{2}{T(2I+1)^2}\right]\left[\Gamma + \frac{1}{T}\right] + \omega^2\right\}^2 + \frac{\omega^2}{T^2(2I+1)^2}},$$

where R is the mean pumping rate, $\omega = g_F \mu_o H$ is the Larmor-precession frequency, T is the characteristic electron-randomization time, and Γ is the natural decay rate.

This equation differs slightly from a Lorentzian, which is the curve obtained for the Hanle signal when no nuclear spin exists. This equation can be used to determine the functional dependence of the Hanle-signal maximum on the foreign gas-randomization rate $\gamma = 1/T$, and following is a plot of such a function for a nuclear spin of 0, 3/2, 5/2, and 7/2 (see Fig. 8).

It can be seen that the experimental curves for Rb^{85}, $I = 5/2$ and Rb^{87}, $I = 3/2$ agree very well with the theoretical curves for $I = 5/2$ and $3/2$ (see Fig. 9). By fitting the experimental points to the curves and by using only one adjustable parameter α such that $\alpha p = 1/\Gamma T$, we obtain $\alpha = 0.380$ torr^{-1}, from which we determine an electronic randomization cross section for helium of 23×10^{-16} cm^2. This number is to be compared with 9×10^{-16} cm^2, which was obtained by Gallagher[4] by ignoring

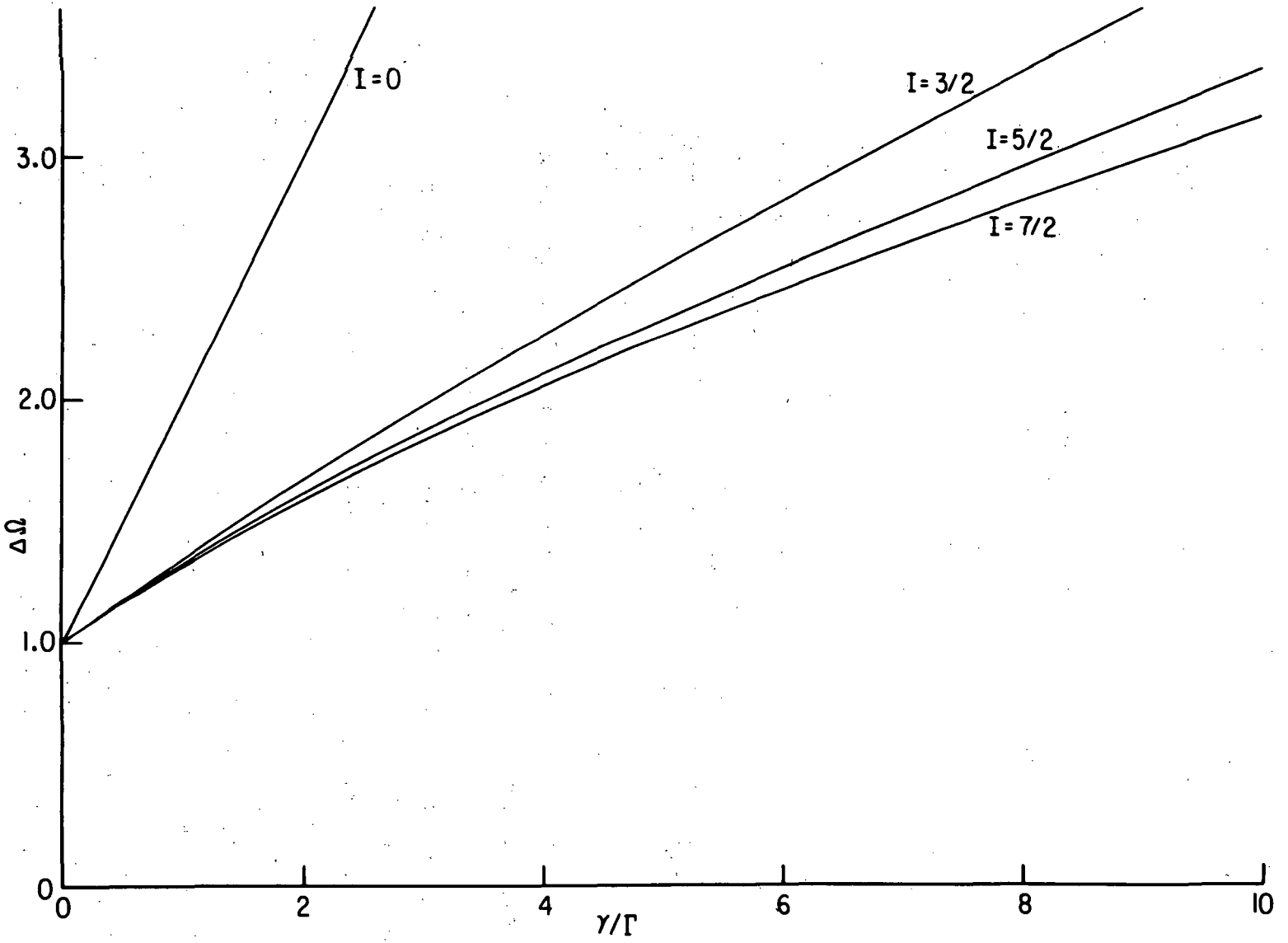

Fig. 8. Calculated values of the relative broadening as a function of the relative depolarization rate for I = 0, I = 3/2, I = 5/2, and I = 7/2.

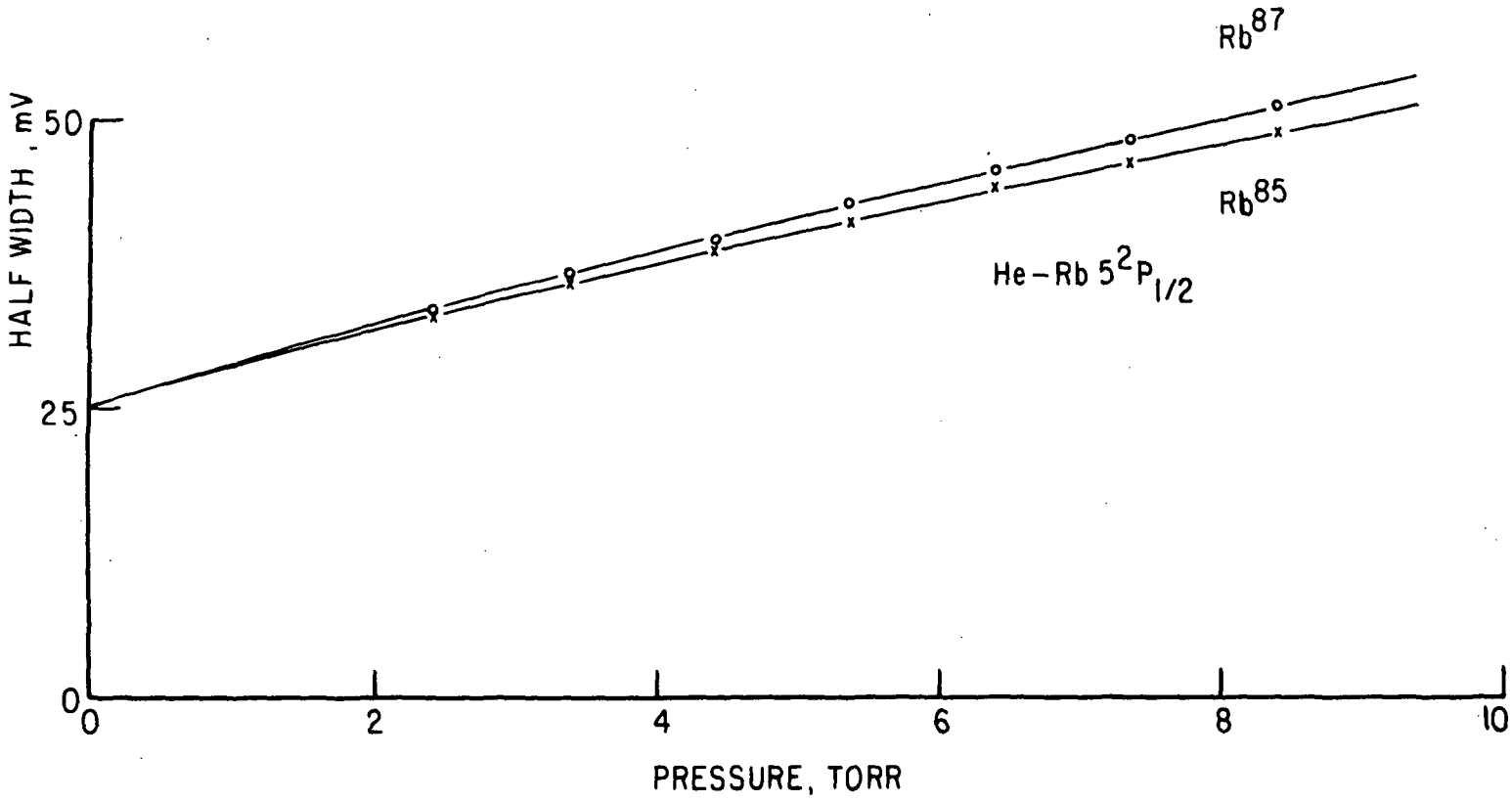

Fig. 9. Experimental values of the broadening as a function of helium-gas pressure for the $5^2P_{1/2}$ state of Rb^{85}, I = 5/2 and Rb^{87}, I = 3/2.

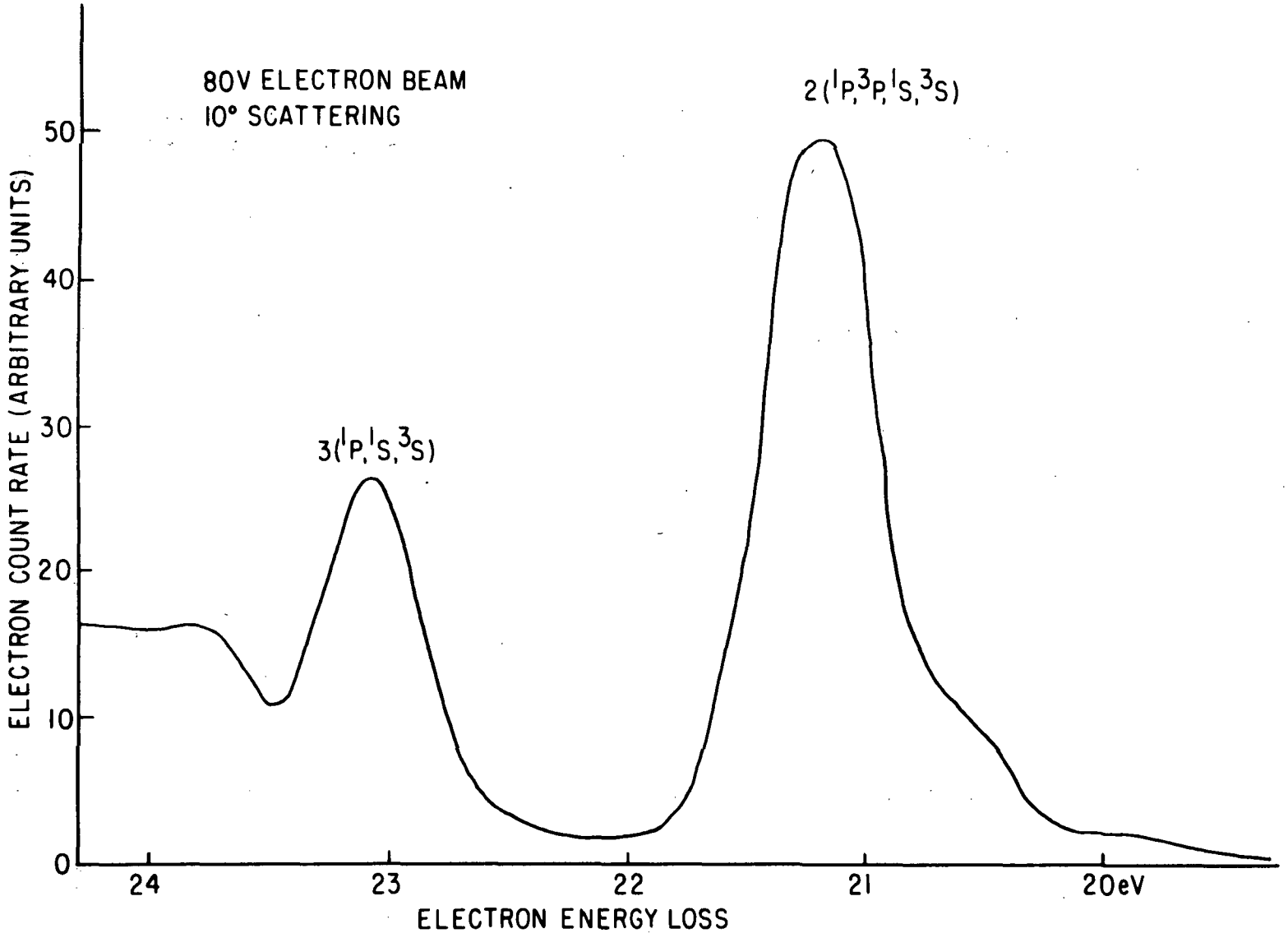

Fig. 10. A sample energy-loss spectrum at a fixed 10° scattering angle.

nuclear spin. Our value is larger than his, as is predicted by the foregoing analysis.

Further work on the depolarization of the $^2P_{3/2}$ state of alkalis will be done in the near future.

*This research was supported by the Air Force Office of Scientific Research under Grant AFOSR-68-1454.

(1) CRL Progress Report, June 30, 1970, p. 20.

(2) H. M. Gibbs, Phys. Rev. 139, A1374 (1965).

(3) W. Hanle, Z. Physik 30, 93 (1964).

(4) A. Gallagher, Phys. Rev. 157, 68 (1967).

---

2. Study of Electron-Impact Excitation of Atoms by a Coincidence Technique

(M. Eminyan, M. Levitt, R. Novick)

We have used the 127° electron-energy analyzer described in previous Progress Reports[1] to observe the electron-energy-loss spectrum at a fixed scattering angle of 10° and at a number of electron energies from 30 to 100 eV. A sample energy-loss spectrum is shown in Fig. 10. The energy spread of the electron gun is on the order of 0.3 eV, and, consequently, the n = 2 and n = 3 peaks are not resolved.

This spectrum was observed as a preliminary measurement to the search for electron-photon coincidences. We expected that the poor energy resolution of the electron gun would not be of significant importance when the scattered electrons were measured in coincidence with the photons. A number of runs taken in the coincidence mode did not show any electron-photon coincidences. While trying to observe the 5016-Å line, which had a bandwidth of 3 Å, we discovered that the interference filter for this line had shifted and gave a transmission of $\leq$ 1%.

In addition to using the correct filter, we will now try to improve the reduction of the light background, and we plan to use a 127° electron monochromator to get a better energy resolution.

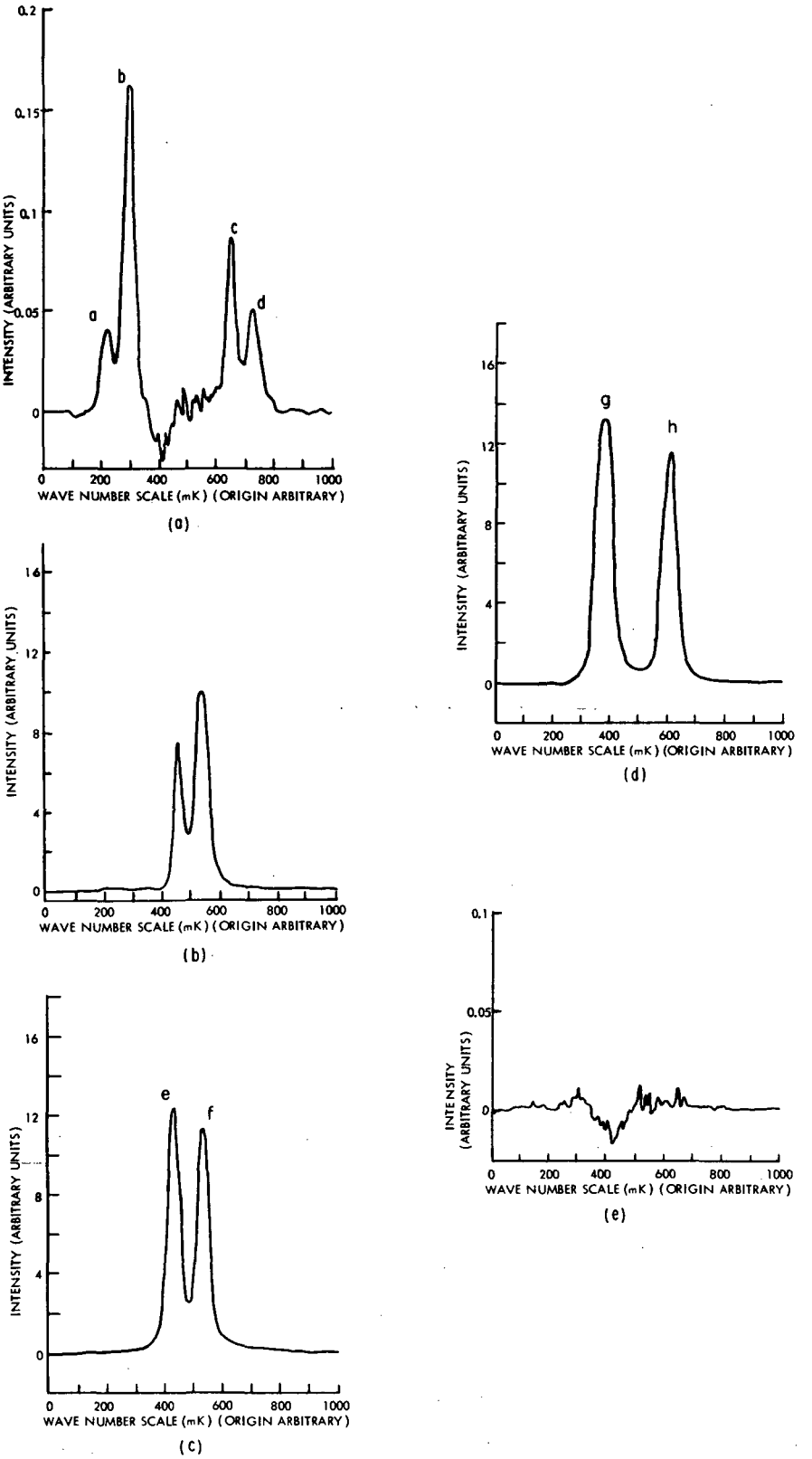

Fig. 11. (a) Spectral profile of sidebands observed with lock-in detection; (b) spectral profile of transmitted carrier; (c) spectral profile of Rb^{85} D_1 light from probing lamp; (d) spectral profile of Rb^{87} D_1 light; and (e) spectral profile observed when the probing lamp was removed.

Program for the next interval: As of Fall, 1970, this project was transferred from the Columbia Radiation Laboratory to the University of Stirling, Scotland, Great Britain.

(1) CRL Progress Reports, October 31, 1968, p. 37; August 31, 1969, p. 35; June 30, 1970, p. 22.

D. ATOMIC FREQUENCY STANDARDS

1. Interaction of Light with Atomic Vapors*
(W. Happer, H. Tang)

We had previously reported[1] the direct observation of sidebands in the spectral profile of Rb^{85} resonance light that had passed through Rb^{87} vapor with "0-0" hfs coherence. During the last period we have made a detailed study of the parametric interaction between light and microwaves in optically pumped Rb^{87} vapor, and our results are in excellent qualitative agreement with the theory.[2,3,4]

The apparatus used for this study is the same as that shown in Fig. 11 of the previous Progress Report,[5] except that lower buffer-gas pressure (~8 torr) was used in the resonance cell, and the guide wavelength of the cavity was adjusted to provide better phase matching than we had achieved previously.[6] We also used a new photomultiplier tube with an extended red-response photocathode[7] to monitor the central fringe of the interference pattern from the etalon. The spectral profiles observed with the improved apparatus are shown in Fig. 11. Figure 11c shows the initial spectral profile of Rb^{85} D_1 light (carrier light). Figure 11b shows the transmitted carrier light from the vapor, observed with polarized P_1 and P_2 parallel.[8] For comparison, the spectral profile of Rb^{87} D_1 light is shown in Fig. 11d. The spectral profile of the sidebands observed with the polarizers P_1 and P_2 crossed is shown in Fig. 11a. We note in Fig. 11a that four sideband components a,b,c, and d are

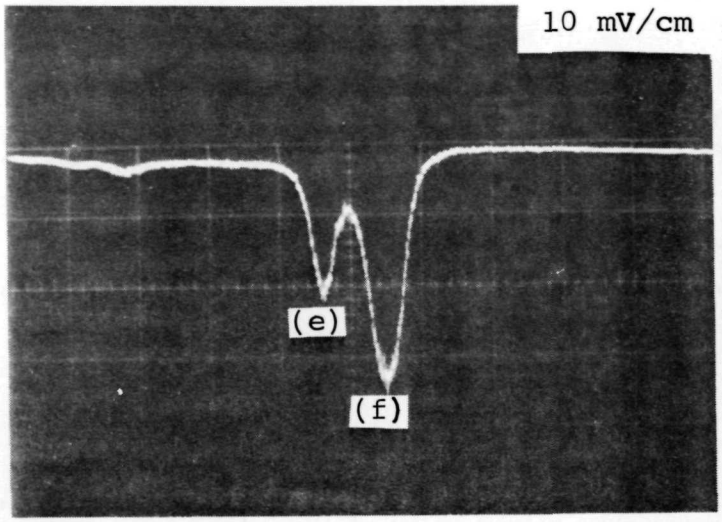

(a)

Oscillogram of photomultiplier-tube output when the polarizers P_1 and P_2 were parallel.

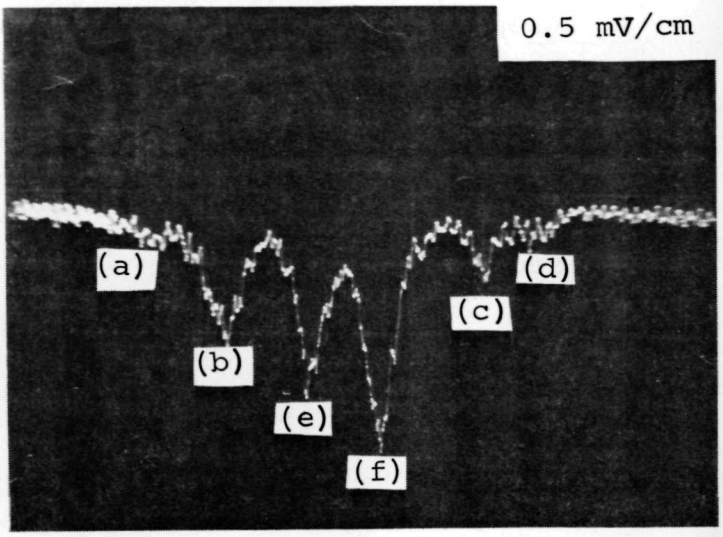

(b)

Oscillograms of photomultiplier-tube output when the polarizers P_1 and P_2 were crossed.

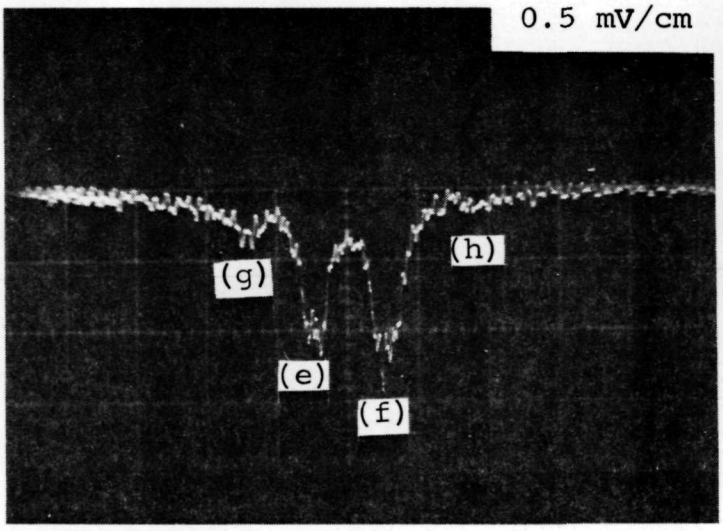

(c)

Oscillogram of photomultiplier-tube output when the polarizers P_1 and P_2 were crossed but the probing lamp was removed.

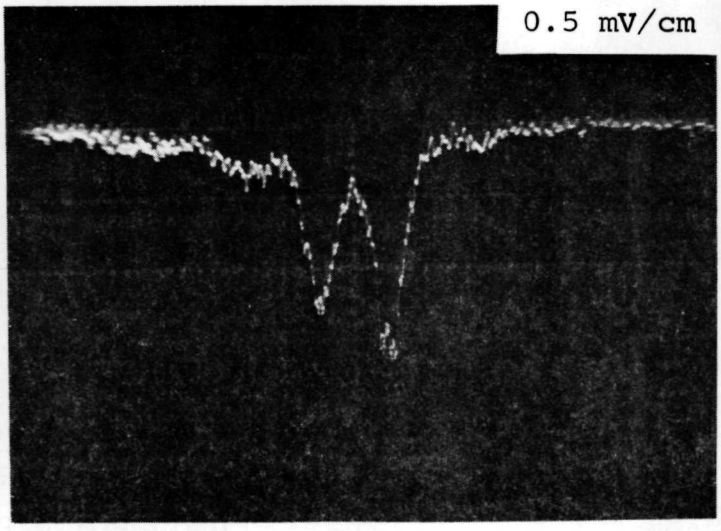

(d)

Oscillograms of photomultiplier output when the polarizers P_1 and P_2 were crossed; the probing lamp was in place, but the microwaves were off resonance.

Fig. 12.

present. The components a and b are displaced by 228 mk on the low frequency side of the components e and f, respectively, of Fig. 11c, while components c and d are displaced by 228 mk on the high frequency side of the components e and f, respectively, of Fig. 11c. The quantity 228 mk is equal to the microwave frequency, 6.835 GHz. The largest sideband component is the lower sideband component b, whose peak intensity is about 1.3% of the intensity of the carrier component e. Figure 11e shows the spectral profile that was observed when the carrier beam was blocked.

With the improved photomultiplier tube, the signal-to-noise ratio of the sideband signal was good enough to permit the observation of the sideband spectral profile on an oscilloscope. These oscillograms are shown in Fig. 12. Figure 12a shows the spectral profile of the transmitted carrier light (polarizers P_1 and P_2 were parallel). The spectral profile observed when the polarizers P_1 and P_2 were crossed is shown in Fig. 12b. We note that the sideband components a,b,c, and d are visible along with the components e and f of the Rb^{85} light. The components e and f are present in Fig. 12b despite the crossed polarizers because an appreciable amount of light from the Rb^{85} pumping lamp is scattered in the forward direction by the resonance-cell walls and by the plates of the cavity. Figure 12c shows the spectral profile observed when the carrier beam is removed. The sidebands have disappeared, but components e and f are still present along with the small components g and h, which are caused by Rb^{87} light fluorescently scattered from the vapor. The spectral profile observed when the carrier-light beam was replaced, but with the microwave frequency tuned off-resonance, is shown in Fig. 12d, and we note that the sideband components are again absent. The oscillograms of Fig. 13 (a-d) show the behavior of the sideband components as the microwave power fed to the cavity was varied. The amount of attenuation of the microwave power is indicated on each oscillogram. We observe that the sideband components decrease

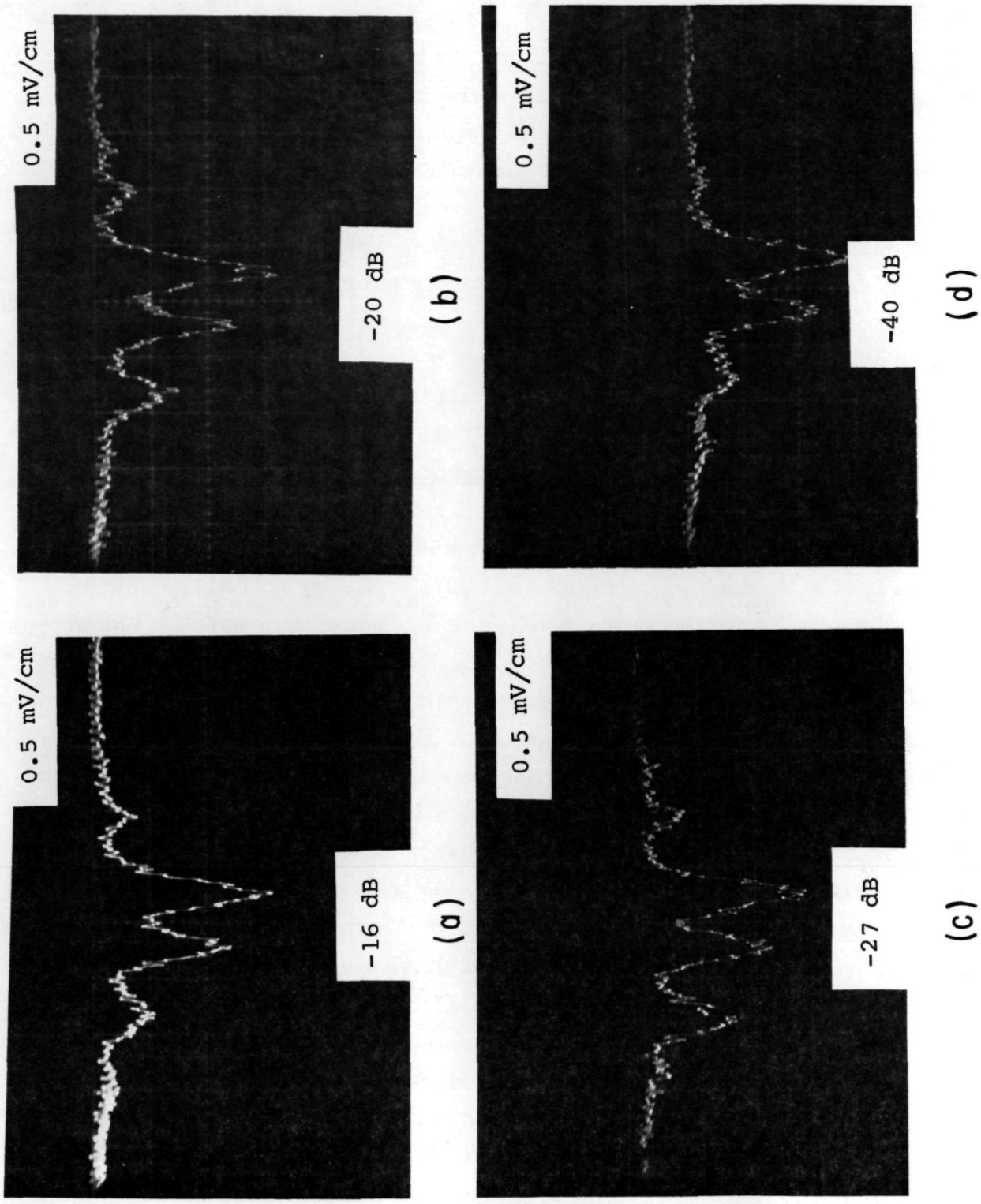

Fig. 13. Oscillogram of the photomultiplier output when the polarizers P_1 and P_2 were crossed, for different values of microwave power.

for high and low microwave power. This is in accordance with the theory, since the sidebands are related to the magnitude of the microwave coherence in the vapor.[9]

We had predicted in the previous Progress Report[10] (see Fig. 15 of Ref. 1) that under the conditions of perfect phase matching, the sideband spectral profile should exhibit only one intense sideband component. In Fig. 11a we see that all four sideband components are present, which indicates that we had still not achieved perfect phase matching. The phase matching is adjusted via the guide wavelength Λ_G of the microwaves in the cavity. The correct value of Λ_G required for perfect phase matching depends critically on the number density N of Rb^{87} atoms in the vapor and on the degree of hyperfine polarization, $\langle \vec{I} \cdot \vec{J} \rangle$, of the vapor. Because of the difficulty involved, we did not attempt to measure the absolute atomic densities. Instead, we based our estimates of the atomic density on published data giving the saturated vapor pressure of rubidium.[11] However, it is well known that the atomic number density in a resonance cell depends on many factors and may deviate considerably from the saturated value.[12] We had also attempted to measure the quantity $\langle \vec{I} \cdot \vec{J} \rangle$ of the vapor, but the accuracy of our measurements was less than that required to precisely determine Λ_G. It can be shown that if the value of Λ_G which is used in the theoretical calculation differed from the correct value for perfect phase matching by only a few percent, the calculated sideband profile would very much resemble that shown in Fig. 11d.

To study the effects of phase matching on the sideband-conversion efficiency, we observed the dependence of the integrated intensity of all the sideband components shown in Fig. 11a as a function of the active cell length. This length was varied by blocking off a portion of the resonance cell from the pumping light. In the unpumped portions of the vapor, there is no coherence; hence no sidebands are generated in these

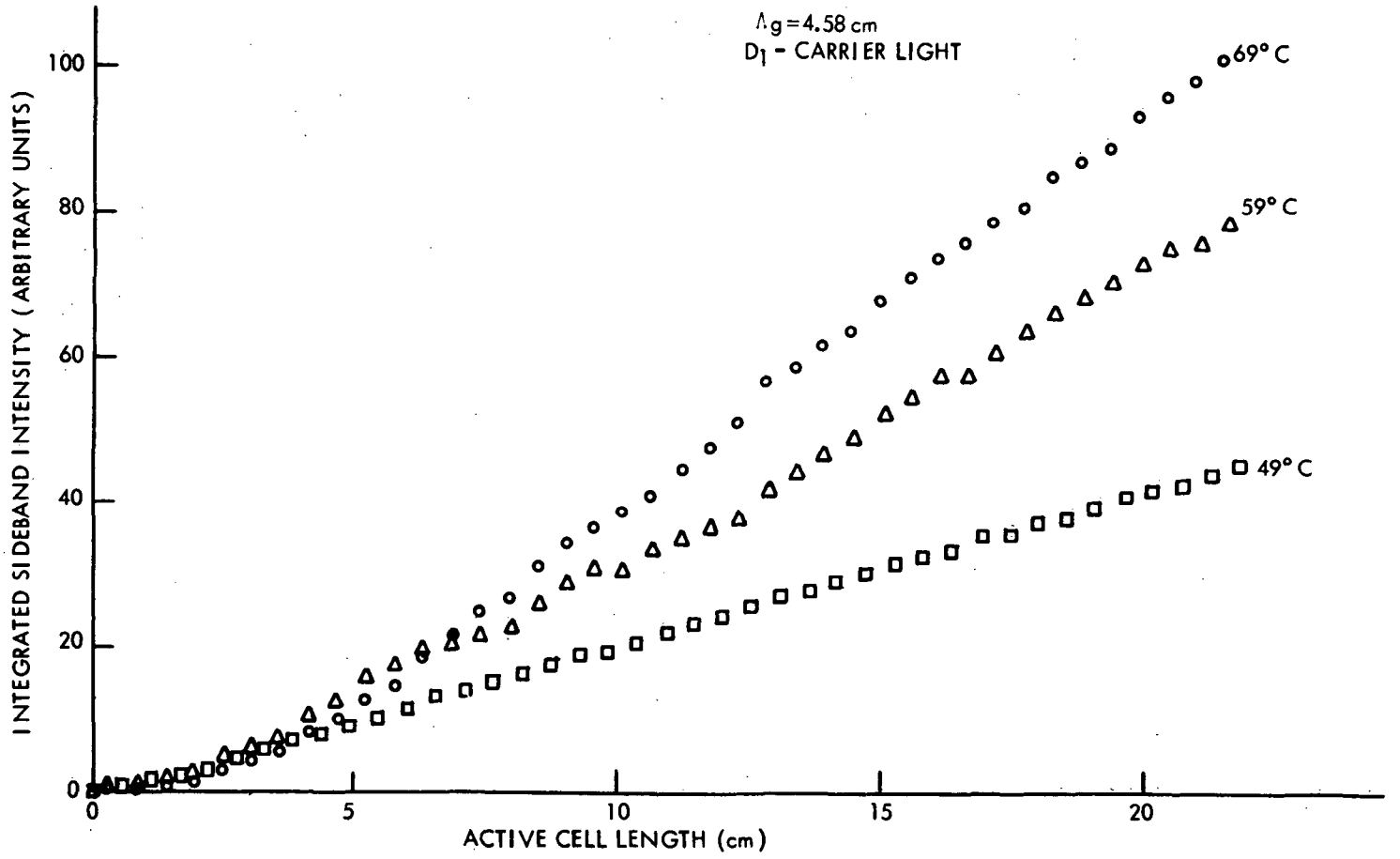

Fig. 14. Integrated sideband intensity versus active length for various values of cell temperature (Λ_G = 4.58 cm).

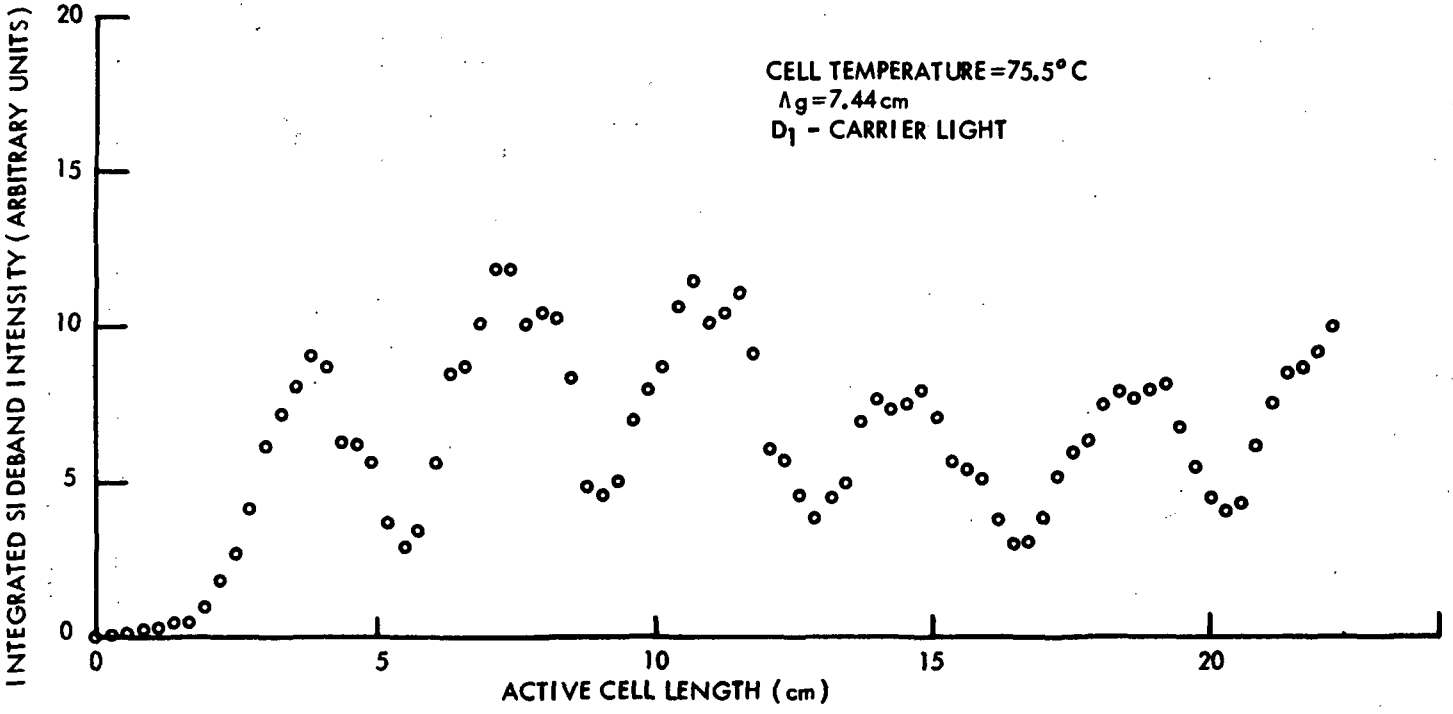

Fig. 15. Integrated sideband intensity versus active length (Λ_G = 7.44 cm).

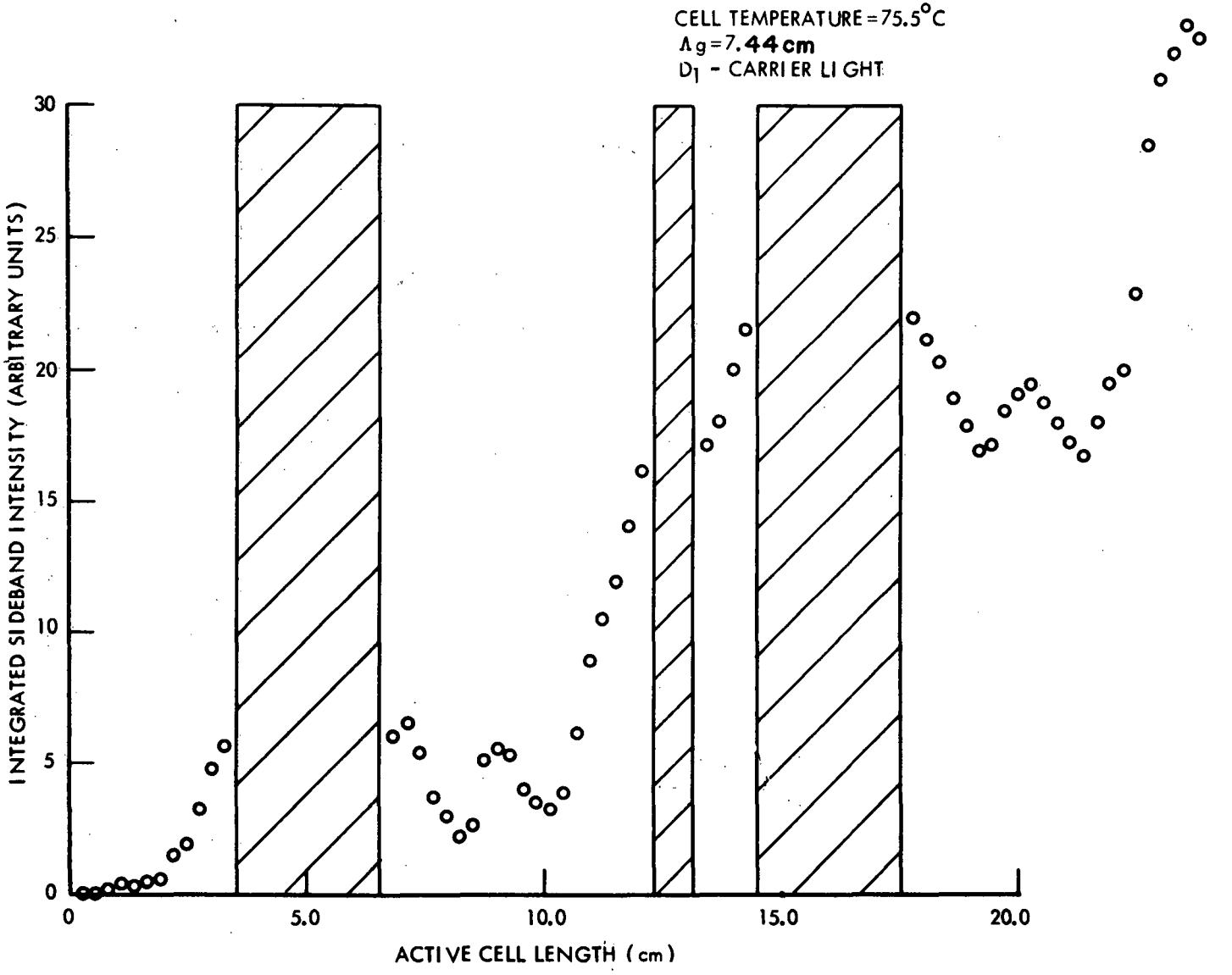

Fig. 16. Integrated sideband intensity versus cell length for a cell which had segments blocked off from the pumping light (Λ_G = 7.44 cm). The blocked-off regions of the cell are represented by the shaded areas.

regions. Furthermore, since the sideband components do not overlap the Rb^{87} absorption line, they suffer no attenuation in the unpumped Rb^{87} vapor. Figure 14 shows a plot of the integrated sideband intensity versus the active cell length for the case in which Λ_G = 4.58 cm. Data taken at several values of cell temperature are shown in this figure, and we see that at each cell temperature, the integrated sideband intensity grows monotonically with the active cell length. Figure 15 shows a plot of the integrated sideband intensity versus the active cell length for the case in which Λ_G = 7.44 cm. We note that the integrated sideband intensity no longer grows monotonically with active cell length but exhibits an oscillatory behavior. The rapid oscillations whose period is equal to $\Lambda_G/2$ are believed to arise because the carrier-light waves can couple to microwaves travelling in both the forward and backward directions in the cavity. The sideband waves which are generated by the forward wave interaction will interfere with the sideband waves generated by the backward wave interaction, with the minima of the sideband intensity occurring at the nodes of the microwave fields in the cavity. The backward wave interaction is usually small because it is poorly phase matched; however, it becomes better phase matched for large values of Λ_G. One can also observe in Fig. 15 that the integrated sideband intensity exhibits a slower oscillatory behavior with a period of about 17 cm. These latter oscillations are caused by poor phase matching.

It was found that in poorly phase-matched situations such as the one shown in Fig. 15 the sideband-conversion efficiency can be enhanced by blocking off certain segments of the resonance cell from the pumping light. Figure 16 shows the integrated sideband intensity versus the active cell length in the case where the cell temperature and Λ_G are the same as in the example shown in Fig. 14, but where segments of the resonance cell have been blocked off from the pumping light.

The shaded regions in Fig. 16 represent the unpumped regions of the resonance cell. We note that the sideband-conversion efficiency has improved. This effect is not yet fully understood, but it can be used to increase conversion efficiency in poorly phase-matched situations.

*This research was also supported by the Air Force Office of Scientific Research under Grant AFOSR-68-1454.

(1) CRL Progress Report, June 30, 1970, p. 31.

(2) W. Happer "Light Propagation and Light Shifts in Optical Pumping Experiments, "Progress in Quantum Electronics, eds., K. W. H. Stevens and J. H. Sanders (Pergamon Press, Oxford, England, 1970), Vol. 1, Part 2, p. 1.

(3) B. S. Mathur, H. Tang, and W. Happer, Phys. Rev. A 2, 2 (1970).

(4) H. Tang and W. Happer, Proceedings of the 24th Annual Symposium on Frequency Control, Atlantic City, N.J. April 27 - 29, 1970, p. 285.

(5) CRL Progress Report, op. cit., p. 31.

(6) Previously we had used a guide wavelength of 4.4 cm. Because of improved estimates of the vapor parameters, we changed the guide wavelength to 4.58 cm.

(7) EMI 9658 RA.

(8) For a linearly polarized carrier, the sidebands are also linearly polarized, but in a direction which is orthogonal to that of the carrier polarization. Hence, when the polarizers P_1 and P_2 shown in Fig. 11 of Ref. 1 are parallel, then only the carrier light passes P_2. However, when P_1 and P_2 are crossed, then only the sidebands pass P_2.

(9) H. Tang and W. Happer, Phys. Rev. Letters 24, 551 (1970).

(10) CRL Progress Report, op. cit., p. 31.

(11) T. J. Killian, Phys. Rev. 27, 578 (1926).

(12) Rubidium is known to react chemically with the resonance cell walls (quartz). Therefore, the vapor pressure in the cell is not solely a function of the temperature of the coldest region of the cell, but also depends on the wall material and the past history of the walls.

2. An Optically Pumped Rb^{85} Maser Oscillator
(R. Novick, W. A. Stern)

At 3035.73... MHz, continuous self-sustained oscillation between the field-independent ground-state hyperfine levels of Rb^{85}, $5^2S_{1/2}(F=3, m_F=0)$ to $5^2S_{1/2}$ $(F=2, m_F=0)$, has been obtained in a magnetically unshielded optically pumped maser.

The maser oscillator operates on the field-independent transition in fields as high as 0.8 G with inhomogeneities of up to 0.2 G. This relative insensitivity to magnetic disturbances together with an observed power output of 8×10^{-10} W gives this maser oscillator good short-term frequency characteristics. Simple estimates indicate a stability of better than 1 part in 10^{13} for averaging times between 1.0 and 0.01 sec.

The Rb^{85} maser will be limited in its long-term stability by cavity pulling and changes in the pumping-lamp profile, as well as chemical changes in the buffer gas caused by outgassing.

The pumped Rb^{85} is contained in a vacuum-tight TE_{021} microwave cavity resonant at 3035.73... MHz and filled with nitrogen gas at a pressure of 8 torr. The nitrogen buffer gas reduces the collision frequency of the aligned Rb^{85} atoms with the walls and quenches reradiation from the upper P states. The cavity is made of copper-plated 305 nonmagnetic stainless steel. Pumping light is admitted through Pyrex windows sealed to the ends of the cavity with nonmagnetic stainless steel housekeeper seals. The light enters the cavity region through perforated end walls. Tuning is accomplished over a 2-MHz range by use of a tuning stub. A movable microwave loop provides proper coupling to the desired mode. After evacuation, 25 mg of Rb^{85} metal (99.85% pure) is introduced into the cavity and settles in a pool on the bottom of the cavity. Very severe Rb^{85} density gradients appear initially and inhibit operation of the maser until the Rb^{85} is uniformly distributed throughout the cavity and uniformly coats the walls. After proper mixing with the buffer gas the Rb^{85} density gradients disappear.

The unloaded cavity Q of 85,000 is high enough to permit oscillation with a relatively small cavity-filling factor and pumping-light intensity. In addition to the high cavity Q, the large cavity volume (9×10^3 cm^3) permits high power output for low vapor densities and facilitates the study of various relaxation processes within the vapor.

The maser is operated at 50 °C by a simple temperature-control system. The nitrogen buffer-gas pressure is not critical, and the maser has been operated over a range of pressures from 6 to 12 torr with little change in output power.

The frequency shift caused by the buffer gas is 274.5 Hz/torr. Insufficient light intensity was available to quench oscillation. The maser oscillates over a 2:1 range of light intensity, and the corresponding change in frequency (light shift) is 10 Hz.

Since the Rb^{85} pumping lamp profile almost overlaps the Rb^{85} absorption line in the maser, the light shifts predicted by the theory for low light fluxes are small. However, if natural rubidium is used as a resonance lamp, the lamp profile would be asymmetric and strongly dependent on the filter-cell temperature. Hence for a natural rubidium lamp the light shifts would be larger and more sensitive to filter-cell temperature than they would be for a Rb^{85} resonance lamp.

Since the light causes shifts of ~20 Hz for a change of 100% light intensity, the lamp intensity must be stable to 1 part in 10^4 to achieve a maser stability of 1 part in 10^{13}. It is possible to obtain this lamp stability, especially over a short term.

Table II summarizes the measured frequency shifts observed with various buffer gases. It is interesting to compare the buffer-gas shift in Rb^{87} with that in Rb^{85}. For example, the Rb^{85}-neon shift is +170 Hz/torr, while the Rb^{87}-neon shift is 392 Hz/torr. Similarly, the Rb^{85}-nitrogen shift is 247.5 Hz/torr, while the Rb^{87}-nitrogen shift is 543 Hz/torr. In order to make a

TABLE II. Frequency Shift Caused by Buffer Gas.

Buffer Gas	Rb^{85} Hyperfine Shift (0-30 torr)
Helium	+308 Hz/torr
Nitrogen	+274.5 Hz/torr
Neon	+170 Hz/torr
Argon	- 22.2 Hz/torr
Methane	-203.8 Hz/torr

comparison between the two isotopes, it is useful to consider that the shift caused by the buffer gas is simply a result of a distortion of the ground-state wave function $\psi(0)$. The ground-state hyperfine splitting for either isotope is given by

$$\nu_o = (16\pi/3)\ \mu_B^2 (I + 1/2) g_I |\psi_{(o)}|^2.$$

If the term $\frac{\partial |\psi_{(o)}|^2}{\partial P}$ is the same for each isotope, then the ratio of the pressure shifts of each isotope for a particular buffer gas should be in the same ratio as the ground-state hyperfine splitting. In the case of the Rb^{85}- Rb^{87} isotope system this ratio is $6834/3035 \cong 2.25$. Observed ratios of pressure shifts are 2.25 for neon and 2.2 for nitrogen.

The work described here brings to a successful conclusion a continuing effort at the Columbia Radiation Laboratory to build auto-oscillating rubidium masers. It now appears that the rubidium maser can be brought out of the laboratory and put to work in the field as a practical short-term frequency standard.

One of the most difficult tasks facing scientists involved in time and frequency control is the generation of high frequencies possessing high spectral purity. It is relatively easy using cesium-beam standards to obtain long-term stabilities of 1 part in 10^{13} for averaging times of a few hours or more. However, when the 5-MHz cesium-beam standard output is multiplied into the gigahertz region for practical applications, the spectral impurities that are present at 5 MHz because of a lack of comparable short-term stability render the resulting signal too noisy. Specific examples of this occur in master oscillators for high-speed digital communications, coherent radar, long-base line interferometry, clock synchronization, and extremely precise navigation.

Rubidium masers permit direct generation of X-band or S-band frequencies with short-term stabilities of better than 1 part in 10^{13}. Although the long-term stabilities would be

on the order of 1 part in 10^{12} for 1-hr averaging, this can be improved by phase locking the maser to a cesium device. The rubidium-cesium combination would then be a primary standard with the short-term stability of the rubidium maser and the long-term stability of the cesium beam. Either alone or in combination with the cesium beam, the rubidium maser is a small, relatively simple frequency standard that will probably have many applications in the communications and the navigation systems of the future.

II. PHYSICS OF MOLECULES

A. MOLECULAR SPECTRA OF CESIUM*
(M. M. Hessel, P. Kusch)

This project has been transferred to Fordham University, Bronx, New York.

*This research was also supported in part by the Air Force Office of Scientific Research under Grant AFOSR-68-1454 and in part by the Office of Naval Research under Contract N00014-67-A-0108-0002.

B. MICROWAVE SPECTROSCOPY*
(R. Nerf, P. Thaddeus)

Several investigations in microwave spectroscopy of interest to the radio astronomy of interstellar molecules have been pursued during the past six months. During this time we have measured the pressure broadening of the $1_{10} \rightarrow 2_{11}$ rotational transition of formaldehyde at 150,498.36 MHz. The effects of formaldehyde, argon, and helium collisions on the width of the line have been studied.

The millimeter-wave spectrum of formaldehyde has been investigated in considerable detail. Twenty-eight lines of the C^{12} and C^{13} isotopic species of formaldehyde, ranging in frequency from 45 to 300 GHz, have been measured to a precision of six parts in 10^7 or higher. An analysis of the spectrum to obtain the centrifugal distortion coefficients of both isotopic species is nearly completed and will be published soon.

We have also measured a number of millimeter-wavelength lines of the ground and excited vibrational states of cyanoacetylene. Accurate frequencies for these lines have been used to refine the values of the rotation constant and the centrifugal distortion coefficient of the molecule.

*This research was also supported by the National Aeronautics and Space Administration under Grant NGR 33-008-012: Scope F.

C. MOLECULAR BEAM-MASER SPECTROSCOPY*

(R. DeZafra, L. Lurie, P. Thaddeus, G. Tomasevich, K. Tucker)

The microwave spectra of a number of light molecules are being investigated in a high-resolution beam-maser spectrometer. The molecules under study are of interest to radio astronomy, which requires precise laboratory measurements of absolute transition frequencies. In addition, they possess interesting magnetic and electric hyperfine structure (hfs), which can be resolved only in a molecular-beam device.

The first molecule under study is formaldehyde, H_2CO, and its isotopic species, $H_2{}^{13}C^{16}O$, $H_2{}^{12}C^{18}O$, and $HD^{12}C^{16}O$. Work on the $1_{10} \rightarrow 1_{11}$ rotational transition has nearly been completed. Because of the high sensitivity of our spectrometer, the ^{13}C and ^{18}O species could be studied in natural abundance. Absolute transition frequencies were measured to an accuracy of a few parts in 10^8. The analysis of these spectra yielded hyperfine interaction parameters for H, D, and ^{13}C nuclei. The measured frequencies and hyperfine parameters appear in Tables III and IV. The $D_2{}^{12}C^{16}O$ molecule and, hopefully, the $H_2{}^{12}C^{17}O$ molecule will be studied in the same way.

In addition, a hot-nozzle beam source was constructed for studying excited vibrational states of H_2CO. With this source, the $1_{10} \rightarrow 1_{11}$ transition was measured in the first bending vibrational modes ν_5 and ν_6, which lie 1250 and 1160 cm^{-1}, respectively, above the ground state. Since these modes have the opposite symmetry (with respect to 180° rotation about the symmetry axis of the molecule) as the ground vibrational state, nuclear statistics require that the two H spins couple to 0 in the 1_{10} and 1_{11} rotational states. Consequently, all hyperfine interactions vanish, and the transition appears as a single line.

In the case of $H_2{}^{13}CO$, not all of the hyperfine components of the upper rotational state could be state-selected; and therefore an additional resonance region was added between the state-selector and the microwave cavity. The application of perpendicular static and alternating electric fields in this region

TABLE III. Measured Hyperfine Frequencies of $1_{10} \rightarrow 1_{11}$ Formaldehyde Transitions.

Molecule	Transition[a] $F \rightarrow F'$ or $F_1F \rightarrow F_1'F'$	Line Center (ν_o) (kHz)	Relative Intensity	$\nu-\nu_o$ (kHz)
H_2CO		4 829 659.96 ± 0.05		
	1 → 0		4	-18.53 ± 0.06
	0 → 1		4	-1.34 ± 0.12
	2 → 2		15	-0.35 ± 0.05[b]
	2 → 1		5	+4.05 ± 0.05
	1 → 2		3	+6.48 ± 0.05
	1 → 1		3	+11.08 ± 0.05
$H_2C^{13}O$		4 593 088.54 ± 0.06		
	$\frac{1}{2}\frac{1}{2} \rightarrow \frac{3}{2}\frac{1}{2}$		1.05	-132.22 ± 0.14
	$\frac{1}{2}\frac{1}{2} \rightarrow \frac{3}{2}\frac{3}{2}$		1.06	-114.78 ± 0.14
	$\frac{1}{2}\frac{3}{2} \rightarrow \frac{3}{2}\frac{1}{2}$		0.04	-112.65 ± 0.25[b]
	$\frac{1}{2}\frac{3}{2} \rightarrow \frac{3}{2}\frac{5}{2}$		2.98	-102.87 ± 0.09
	$\frac{1}{2}\frac{3}{2} \rightarrow \frac{3}{2}\frac{3}{2}$		1.62	-95.19 ± 0.14
	$\frac{1}{2}\frac{1}{2} \rightarrow \frac{1}{2}\frac{1}{2}$		0.37	-39.16 ± 0.16
	$\frac{1}{2}\frac{3}{2} \rightarrow \frac{1}{2}\frac{1}{2}$		3.83	-19.57 ± 0.07

TABLE III. (cont'd)

Molecule	Transition[a]	Line Center (ν_o) (kHz)	Relative Intensity	$\nu-\nu_o$
$H_2C^{13}O$		4 593 088.54 ± 0.06		
	$\frac{1}{2}\,\frac{1}{2} \rightarrow \frac{1}{2}\,\frac{3}{2}$		4.18	-8.59 ± 0.25
	$\frac{3}{2}\,\frac{1}{2} \rightarrow \frac{3}{2}\,\frac{1}{2}$		2.74	-7.39 ± 0.10
	$\frac{3}{2}\,\frac{3}{2} \rightarrow \frac{3}{2}\,\frac{1}{2}$		2.84	-2.16 ± 0.25[b]
	$\frac{3}{2}\,\frac{5}{2} \rightarrow \frac{3}{2}\,\frac{5}{2}$		14.00	-2.00 ± 0.05
	$\frac{3}{2}\,\frac{5}{2} \rightarrow \frac{3}{2}\,\frac{3}{2}$		2.31	+5.70 ± 0.15
	$\frac{3}{2}\,\frac{3}{2} \rightarrow \frac{3}{2}\,\frac{5}{2}$		3.02	+7.58 ± 0.15
	$\frac{3}{2}\,\frac{1}{2} \rightarrow \frac{3}{2}\,\frac{3}{2}$		2.44	+9.97 ± 0.15
	$\frac{1}{2}\,\frac{3}{2} \rightarrow \frac{1}{2}\,\frac{3}{2}$		4.86	+10.89 ± 0.25[b]
	$\frac{3}{2}\,\frac{3}{2} \rightarrow \frac{3}{2}\,\frac{3}{2}$		5.90	+15.37 ± 0.11
	$\frac{3}{2}\,\frac{1}{2} \rightarrow \frac{1}{2}\,\frac{1}{2}$		1.40	+85.54 ± 0.10
	$\frac{3}{2}\,\frac{3}{2} \rightarrow \frac{1}{2}\,\frac{1}{2}$		1.07	+90.93 ± 0.10
	$\frac{3}{2}\,\frac{5}{2} \rightarrow \frac{1}{2}\,\frac{3}{2}$		3.69	+111.78 ± 0.08
	$\frac{3}{2}\,\frac{1}{2} \rightarrow \frac{1}{2}\,\frac{3}{2}$		0.09	+116.04 ± 0.25[b]
	$\frac{3}{2}\,\frac{3}{2} \rightarrow \frac{1}{2}\,\frac{3}{2}$		0.51	+121.38 ± 0.20

TABLE III. (cont'd)

Molecule	Transition[a]	Line Center (ν_o) (kHz)	Relative Intensity	$\nu-\nu_o$
H_2CO^{18}		4 388 796.98 ± 0.12		
	1 → 0		4	-18.43 ± 0.14
	0 → 1		4	-1.02 ± 0.30[b]
	2 → 2		15	-0.68 ± 0.08
	2 → 1		5	+4.09 ± 0.10
	1 → 2		5	+6.56 ± 0.17
	1 → 1		3	+11.45 ± 0.13
HDCO[c]		5 346 141.59 ± 0.09		
	$1\frac{1}{2} \rightarrow 1\frac{1}{2}$		0.89	-46.07
	$1\frac{3}{2} \rightarrow 1\frac{1}{2}$		0.65	-45.17
	$1\frac{1}{2} \rightarrow 1\frac{3}{2}$		0.67	-39.00
	$1\frac{3}{2} \rightarrow 1\frac{3}{2}$		2.76	-38.10
	$1\frac{1}{2} \rightarrow 2\frac{3}{2}$		2.66	-19.93
	$1\frac{3}{2} \rightarrow 2\frac{3}{2}$		0.96	-19.03
	$2\frac{3}{2} \rightarrow 1\frac{1}{2}$		2.91	-18.22
	$1\frac{3}{2} \rightarrow 2\frac{5}{2}$		4.76	-15.78
	$2\frac{5}{2} \rightarrow 1\frac{3}{2}$		5.20	-13.71
	$2\frac{3}{2} \rightarrow 1\frac{3}{2}$		0.27	-11.14

TABLE III. (cont'd)

Molecule	Transition[a]	Line Center (ν_o) (kHz)	Relative Intensity	$\nu-\nu_o$
HDCO[c]		5 346 141.59 ± 0.09		
	$2\frac{5}{2} \rightarrow 2\frac{3}{2}$		0.80	+5.38
	$2\frac{3}{2} \rightarrow 2\frac{3}{2}$		0.89	+7.92
	$2\frac{5}{2} \rightarrow 2\frac{5}{2}$		14.00	+8.62
	$2\frac{3}{2} \rightarrow 2\frac{5}{2}$		1.24	+11.17
	$1\frac{1}{2} \rightarrow 0\frac{1}{2}$		2.44	+16.44
	$1\frac{3}{2} \rightarrow 0\frac{1}{2}$		4.21	+17.34
	$0\frac{1}{2} \rightarrow 1\frac{1}{2}$		2.21	+18.03
	$0\frac{1}{2} \rightarrow 1\frac{3}{2}$		4.44	+25.11
H_2CO, $V_4 = 1$[d]		4 235 952.38 ± 0.11		
H_2CO, $V_6 = 1$[d]		4 968 862.47 ± 0.16		

(a) F (F_1F) refers to the upper level of the transition, and F' (F_1'F') to the lower level.

(b) Calculated frequency.

(c) Frequencies listed are best-fit hyperfine frequencies; the estimated uncertainty is ±0.10 kHz.

(d) Because of the symmetry properties of the first excited vibrational states of ν_6 and ν_4, no hfs is present in the $1_{10} \rightarrow 1_{11}$ transition.

TABLE IV. Hyperfine Coupling Constants.

Molecule	Hyperfine Constant (kHz)
H_2CO	$C_H\ (1_{10}) = -0.82 \pm 0.04$
	$C_H\ (1_{11}) = -3.05 \pm 0.04$
	$g_H\mu_N{}^2 r^{-3} = 17.68 \pm 0.10$
$H_2C^{13}O$	$C_C\ (1_{10}) = 73.87 \pm 0.14$
	$C_C\ (1_{11}) = 67.79 \pm 0.14$
	$C_H\ (1_{10}) = -0.77 \pm 0.06$
	$C_H\ (1_{11}) = -3.03 \pm 0.06$
	$g_H{}^2\mu_N{}^2 r_{HH}{}^{-3} = 17.52 \pm 0.17$
	$g_H g_C \mu_N{}^2 r_{HC}{}^{-3} = 21.65 \pm 0.18$
H_2CO^{18}	$C_H\ (1_{10}) = -0.98 \pm 0.10$
	$C_H\ (1_{11}) = -2.98 \pm 0.10$
	$g_H{}^2\mu_N{}^2 r^{-3} = 17.90 \pm 0.25$

TABLE IV. (cont'd)

Molecule	Hyperfine Constant (kHz)
HDCO	$C_D\ (1_{10}) = 0.11 \pm 0.04$
	$C_D\ (1_{11}) = -0.12 \pm 0.04$
	$C_H\ (1_{10}) = -1.43 \pm 0.08$
	$C_H\ (1_{11}) = -3.70 \pm 0.12$
	$g_H g_D \mu_N^2 r^{-3} = 2.75 \pm 0.10$
	$(eV_{\xi\xi}Q)_D = 167.30 \pm 0.90$
	$(eV_{\xi\xi}Q) = -82.55 \pm 0.90$

induced transitions among the hyperfine components of the focusing state, so that all the missing maser transitions were reproduced.

The formaldehyde-maser oscillator operating on the $1_{10} \rightarrow 1_{11}$ transition was examined further. Four of the hyperfine components could be made to oscillate simultaneously, and audio beat frequencies could be monitored in the microwave receiver output. The total oscillator power was 1.4×10^{-10} W with 8% coupling in a cavity with a Q of about 2×10^{4}.

Other molecules to be studied include the chemically related furan (C_4H_4O), pyrrole (C_4H_5N), and pyridine (C_5H_5N), all rings compounds. The $1_{10} \rightarrow 1_{11}$ (4575.910-MHz) and $2_{20} \rightarrow 2_{11}$ (4381.949-MHz) transitions in furan have already been measured. This is the most complex molecule ever observed in a maser spectrometer. Two pyrrole lines have also been observed but not measured accurately.

The $2_{11} \rightarrow 2_{12}$ transition in formic acid (CH_2O_2) and the J = 1 to 0 transition in cyanoacetylene (HC_3N) have also been observed.

To facilitate the search for new molecular resonances that are not well predicted, a Stark-cell microwave spectrometer has been constructed. Since a maser utilizes a resonant cavity, which is an intrinsically narrow-banded device, it is not well suited for wideband searching. The Stark cell allows searching over an entire microwave band, although with much poorer resolution than a beam maser. One can also combine direct detection and Stark modulation in order to determine whether a complex spectrum has a suitable Stark effect for molecular beam-maser observability.

To increase the sensitivity of the maser, a digital laboratory-control computer is being acquired. It will permit us to extend practical signal-detection time constants with repetitive signal averaging and automatic experiment control.

Also under construction is a millimeter-wave-maser spectrometer. This device will utilize a Fabry-Perot resonator in place of the conventional microwave cavity. A preliminary version of the Fabry-Perot is now being tested; and it will be tested in the near future on the well-known 3-3 inversion line of ammonia.

*This research was also supported by the National Aeronautics and Space Administration under Grant NGR 33-008-012: Scope F.

D. LEVEL-CROSSING AND OPTICAL RADIO-FREQUENCY DOUBLE-RESONANCE STUDIES OF MOLECULES*

(T. Bergeman, E. Weinstock, R. N. Zare)

During this period, we have used a coincidence with an atomic tellurium line at 2147.5 Å as a source of excitation to carry out Hanle-effect measurements on the ($v = 1$, $N = 10$) level of the $A\ ^2\Sigma^+$ state of the NO molecule. These measurements extrapolated to zero pressure yield the product of the molecular g factor and the molecular radiative lifetime τ. The value of $g\tau$ for the ($v = 1$, $N = 10$) level is found to be consistent with the previously reported value of $g\tau$ for the ($v = 1$, $N = 13$) level. In both cases if the g value is that predicted for Hund's case (b) coupling, namely, $g_N = \pm(N + 1/2)^{-1}$ for the two spin components $J = N \pm 1/2$, then the radiative lifetime τ is determined to be 2×10^{-7} sec.

The measurement of the spin doubling and the hyperfine interactions for the NO $A\ ^2\Sigma^+$ molecular state remains the principal goal of our work. For this purpose, we have calculated the resonance-fluorescence intensities for $^2\Pi \rightarrow {}^2\Sigma^+ \rightarrow {}^2\Pi$ transitions with hyperfine structure and excited-state radio-frequency resonances. These calculations allow us to select the optimum experimental arrangement for carrying out optical radio-frequency double-resonance experiments, and they will facilitate the identification of resonances when the latter are observed. The hyperfine splitting is expected to be dominated by the term which includes the Fermi contact interaction, $b(I \cdot S)$, in the

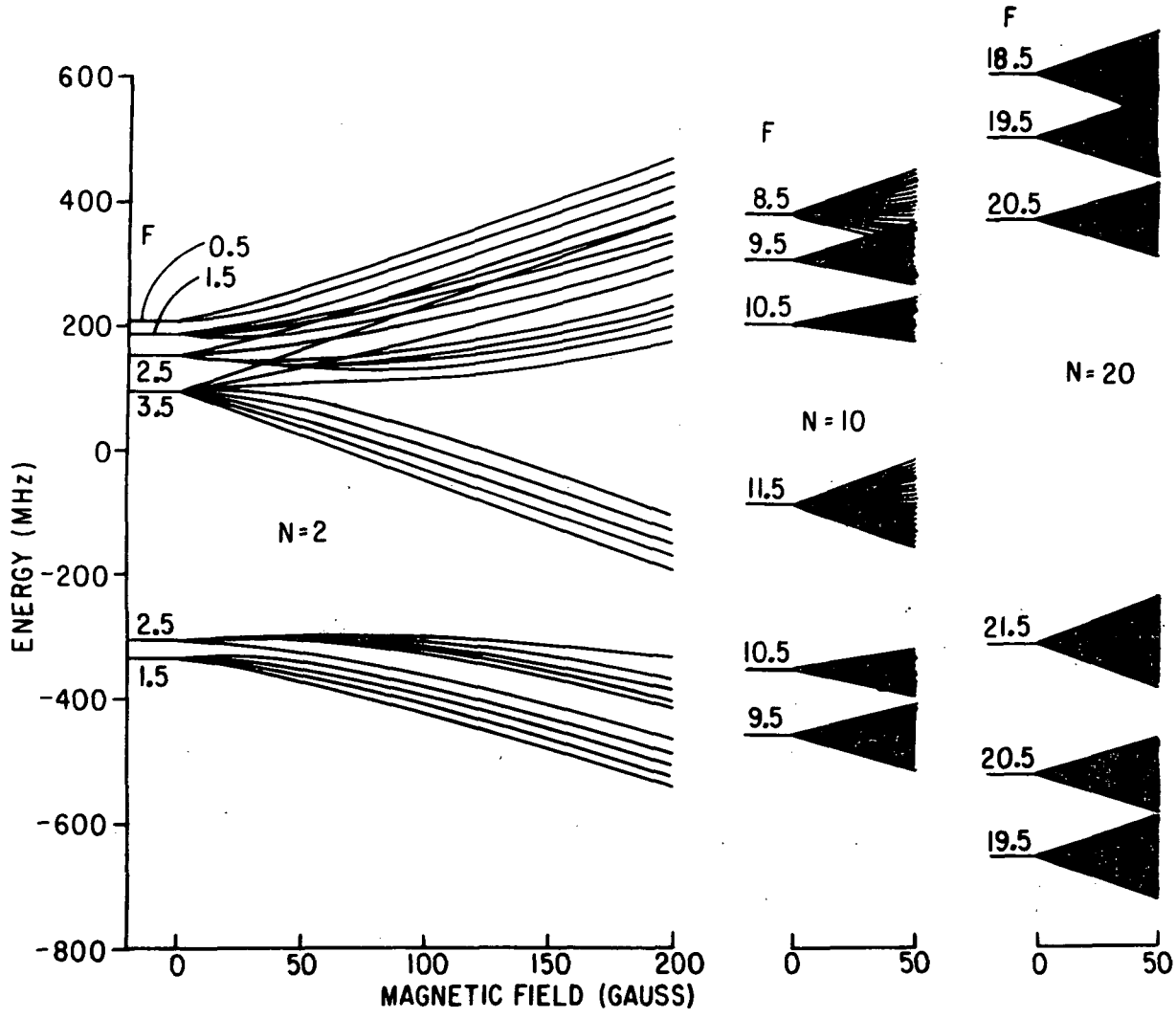

Fig. 17. Hyperfine and Zeeman level structure of the $^{14}N^{16}O$ A $^2\Sigma^+$ state derived from estimated parameters, b = 300 MHz and γ = -45 MHz. This shows the levels to be studied by double resonance. For K = 2, $b(\vec{I}\cdot\vec{S})$ predominates; there are four F states for $|\vec{I} + \vec{S}| = 3/2$, and two F states for $|\vec{I} + \vec{S}| = 1/2$, where $\vec{F} = \vec{I} + \vec{S} + \vec{K}$. This is coupling case (bβS). The Paschen-Back effect divides all sublevels into blocks of $S_z = +1/2$ and -1/2. For high K, spin rotation $\gamma\vec{K}\cdot\vec{S}$ predominates, and there are three F states each for $J = K \pm 1/2$. This is case (bβJ). The case K = 10 is intermediate. The 2F + 1 Zeeman sublevels for each F state with K = 10 and K = 20 are not resolved on this scale.

notation of Frosch and Foley.[1] We estimate from simple molecular orbital theory that the b parameter has the approximate value b = 300 ± 100 MHz. The spin doubling can be estimated from recent optical emission spectroscopy to have the approximate value $\rho_N = -(N + 1/2)(45 \pm 20)$ MHz. Note that for the lowest rotational levels the hyperfine splittings should be larger than the spin doubling, but for large N the latter dominates. The Hanle-effect observations on the N = 10 level confirm these estimates to the extent that the observed intensities of the individual resolved fluorescent lines do not show the effects of hyperfine mixing as would be expected if $b \geq \rho_{10}$. Precise knowledge of these fine structure and hyperfine structure parameters is of interest in the interpretation of spectra and as a test of electronic wavefunction calculations now being developed for open-shell configuration of diatomic molecules.

The primary difficulty in performing these measurements arises from the overabundance of sublevels in a $^2\Sigma^+$ state with a nuclear spin I = 1. There are in general 12N + 6 different $|F,M\rangle$ Zeeman sublevels for each rotational level N (see Fig. 17). Because of the poor state selection attainable for optical transitions from and to the $^2\Pi$ ground state, the usual techniques of high-field level crossing or fixed-frequency magnetic-field-swept rf resonances do not yield a useful signal except possibly for excitation of the N = 1 level by atomic line coincidences. The options are therefore limited.

At present, the best available method of optically pumping selected rotational levels of the excited electronic state uses atomic spectral line coincidences. A well-known cadmium-ion line at 2144 Å which pumps N = 13, the tellurium 2147.5-Å line which pumps N = 10, also of v = 1, and a selenium line which pumps a less adventitious transition to N = 1 of v = 3[2] have been used to excite fluorescence. There are also coincidences with much weaker lines from the CO molecular spectrum which pump several rotational levels, including N = 1 of v = 0. Excitation by the discharge of NO itself, a possibility considered earlier, is not

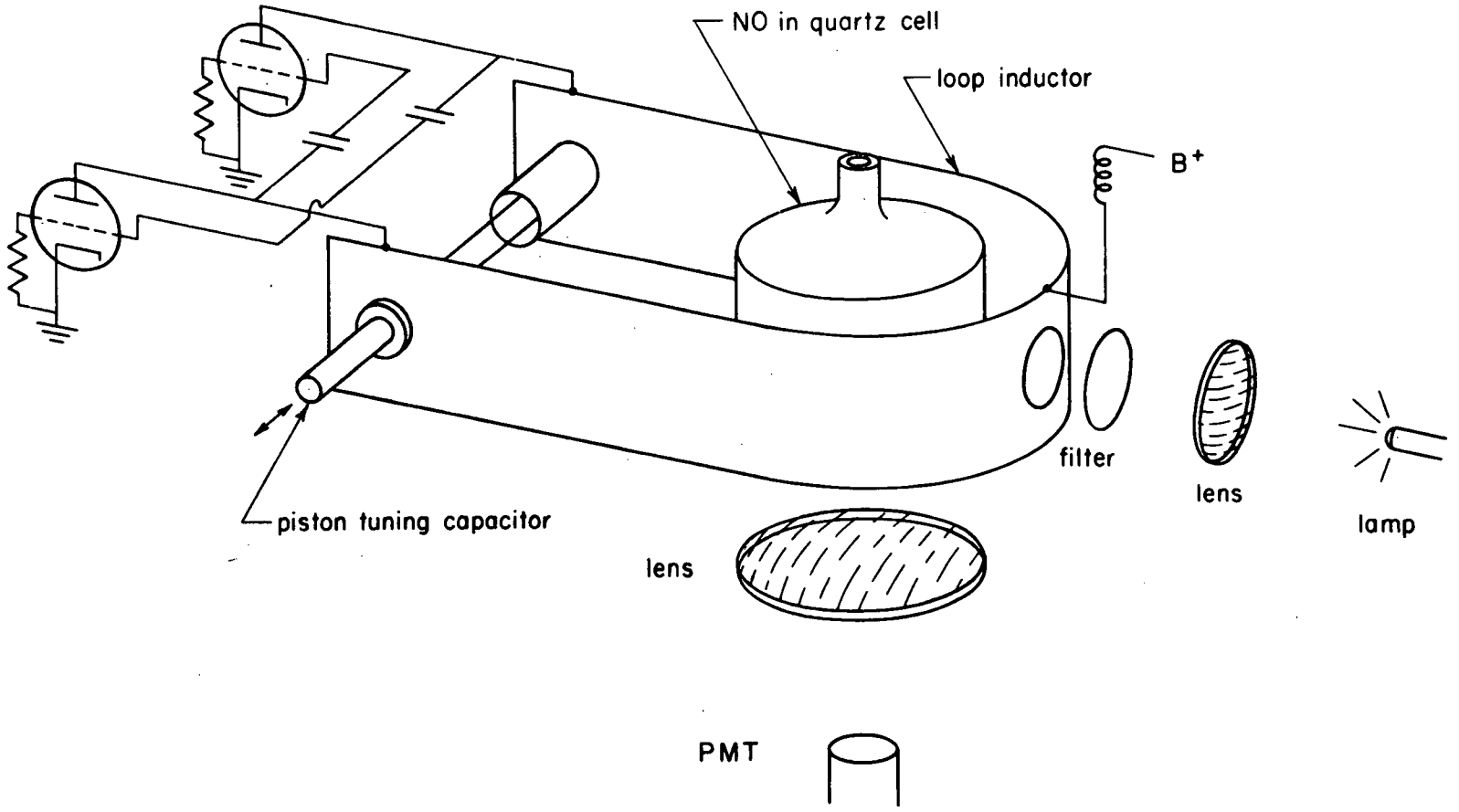

Fig. 18. Schematic diagram of the oscillator used along with the optical elements for double-resonance zero-field radio-frequency sweeps. For simplicity, the vacuum tubes are shown as triodes; actually a 5894 dual tetrode, 4X150A ceramic tetrodes, and 3CX100A5 planar triodes have been used. For frequencies below 175 MHz, the loop inductor is lengthened beyond the ~4-in length shown.

sufficiently selective to be useful.

In order to measure the hyperfine structure intervals, particularly for $N > 1$, it is best to take advantage of the $2F+1$ -fold degeneracy at zero field. The effect we hope to observe is a slight modification of previous level-crossing and double-resonance techniques. We will utilize those same terms in the excited-state density matrix which are responsible for the Hanle effect (in which the application of a dc magnetic field removes the coherence present within each hyperfine level at zero field and produces a change in the angular distribution of fluorescent light). A radio-frequency field in resonance across the interval between two hyperfine states will also, we predict, reduce the coherence terms in both states. For a 2-G rf field, we calculate a change on resonance of the unpolarized fluorescence perpendicular to the exciting light of 1.3% for the $F = 10.5$ to 9.5 transition at 110 MHz for $N = 10$. In our experimental setup, we detect more than 10^6-photons/sec fluorescence from $N = 10$ when excited by the tellurium 2147.5-Å line.

The use of radio-frequency scans is quite straightforward for KHz linewidths at low power, as in molecular beam-resonance experiments, but we are unaware of the use of this technique for MHz linewidths with the field strength and frequency range required here. In the rf oscillators we have developed to date (see Fig. 18), the fluorescence cell is placed in a plate-tank circuit inductor. The inductor consists of a single wide copper loop designed to minimize the rf electric field responsible for discharge breakdown of the NO-gas sample. The parallel capacitance is varied by a single adjustment, as would not be possible in the more usual oscillator-amplifier-tuned circuit. This single adjustment is actuated by a micrometer screw, which in turn is connected to a stepping motor. This arrangement has been chosen so that the rf scan can ultimately be computer controlled, thus permitting repetitive sweeps for the purposes of signal-averaging. With a dual tetrode operated in the push-pull mode, 40-W plate input is sufficient to achieve 2 rf gauss. The

field strength corresponds to the minimum required to induce transitions within the excited-state lifetime. The rf output is flat to ±2 dB over 30 MHz segments of the spectrum. To date this arrangement has performed satisfactorily from 40 MHz, the low end of the expected rf spectrum, to 220 MHz. We have plans to construct an rf oscillator for the 500-800-MHz region provided the problem of electric field breakdown of the gas sample does not limit us too severely.

*This research was also supported by the National Science Foundation under Grant NSF-GP 16029.

(1) R. A. Frosch and H. M. Foley, Phys. Rev. 88, 1337 (1952).

(2) The Te and Se coincidences have been discovered by L. Melton, Department of Chemistry, Harvard University.

III. RESONANCE PHYSICS

A. INTERACTION BETWEEN A NEUTRAL BEAM AND A CONDUCTING SURFACE*

(S. R. Hartmann, P. Kusch, D. Raskin, A. Shih)

We are now completing our study of the interaction between polar molecules and conducting surfaces. This investigation has been made by measuring the deflection of a molecular beam that passes close (~100 - 500 Å) to a cylindrical conducting surface. We have made the following observations:

(a) The dependence of the measured deflections on the radius of the conducting surface was in accord with a $-k/r^{-3}$ potential, where r is the separation between molecule and surface, and k is the interaction constant. This dependence is shown in Fig. 19, where β equals $k/1.4\,\kappa T$, κ is the Boltzmann constant, and T is the evaporation temperature of the beam. Recent physical absorption experiments by Lando and Slutsky[1] indicate a potential of the form $V(r) = -k'r^{-2}$ for a molecule and a metal surface. Our result (see Fig. 20) shows disagreement with the form of that potential.

(b) The interaction constant k mentioned above depends on the material of the surface as well as on the species of molecules. We have used the molecules CsCl and CsF in interactions with stainless steel surfaces and nickel-coated stainless steel cylinders. The results of our research are summarized in Table V.

From the table we may see that the potential derived from the measured beam profile is proportional to μ^2/T, where μ is the permanent electric dipole moment of the molecule.

We are now measuring the interaction of CsF with 10-cm diameter stainless steel surfaces.

*This research was also supported by the Army Research Office (Durham) under Grant DA-ARO-D-31-124-G972.

(1) D. Lando and L. J. Slutsky, J. Chem. Phys. 52, 1510 (1970).

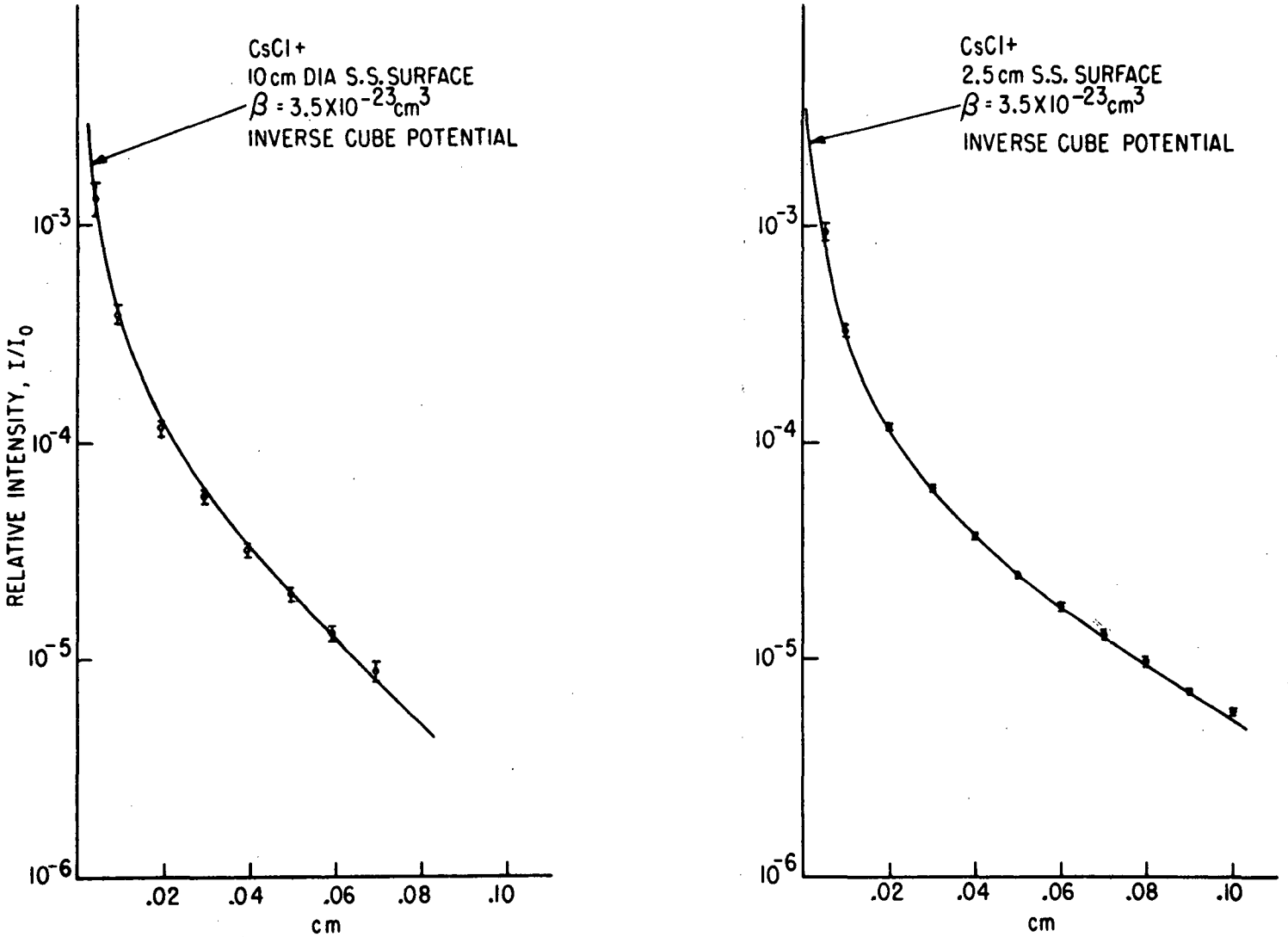

Fig. 19. The theoretical profiles generated by an inverse cube potential for a single β value for surfaces of two different radii are seen to fit the experimental profiles resulting from deflection of CsCl by surfaces of the respective radii.

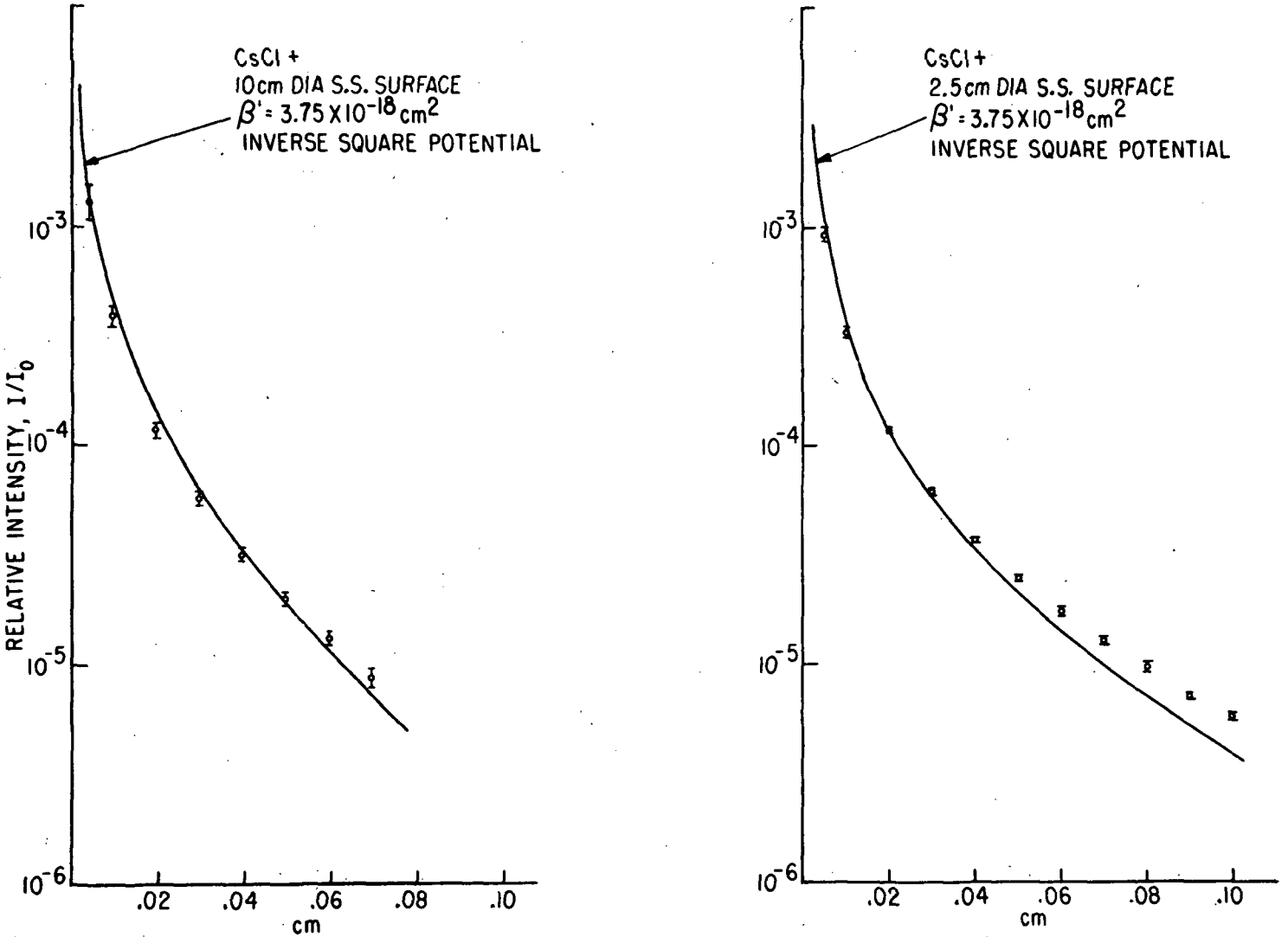

Fig. 20. This shows that theoretical curves generated by an inverse potential of $\beta' = 3.75 \times 10^{-18}$ cm^2 for surfaces of two radii do not fit both experimental profiles of the respective radii. In fact, no such pair with any β' value fit both experimental profiles.

TABLE V. Experimental β Value.

	Stainless Steel[a]	Nickel Surface 1	Nickel Surface 2
CsCl	3.6×10^{-23} ±13%	2.0×10^{-23} ±9%	2.3×10^{-23} ±11%
CsF	1.8×10^{-23} ±12%	1.1×10^{-23} ±9%	1.2×10^{-23} ±17%
$\frac{\beta(CsF)}{\beta(CsCl)}$	0.52	0.56	0.53
$\frac{\frac{\mu^2}{T}(CsF)}{\frac{\mu^2}{T}(CsCl)}$ [b]	0.54	0.54	0.54

(a) All surfaces indicated are 2.5 cm in diameter.

(b) The value for μ is to be found in P. Kusch and V. W. Hughes, Handbuch der Physik XXXVII/1 (1959), p. 47.

B. ADIABATIC DEMAGNETIZATION IN THE ROTATING FRAME*
(S. R. Hartmann, N. Lin)

When the first order spin diffusion is eliminated by the application of intense rf fields at the magic angle, the relaxation of the spin system for the case of $\omega_o\tau_c \gg 1$ with moderately high impurity concentration may be considered to result from the direct interaction between the nuclei and the paramagnetic impurities alone, and a decay described by $\exp[-(t/\tau_1)^{1/2}]$ is observed.[1] As ω_e is reduced, the first order spin diffusion remains zero, but the second order spin diffusion increases. At moderate impurity concentrations with $\omega_o\tau_c \gg 1$, the second order effect cannot be observed experimentally because the spin system will reach thermal equilibrium before the second order spin diffusion has any appreciable chance to cause relaxation. In order to bypass this difficulty, we use CaF_2 doped with impurities with smaller τ_c. For the commercially available CaF_2 doped with trivalent rare earth ions such as Tb^{3+}, Ce^{3+}, and Sm^{3+}, τ_c ranges from 10^{-12} sec to 10^{-14} sec at 77°K. These values of τ_c are quite small, and the resulting T_1 would be too long if the same concentration were used. As the transmitter has the drawback of producing a very long, intense pulse, we must compensate for the weak τ_c by using a higher impurity concentration. With a suitable combination of the effective field, impurity concentration, and τ_c, the relaxation of the spin system will fall in the diffusion-limited region, and the effect of the second order diffusion can be observed easily. An outline for estimating the second order diffusion coefficient is given as follows:

The first order spin-diffusion coefficient resulting from secular dipolar interaction was evaluated using the moment method by Redfield and Yu.[2] For the second order spin-diffusion coefficient, we follow the same line of reasoning. At time $t = 0$, we assume $M_z = M_o + G(0)\cdot\sin kx$. Such a nonuniform magnetization could be produced by adding a nonuniform field to the uniform effective field for $t < 0$ and switching this added field off at $t = 0$. By satisfying the magic angle condition, $3\cos^2\Phi - 1 = 0$,

we can write the Hamiltonian in the tilted rotating frame as

$$\mathcal{H}^* = \hbar\omega_e I_z + \epsilon\cdot\hbar\omega_e \sum_j \sin kx_j \cdot I_{jz} + \frac{1}{8}\sum_{j,k}{}' \gamma^2\hbar^2 r_{j,k}^{-3}$$

$$\times\left[-\frac{3}{2}\sin^2\Phi\ (I_{j+}I_{k+} + I_{j-}I_{k-}) + 3\cos\Phi\cdot\sin\Phi\right.$$

$$\left.\times\ (I_{jz}I_{k+} + I_{jz}I_{k-} + I_{kz}I_{j+} + I_{kz}I_{j-})\right], \qquad (1)$$

where $\epsilon = 0$ holds for $t \geq 0$. Based on the above initial condition of M_z, the magnetization which obeys the diffusion equation leads to $M_z = M_o + G(t)\cdot\sin kx$, where we have

$$G(t) = \frac{\sum_{j,k} \sin kx_j \cdot \sin kx_k \cdot \mathrm{Tr}[I_{jz}\exp(i\mathcal{H}^*t/\hbar)\ I_{kz}\exp(-i\mathcal{H}^*t/\hbar)]}{\sum_j (\sin kx_j)^2 \cdot \mathrm{Tr}(I_{jz})^2}, \qquad (2)$$

and $\mathcal{H}^*$ is Eq. (1) with $\epsilon = 0$.

The nonsecular part in the Hamiltonian $\mathcal{H}^*$ will cause $G(t)$ to have oscillating components at $M\omega_e$. If $G(t)$ is to be the time part of the diffusion equation, it must be a slow function of t. In order to separate out that part of the function that varies slowly with time, $G(t)$ is expanded as

$$G(t) = \sum_{M=0}^{\infty} G_M(t),$$

where the components of $G_M(t)$ oscillate at $M\omega_e$. We use the perturbation method of Lee and Goldburg[3] to perform the above expansion. In this method, one seeks an operator, $\exp(is)$, which transforms the Hamiltonian $\mathcal{H}^*$ into a new effective Hamiltonian

$$\exp(-is)\ \mathcal{H}^*\ \exp(is) = \mathcal{H}_o^* + \mathcal{H}_s^* .$$

The Hermitian operator S must be determined by requiring the condition $[\mathcal{H}_o^*, \mathcal{H}_s^*] = 0$; this results in

$$\mathcal{H}_o^* = \hbar\omega_e I_z$$

and

$$\mathcal{H}_s^* \sim \sum_{n=1}^{\infty} (1/\omega_e)^n .$$

Using the transformed Hamiltonian, we find $G_M(t)$ to have the following form:

$$G_M(t) = E_M(t) \cdot \cos M\omega_e t + O_M(t) \cdot \sin M\omega_e t,$$

where $E_M(t)$ and $O_M(t)$ are even functions and odd functions of time respectively.

The above expansion of $G(t)$ is valid only when ω_e is appreciably greater than $\langle (\Delta\omega)^2_{lab} \rangle^{1/2}$. We find that with the condition $M \neq 0$, $G_M(t)$ is smaller than $G_o(t)$ by a factor of at least $\langle (\Delta\omega)^2_{lab} \rangle / \omega_e^2$. To calculate the lowest order diffusion coefficient, only the dominant term, $G_o(t)$, will be considered. We assume that if the magnetization obeys the diffusion equation, then we have $G_o(t) = \exp(-t/\tau_o)$. Taking into account the non-exponential behavior near $t = 0$,[4] we find the Fourier transform of $G_o(t)$ to be

$$A_o(\omega) = \frac{2\tau_o/\pi}{1 + \omega^2\tau_o^2} \times g(\omega).$$

Using a Gaussian function for $g(\omega)$, we find that the same argument as that used by Redfield in the evaluation of the first order diffusion coefficient leads to

$$D = \frac{M_2}{k^2} \left(\frac{\pi M_2}{2M_4} \right)^{1/2} .$$

To the lowest order for ω_e, $M_2 \sim 1/\omega_e^2$, and $M_4 \sim 1/\omega_e^4$, we have

$$D = R/\omega_e,$$

where R is a complicated constant resulting from the evaluation of the traces for M_2 and M_4.

In the case of the diffusion-limited region, we have $1/T_1 = 4\pi N\beta D$,[5] or $T_1 = (2.8\pi NC^{1/4}R^{3/4})^{-1}(\omega_e)^{3/4}$. By measuring T_1 for different ω_e, we can determine the experimental dependence of the second order diffusion coefficient D on ω_e. Experiments are being carried out to verify the field dependence of the second order diffusion coefficient.

*This research was also supported by the National Science Foundation under Grant NSF-14243.

(1) D. Tse and S. R. Hartmann, Phys. Rev. Letters 21, 511 (1968).

(2) A. G. Redfield and W. N. Yu, Phys. Rev. 169, 443 (1967).

(3) M. Lee and W. I. Goldburg, Phys. Rev. 140, A1261 (1965).

(4) Redfield and Yu, op. cit., p. 443.

(5) P. G. De Gennes, J. Phys. Chem. Solids 3, 345 (1958).

C. PHOTON-ECHO RESONANCE*

(S. Chandra, S. R. Hartmann, P. Hu, R. Leigh, M. Matsuoka)

We are continuing our efforts to see photon echoes in neodymium-doped samples. Our earlier method of using the stimulated Raman scattering of ruby-laser light to obtain pulses at 880 nm proved unsatisfactory because of persistent damage to the ruby laser caused by stimulated Brillouin scattering in the backward direction. As an alternative, we constructed a laser-pumped dye laser. Using a simple cavity with two plane mirrors, we obtained 1-MW, 880-nm pulses having a spectral width of 150 Å. Such a laser should pump 2×10^{13} Nd^{3+} atoms of a 0.15% Nd-doped glass sample into the $^4F_{3/2}$ state, so that photon-echo experiments at the 1060-nm transition ($^4F_{3/2} - {}^4I_{11/2}$) would be possible.

However, for photon-echo experiments at 880 nm ($^4I_{9/2} - {}^4F_{3/2}$) we replaced the output mirror of the dye laser by a grating to achieve a linewidth of 6Å at 500-kW power. The linewidth narrowing is important because the contribution to the echo intensity from each mode is proportional to the cube of the power per mode. We expect to get 10^6 photons in the echo.

We studied fluorescence excited in a 5% Nd_2O_3 -doped glass sample by a 250-kW dye laser at various sample temperatures between the room temperature and 6°K. From the amount of 1.06-μ fluorescence incident on the photomultiplier tube, we estimated that nearly 10^{14} atoms were excited by the laser. This was roughly in agreement with the theoretically calculated value. We made two attempts to look for the echo. We were unsuccessful in detecting the photon-echo signal because of the saturation, caused by the scattered laser light, of the photomultiplier tube of the detection system. We noticed that the electro-optic shutter that we had built using a Pockels cell, although effective against a well-collimated beam, performed poorly against scattered light. We plan to improve the shutter by replacing the Pockels cell by a Kerr cell that we have recently constructed. We further realized that 5% Nd_2O_3 doping is too high for photon-echo experiments because of electron spin-spin interactions between neighboring Nd^{3+} atoms. The experience with photon echoes in ruby suggests that we should keep the concentration down to about 0.15%. We plan to run the experiment with 880-nm echoes in the diluted concentration soon.

Concurrently, we are also preparing the first version of the experiment to see 1060-nm echoes in Nd^{3+} in glass by using pulses from a neodymium laser to excite the echo after the Nd^{3+} atoms are pumped into the $^4F_{3/2}$ state by the dye laser. We estimate that there will be 2×10^6 photons in the echo.

Experiments with photon echoes in ruby have largely centered around gaining an understanding of the marked dips in echo amplitude at applied magnetic fields of 2 and 4 kG. The quartet ground state of Cr^{+++} in ruby ($^4A_2$) has a level crossing

between the +3/2 and the -1/2 states at 2 kG and one between the +3/2 and the +1/2 at 4 kG. Our experiments have used σ^+ light to excite the $^4A_2(-1/2) \rightarrow \bar{E}(^2E)(-1/2)$ transition, or σ^- light to excite the $^4A_2(+1/2) \rightarrow \bar{E}(^2E)(+1/2)$ transition, and we have examined and compared the behavior of the echo at the level crossings.

The dip at 2 kG, which is present in both transitions, has a width of about 15 G (approximately the EPR linewidth). In this region, the echo amplitude is reduced by a factor between 1.5 and 10. The depth of the dip depends on the time interval between the excitation pulses in both cases. For the σ^- transition, this depth seems to be a simple exponential in time, while for the σ^+ transition, where the ground-state sublevel is actually involved in the level crossing, the behavior is more erratic. These dips have been observed in both 0.05% and 0.005% by weight Cr ruby and are deeper in the more concentrated sample. In an attempt to ascertain their behavior in a very dilute sample, we have observed photon echoes in "sapphire," which we estimate has a Cr concentration on the order of 10^{-6}% by weight, but the echoes were too small for detailed study.

We are currently working out theories to explain the behavior of the echoes at 2 kG. We believe the dip for the σ^- transition to result largely from mutual spin flip between pairs of neighboring Cr^{+++} ions in the ground state, for which more channels are open at the level crossing. The σ^+ transition, which is much more erratic, probably arises in part from the modulating effect of the neighboring Al nuclear spins,[1] although spin flip must also influence this transition.

At 4 kG, there is a large dip in the amplitude of the echo for the σ^- transition, but none for that of the σ^+ light. The dip is about 500 G in width, with the amplitude falling off by at least a factor of 10^4. Since at the 4-kG level crossing there is the possibility of both enhanced Al interactions and enhanced spin flip for the σ^- transition, and of neither for the σ^+, we have clear qualitative agreement with our theories but

have as yet been unable to determine the relative importance of the two effects.

We have also observed modulation of the echo amplitude but do not yet have enough data to compare our results with theory.[2]

Program for the next interval: We intend to refine our data and theories for the 2- and 4-kG dips, and we hope to bring the two into agreement, thereby arriving at a much better understanding of relaxation mechanisms in the ground state of ruby. We will also study in more detail the gross magnetic field and time dependence of the echoes, attempting to relate these results to theory.[3]

*This research was also supported by the Army Research Office under Contract DA-31-124-ARO-D-341.

(1) D. Grischkowsky and S. R. Hartmann, Phys. Rev. Letters 20, 43 (1968).

(2) D. Grischkowsky and S. R. Hartmann, Phys. Rev. 2, 60 (1970).

(3) Ibid.

D. ECHO BEHAVIOR IN RUBY*

(S. R. Hartmann, P. Liao)

A microwave spectrometer that operates in the frequency range of 16.0 to 16.5 GHz has been constructed and tested. This spectrometer, which has pulse and c. w. capabilities, will be needed to observe electron-spin echoes in the $\overline{E}(^2E)$ excited state of ruby.[1]

We have been able to extend the range of pulse separations for which electron-spin echoes at 9.31 GHz in the $^4A_2$ ground state of ruby can be observed. These echoes involve the +1/2 and -1/2 Zeeman levels in a magnetic field of approximately 3.3 kG. The range was increased from 0.8 - 2.5 μsec to 0.8 - 7.0 μsec. Because the echo amplitude decays as the time separation between the exciting microwave pulses is increased, the observa-

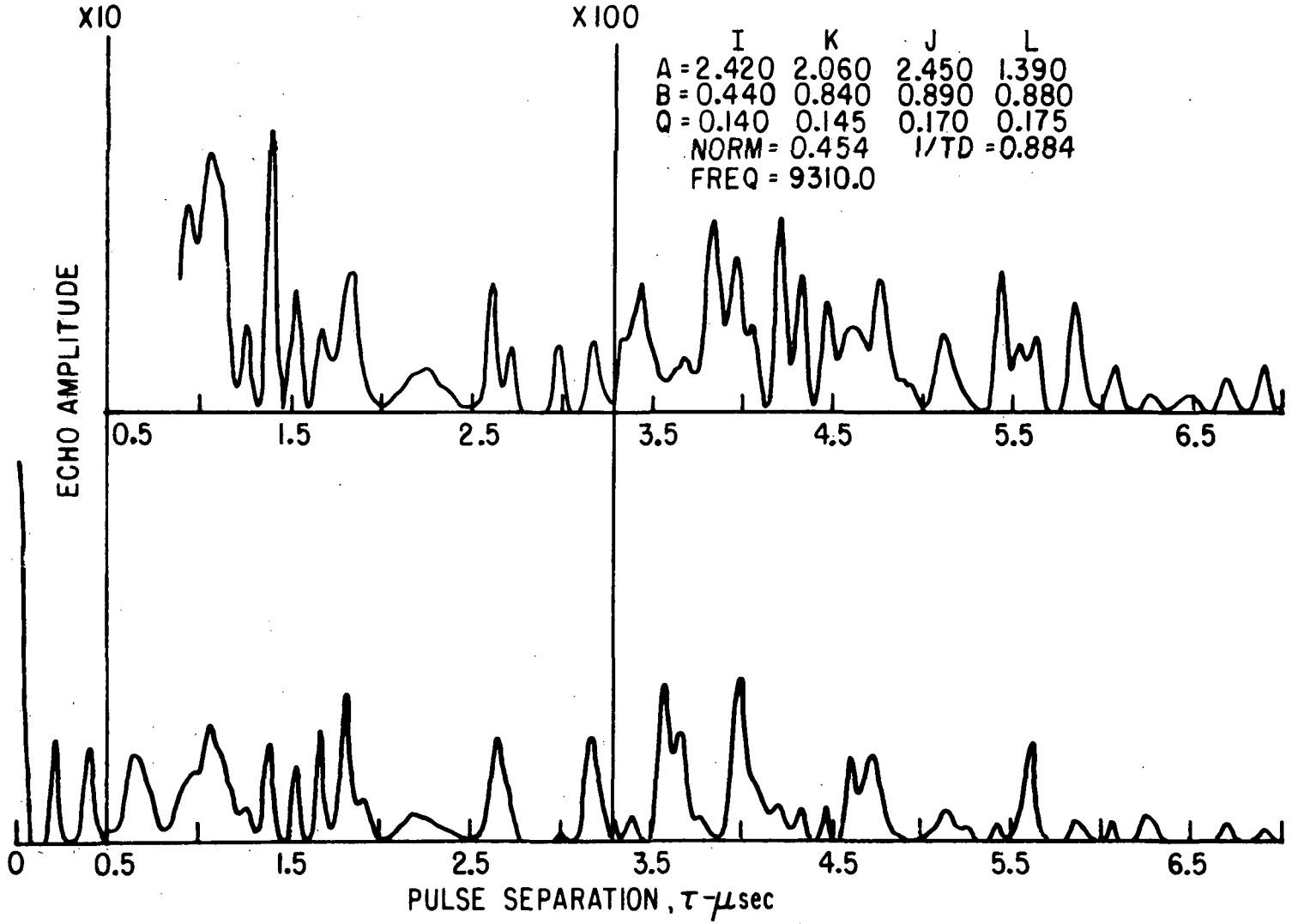

Fig. 21. Experimental and theoretical spin-echo amplitude versus pulse separation at 9.31 GHz with hyperfine parameters as determined by an ENDOR experiment.

tion of echoes for the longer pulse separations was achieved by signal averaging. Both signal averaging and data taking were accomplished with a 10-channel analyzer,[2] which was interfaced into a PDP-8 computer. The time separation between the microwave pulses was generated by an electronic oscillator whose frequency (and hence the separation) was measured by a frequency counter. This counter was also interfaced into the computer. The echoes were measured at the temperatures of liquid helium and with microwave pulselengths of approximately 30 nsec. The optic axis of the ruby crystal was aligned parallel to a dc magnetic field, and the Cr_2O_3 concentration was 0.005% by weight. The results are shown by the upper curve plotted in Fig. 21.

Using the following spin Hamiltonian the spin-echo amplitude can be calculated as a function of pulse separation:[3]

$$\mathcal{H} = g\mu_\beta H S_z + D\left[S_3^2 - \tfrac{1}{3}S(S+1)\right]$$

$$+ \sum_j \left\{-h8HI_{z_j} + Q_j\left[I_{z_j}^2 - \tfrac{1}{3}I(I+1)\right] + S_z(A_jI_{z_j} + B_jI_{T_j})\right\},$$

where A_j, B_j, and Q_j are the hyperfine interaction constants of neighboring aluminum nuclei. In our calculation we have included only the 13 nearest neighbors. When the magnetic field is applied to the optic axis, these 13 can be divided into four sets of three equivalent nuclei and one that has no effect on the echo.

We made a least-squares fit to the electron-spin-echo data at 9.31 GHz, in which the nearest-neighbor aluminum hyperfine-interaction constants were treated as adjustable parameters. This fit provides a redetermination of these parameters, which were originally determined in an ENDOR experiment.[4] The lower curve in Fig. 21 is a plot of the theoretical spin-echo amplitude versus pulse separation τ, for which the values of the hyperfine parameters were taken to have these original ENDOR values. An additional simple exponential decay was given to the theoretical spin-echo amplitude to approximate the effect of dephasing inter-

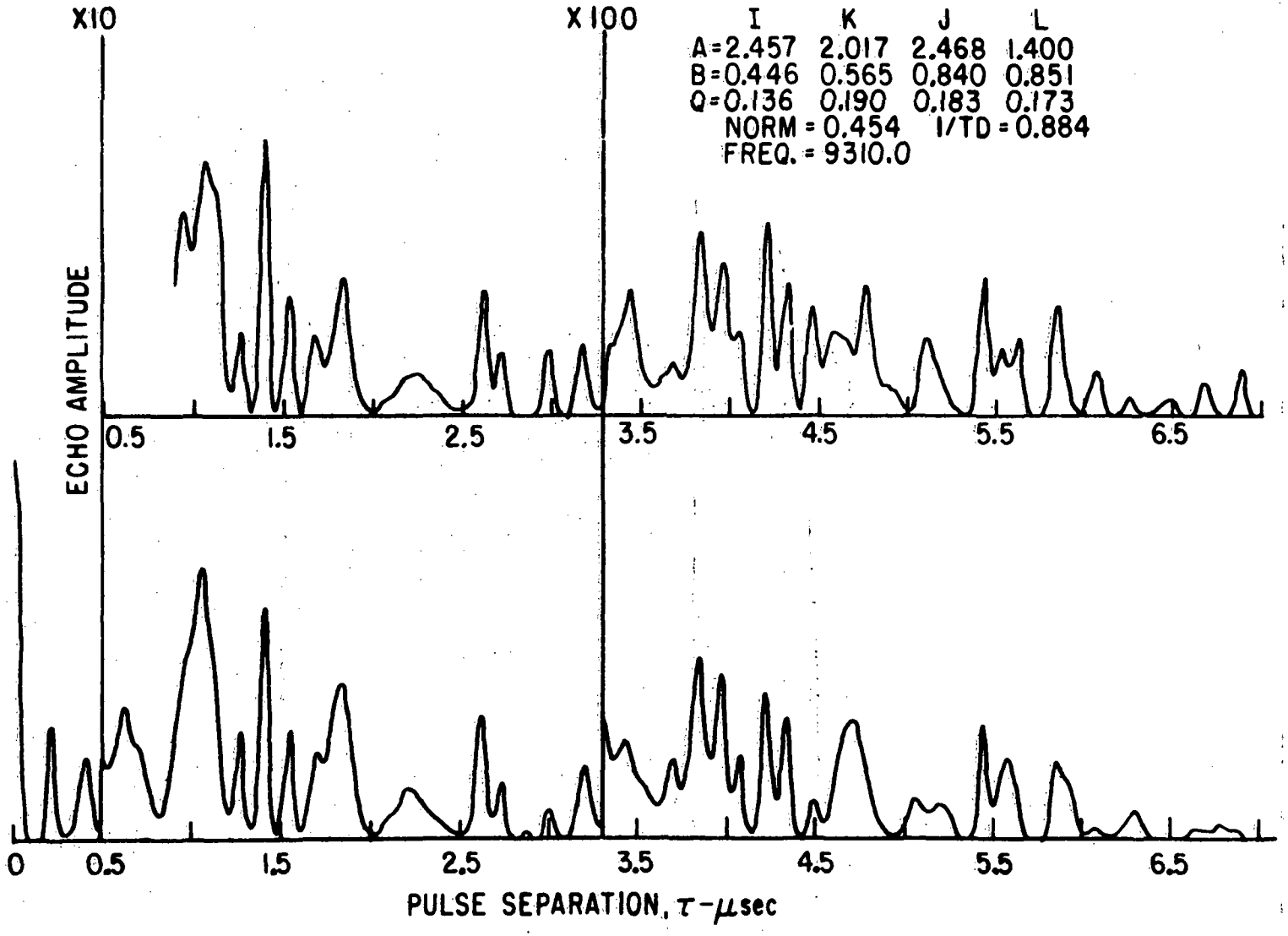

Fig. 22. Experimental and theoretical spin-echo amplitude versus pulse separation at 9.31 GHz with hyperfine parameters determined by a least-squares fit to the experimental spin-echo data.

actions that are not included in the theory. The fit to experimental data is reasonably accurate to about 3.0 μsec, after which it is poor. Figure 22 again shows the experimental data (upper curve), but the theoretical curve is now made with the least-squares adjusted parameters. Here the fit is improved in such a way that it is as good to 6.0 μsec as the original was to 3.0 μsec.

In an effort to confirm the redetermination of hyperfine parameters, we used the new spectrometer to observe electron-spin echoes at 16.24 GHz, where the modulation pattern is entirely changed. The experimental results are shown as the upper curve in Figs. 23 and 24. The lower curve of Fig. 23 is the theoretical curve determined using the original ENDOR values, while Fig. 24 uses the parameters determined by the least-squares fit to the 9.31 GHz data. Note that in a sense no adjustable parameters are used in this curve. The redetermined parameters are seen to considerably improve the fit, thereby confirming these least-squares parameters.

The parameters of the least-squares fit differ in most cases by a few percent from the original and can be considered in essential agreement with the ENDOR results. However, when the parameters of the least-squares fit are used to predict the positions at which ENDOR lines should have been observed, they do not agree exactly with the published experimental data. The discrepancy is larger than the experimental accuracy of the ENDOR experiment and is very puzzling in the light of the spin-echo experiment at 16.24 GHz. This disagreement may result from limitations in the theory of spin echoes. The theory does not take into account the finite pulsewidths of the exciting microwave pulses and assumes the entire line to be excited. Only the nearest 13 neighbors are included in the predictions, and no interactions between neighbors are used in the theory. Furthermore, the assumption of the existence of exponential decay may not be correct. An experimental limitation arises from the inability to align the crystal optic axis exactly parallel to

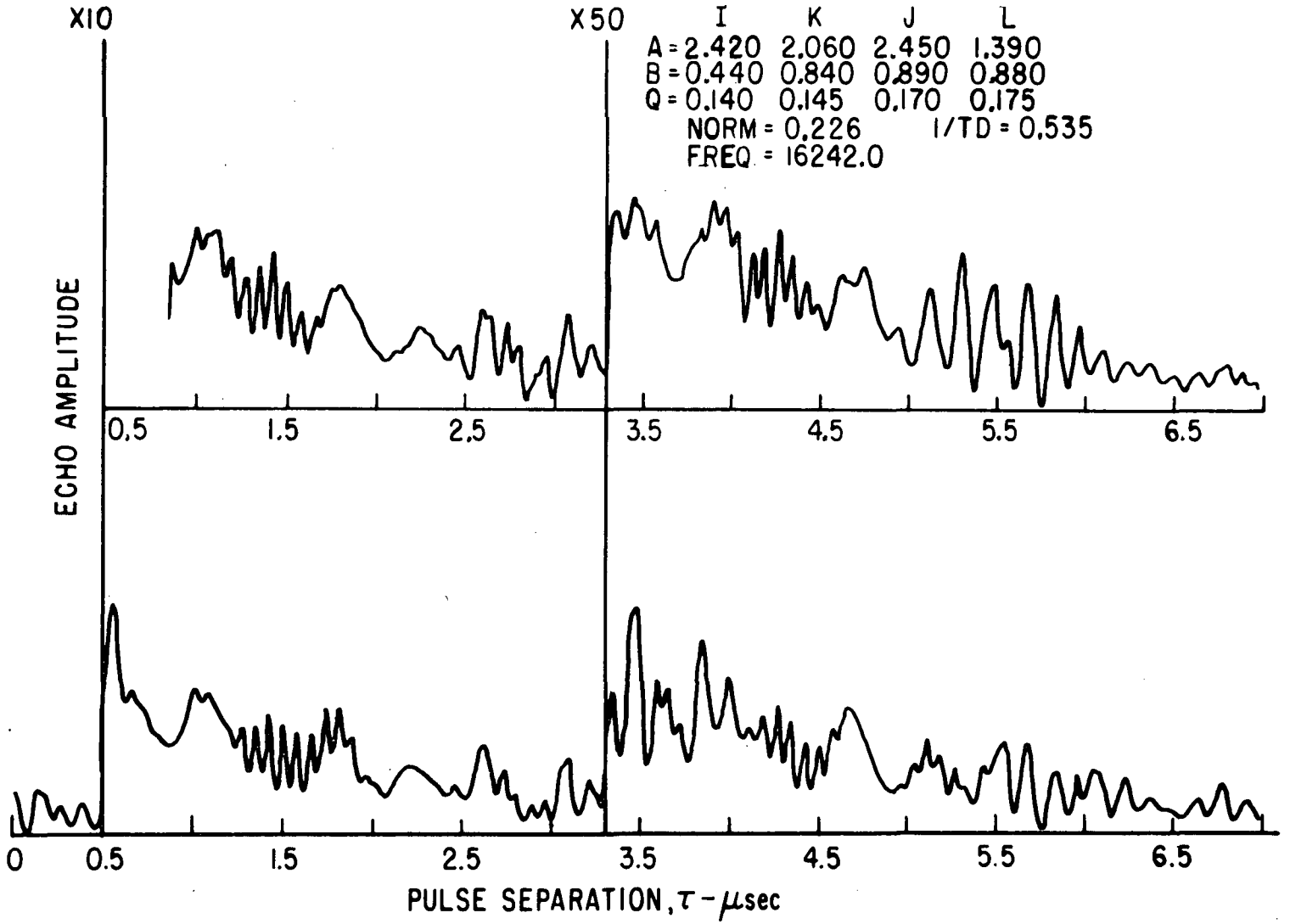

Fig. 23. Experimental and theoretical spin-echo amplitude versus pulse separation at 16.242 GHz with hyperfine parameters as determined by an ENDOR experiment.

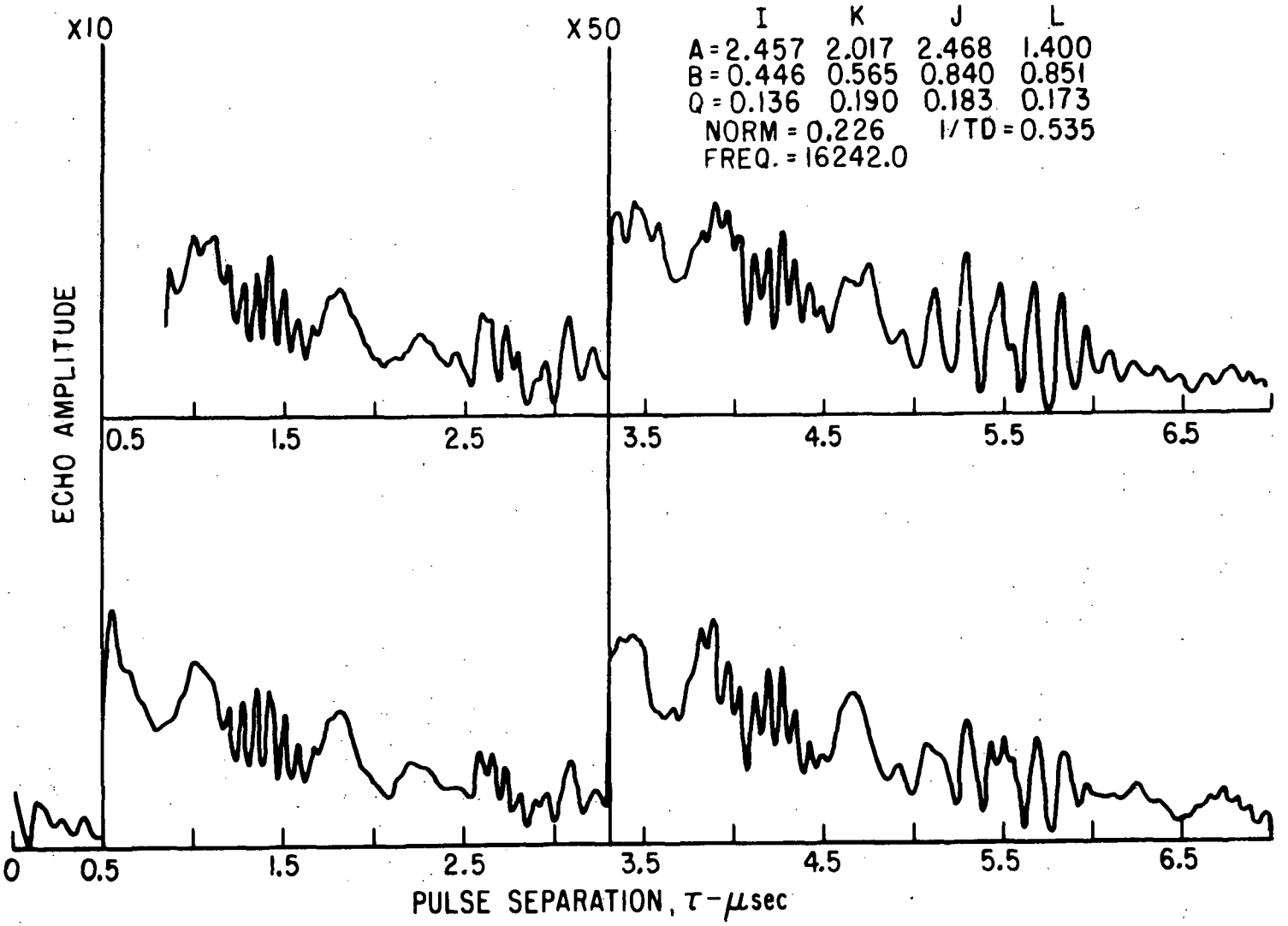

Fig. 24. Experimental and theoretical spin-echo amplitude versus pulse separation at 16.242 GHz with hyperfine parameters determined by a least-squares fit to 9.31-GHz spin-echo data.

the magnetic field. This misalignment can change the modulation pattern. All the above limitations can restrict the usefulness of the least-squares determination.

Program for the next interval: We will attempt to detect spin echoes in the excited state of ruby.

*This research was also supported by the Army Research Office under Contract DA-31-124-ARO-D-341.

(1) CRL Progress Report, June 30, 1970, p. 58.

(2) Ibid., p. 58.

(3) D. Grischkowsky and S. R. Hartmann, Phys. Rev. B 2, 60 (1970).

(4) N. Laurance, E. C. McIrvine, and J. Lambe, J. Phys. Chem. Solids 23, 515 (1962).

E. RAMAN ECHOES*

(A. Flusberg, S. R. Hartmann, L. A. Levin, R. A. Weingarten)

The investigation of stimulated Raman scattering in atomic thallium vapor has now produced a number of interesting results. From classical Raman-scattering theory we can find the dependence of the Stokes polarization on the incident laser polarization. We have found that for forward scattering, the Raman-scattering cross section for a transition from a $J = 1/2$ to $J = 3/2$ state in a spherically symmetric system such as an atom can be written as

$$\sigma_R = k_1(1 - \cos\Phi \cos\theta_L \cos\theta_S + \sin\theta_L \sin\theta_S)$$

$$+ k_2(7 + \cos\Phi \cos\theta_L' \cos\theta_S - 5 \sin\theta_L \sin\theta_S), \quad (1)$$

where $|\tan\theta/2|$ is the ratio of minor to major axes of the ellipse traced out by the polarization vector, and θ is positive for right elliptical polarization and negative for left elliptical polarization. (The subscripts L and S denote laser and Stokes, respectively.) The terms k_1 and k_2 are constants which depend on the scattering-system parameters and the laser and Stokes

frequencies. The angle between the major axes of the ellipses associated with θ_L and θ_S is $\Phi/2$.

The dependence of the Stokes polarization on the incident laser polarization can be deduced from Eq. (1). The Stokes polarization with the largest gain is given by

$$(\theta_S)_{max} = \tan^{-1}\left(\frac{k_1 - 5k_2}{k_2 - k_1} \tan \theta_L\right) . \qquad (2)$$

We have calculated the cross section for excitation of atomic thallium at various wavelengths by using the experimentally-determined energy levels[1] and transition probabilities[2] as parameters to determine k_1 and k_2.

We have investigated the polarization of the Stokes light at 1.513 μ in thallium excited by a ruby laser at 6943 Å. Preliminary results, using the calculated values of k_1 and k_2, are in agreement with Eq. (2). Experiments are now underway to measure the stimulated Raman-scattering gain and, from it, to deduce the spontaneous Raman-scattering cross section as a check of Eq. (1).

An interesting effect has been observed to accompany stimulated Raman-scattering in high pressure (tens of torr) thallium vapor. The ruby-laser beam, which has an apparent uniformly intense profile before entering the thallium cell, becomes concentrated into sharp spots during its passage through the thallium vapor. This implies that some form of self-focusing takes place in the cell. Since self-focusing and intense Raman-scattering only appear together, we believe the self-focusing is caused by the excitation of the thallium atoms from the ground $^2P_{1/2}$ state to the excited $^2P_{3/2}$ state. This excitation occurs during Raman scattering. A calculation of the index of refraction in thallium vapor at 6943 Å shows that creation of a population in the excited $^2P_{3/2}$ state increases the index of refraction and leads to focusing. A similar effect has been observed in cesium vapor.[3]

While self-focusing is an interesting effect, the subsequent defocusing reduces the laser intensity in the second oven. Continued efforts to detect Raman echoes in this oven have thus far been unsuccessful despite continued improvement of the apparatus. In particular, the interrogation dye laser is now tunable in the region of the $^2P_{3/2} \rightarrow {}^2S_{1/2}$ resonance in thallium at 5350 Å, if we use brillant sulphaflavine as the lasing dye and cyclooctatetraene to quench triplets and lengthen the lasing pulse. Future progress appears to depend on increasing the laser and Stokes intensities in the second oven.

Program for the next interval: We shall complete the study of the dependence of the Stokes polarization on the incident laser polarization and continue to study the dependence of the gain on thallium pressure, cell length, and self-focusing. In an effort to detect Raman echoes we will make an attempt to improve the homogeneity and increase the intensity of the laser and Stokes pulses entering the second, or echo, oven.

*This research was also supported by the Army Research Office under Contract DA-31-124-ARO-D-341.

(1) C. Moore, Atomic Energy Levels (Circular NBS 467, Washington, D. C., 1952), Vol. III.

(2) A. Gallagher and A. Lurio, Phys. Rev. 136, A87 (1964).

(3) P. P. Sorokin and J. R. Lankard, IBM Technical Report, RC 3111 (1971).

F. COHERENT EFFECTS IN TWO-PHOTON ABSORPTION*

(Z. Friedlander, S. R. Hartmann, M. Matsuoka)

Experiments on the coherent excitation of Cs atoms by two-photon absorption are proceeding. Theoretical considerations revealed that a new two-photon superradiance should be observed in this experiment. This phenomenon is essentially a two-photon version of Dicke's (one-photon) superradiance. It is, however, an interesting new problem; a new theoretical formalism is required to express the superradiant state, and experimentally

the superradiance may be observed by using fluorescence at a wavelength different from that of the excitation.

The two-photon superradiance should be observed in Cs atoms as an emission of two photons at two wavelengths of the cascading single photon fluorescence; for example, ($9D_J \rightarrow 6P_{J'} \rightarrow 6S_{1/2}$ or $9D_J \rightarrow 7P_{J'} \rightarrow 6S_{1/2}$) but in a shorter decay time and into a smaller solid angle. The decay time is determined by the number of atoms excited, the two-photon absorption linewidth, and the excitation pulsewidth. The solid angle into which the superradiant fluorescence is emitted should be of the same order of magnitude as that into which the excitation laser pulse propagates.

We have observed fluorescence from cesium gas excited by a two-photon absorption. We have constructed a Q-switched, temperature-tuned ruby laser for which a vacuum of 10^{-7} torr is obtained in the cryostat. The ruby can be heated to temperatures above 77°K by means we have described previously.[1] The heat is regulated by a temperature control that can maintain a set temperature in the range 80°K - 193°K with an accuracy of ±0.5°K. This corresponds to a variation of the laser-output wavelength from 6934 Å to 6938 Å. The laser is fired automatically every two minutes, an interval that we have found sufficient to allow the laser to cool to its original temperature after each firing.

We first used passive Q-switching with cryptocyanine dye; however, this proved unsatisfactory because delicate adjustment of the dye concentration was necessary whenever we changed the temperature. The pumping level necessary to break down the dye also caused lasing off the front surface of the rod when the antireflection coating deteriorated. We then substituted Pockels-cell Q-switching and obtained pulses with a peak greater than 2 MW and a 15-nsec width. Fabry-Perot pictures indicate that lasing occurs in only 2 to 3 modes.

The laser-output wavelength was carefully calibrated against temperature. We successfully observed the 5846.68-Å, $9D_{5/2} \rightarrow 6P_{3/2}$ fluorescent decay following absorption of two 6935.76-Å photons in the transition $6S_{1/2} \rightarrow 9D_{5/2}$. The number

of fluorescent photons was 5×10^{10}, and the pulse was about 20-30 nsec wide. The fluorescence disappears when the laser is tuned 0.8°K above or below the optimum temperature.

We will observe the $9D_{5/2} \rightarrow 6P_{3/2}$ and $6P_{3/2} \rightarrow 6S_{1/2}$ decays simultaneously and expect to find the same number of photons in both, with the decay rates being shorter than those of incoherently excited states. The $9D_{5/2} \rightarrow 7P_{3/2}$ and $7P_{3/2} \rightarrow 6S_{1/2}$ fluorescences will be observed in the same manner. We plan to measure the dependence of the fluorescent intensity and decay time on the intensity of the laser and on the density of the cesium. In the experiments described above, the cesium was maintained at a pressure of 0.1 torr, corresponding to a density of 2.21×10^{15} atoms/cm^3. The mean time between collisions is 1.27×10^{-6} sec, about two orders of magnitude longer than our expected radiative lifetimes.

Shot-to-shot fluctuations of as much as 20% occurred in the laser intensity. This suggests that a good way to measure the fluorescent intensity as a function of cesium density is to use two ovens in which the cesium is maintained at two different densities. If we then split the laser beam and send a known fraction into each oven they will both be equally affected every time by any changes in the incoming laser pulse.

Program for the next interval: We will attempt simultaneous observation of the $9D_{5/2} \rightarrow 6P_{3/2}$ and $6P_{3/2} \rightarrow 6S_{1/2}$ as well as the $9D_{5/2} \rightarrow 7P_{3/2}$ and $7P_{3/2} \rightarrow 6S_{1/2}$ decays. We will investigate the dependence of the fluorescent intensity on incident laser power, cesium density, and direction of observation.

*This research was also supported by the Army Research Office under Contract DA-31-124-ARO-D-341.

(1) CRL Progress Report, June 30, 1970, p. 62.

G. FREQUENCY SHIFTS IN RESONANT SYSTEMS*

(R. Friedberg, M. Friedlander, S. R. Hartmann, J. T. Manassah)

We have calculated the frequency shift due to resonant interaction between identical radiating atoms and have shown that in some cases the shift exceeds 1/10 of the pressure-broadened

width.

Let us consider the spontaneous radiation from a system of identical two-level atoms. We assume that J = (0,1) for the (lower, upper) level and that retardation within each atom may be neglected. We write p for the magnitude of the dipole-transition matrix element.

The potential between an excited- and a ground-state atom will consist of a transverse and a longitudinal part, the sum of which will be the Lienard-Wiechert dipole-dipole potential V_{12}.

The radiation from two stationary atoms will be shifted in frequency by the difference in $\mathrm{Re}V_{12}/\hbar$ between initial and final states.[1] To lowest order in density,[2] the same should be true for N stationary atoms with V_{12} replaced by

$$\sum_{i<j} V_{ij}.$$

The "density expansion" should work well on the wings of the line.[3]

A state with (N/2 + m) excited atoms of polarization $\hat{\epsilon}$ may be described by Dicke's quantum numbers[4] m and $r_{\vec{K}}$. Averaging over all initial states of given $r_{\vec{K}}$ and m, we find the frequency shift in spontaneous emission as

$$\overline{\Delta\Omega}_{r_{\vec{K}},m \to m-1} = -(2m-1)(p^2/\hbar)\,\mathrm{Re}\,\overline{W_{ij}\cos\vec{k}\cdot r_{ij}}^{\,i\neq j}, \qquad (1)$$

where $W_{ij} = V_{ij}$ with the dipole moments replaced by $\hat{\epsilon}$.

For a small spherical sample of uniform density we find

$$\Delta\Omega_{r_{\vec{K}},m \to m-1} \simeq +\left(\frac{4}{5}k_o^2 + \frac{2}{25}k^2\right)(2m-1)(p^2/\hbar R), \qquad (2)$$

which was obtained qualitatively and approximately by Fain.[5]

Since in an incoherently excited system with an arbitrary direction $\hat{n}$, all states with the same $r_{\vec{K}}$ ($\vec{k} = k_o\hat{n}$) and m are equally probable and all such states radiate with equal strength into the $\vec{k}$ mode, Eq. (1) gives the "center of gravity" frequency

shift for radiation into the $\vec{k}$ mode from initial states of given $r_{\vec{k}}$ and m. Since Eq. (1) is independent of $r_{\vec{k}}$, if the initial m is known, Eq. (1) gives the "c. of g." shift for all the radiation in any direction.

For a slab of thickness L and uniform density, with essentially infinite lateral extent and faces perpendicular to $\vec{k}$, we obtain for $|k_o-k|L \ll 1$,

$$\overline{W_{ij} \cos \vec{k}\cdot\vec{r}_{ij}}^{\,i\neq j} = (n/N)(A - iB),$$

where n = density of atoms;

$$A = -\frac{4}{3}\pi + \frac{\pi k_o}{3}(k_o-k)L^2 + \frac{2\pi k_o}{k_o+k}\left[1 - \frac{\sin (k_o+k)L}{(k_o+k)L}\right]; \text{ and} \quad (3)$$

$$B = \pi k_o L + \frac{2\pi k_o}{(k_o+k)^2 L}\left[1 - \cos (k_o+k)L\right]. \quad (4)$$

Within the regime $|k_o-k|L \ll 1$, the second term of Eq. (3) can still be very large. However, this formula was obtained by perturbation theory, whereas a correct analysis, as stressed by Stephen and others,[6,7,8,9] should follow the time development of the system. The dipole moment of a coherently excited system will begin to vibrate at a frequency shifted according to Eq. (1), but in a time inverse to this shift, the phase relations between atoms may be altered by position-dependent fields that invalidate Eq. (1).

For an incoherently excited system, normal relaxation processes will restore the completely incoherent ensemble faster than it is distorted by radiation into modes other than $\vec{k}$.

We conclude that radiation normal to the faces of an incoherently excited slab will be shifted in frequency by $-(2m-1)N^{-1}(np^2/\hbar)\, A_{res}$ if only a small fraction of the atoms are excited, where A_{res} is given by Eq. (3) with $k = k_o$.

To test the validity of Eq. (1) for coherent excitation, two of the authors[10] solved Maxwell's equations for a slab

after excitation by a δ-function pulse with normal incidence. The frequency shift was found to be $(-\pi/3)np^2/\hbar$ for $kL \gg 1$, and $(-4/3)\pi np^2/\hbar$ for $kL \ll 1$, which is in agreement with Eq. (3) with $k = k_o$. It is worth emphasizing that this "superradiant" shift is just equal to the "incoherent" shift discussed above.

For a gas, we find that for density $\ll$ (Weisskopf radius)$^{-3}$ and Doppler width smaller than collision width, our results should be augmented by the shift computed by the impact approximation with the static potential, taking into account the change of polarization of the excited atom. This gives the term

$$\Delta\Omega_{coll} = (0.221 \pm 0.001)\,\pi np^2/\hbar,$$

which agrees with the value of Δ_g given by Berman and Lamb.[11]

The total shift of a thick slab of gas, weakly and incoherently excited, is

$$\Delta\Omega = -0.11\ \pi np^2/\hbar = -0.026\ \Gamma_f.$$

Notice that $\Delta\Omega$ and $\Delta\Omega_{coll}$ are of opposite sign. For a thin slab the shift is about ten times as great.

Our method of approximation also gives the collision width as

$$\Gamma_{coll} = (1.1488 \pm 0.0001)\ \Gamma_F,$$

where $\Gamma_F = (4/3)\pi^2 np^2/\hbar$ is the width calculated[12] by neglecting changes of polarization. This result also agrees with previous calculations[13] and with experimental results on helium.[14]

Green's function analysis[15] indicates that all our formulas should apply as well to absorption. The shifts calculated here will appear only in the principal line and not, for example, in the indirect transitions measured by Kuhn et al.[16]

An experiment is being planned to measure the predicted shift in the resonance-transition frequency of atomic gases in the thick sample case. We will study the resonance transitions of cesium vapor in absorption at 8521 Å and 8944 Å. The minimum

usable density of cesium is determined by the requirement that we must be able to resolve the shift at that density using available spectrometers. A density of 2×10^{16} atoms/cm^3, which produces a shift of 0.002 Å, meets this requirement. However, at this density the resonance line becomes artificially broadened. In a cell that is 10 wavelengths long, the 8521-Å line of cesium at this density has a full width at half maximum of 0.6 Å. It therefore becomes advantageous to use as short a cell as possible. For this purpose we are constructing a variable pathlength microcell to contain the cesium vapor. The cell will be adjustable from about 10 to 1000 μ, the lower limit being determined by the flatness of the windows used. The cell is thermally compensated, so that a spacing set at room temperature will be maintained at 200 - 300°C, the working temperature of the cell. Moreover, the thermal compensation will prevent temperature fluctuations from affecting cell length during the experiment. Despite the compensation, fine adjustment of cell length and adjustment of cell parallelism can be accomplished while the cell is hot. Cell length will be determined by observing the spacing of the fringes produced by white light passed through the cell and detected by a scanning grating spectrometer with a photomultiplier tube.

In order to obtain the needed resolution, which will be on the order of 10^7, we will use two Fabry-Perot interferometers with plate finesses in the vicinity of 130 and a grating spectrometer in series.[17] The first Fabry-Perot interferometer will provide the needed resolution, whereas the second interferometer and the grating spectrometer will extend the very limited free-spectral range of the first interferometer, thereby preventing overlap of the adjacent orders of interference.

Two piezoelectrically-scanned Fabry-Perot interferometers of exceptional thermal and mechanical stability have been ordered. The interferometer will be constructed entirely of invar, a variant on the standard construction which involves the use of some thermally-compensated aluminum and brass parts. Others have found the thermal compensation to be less than

perfect; and in addition, the use of dissimilar metals tends to stress the mount, thus creating drift even if the first order compensation were perfect. The piezoelectric translators were chosen for their linearity, lack of hysteresis, and zero coefficient of thermal expansion at room temperature.

In order to meet the finesse requirement, we have ordered two sets of 2-in interferometer plates with a flatness figure of 1/300th of a wavelength and a reflectivity of 99.5%. The reflectivity of the plates will be maintained at 99.5% from 9000 Å to 7600 Å, thereby permitting the possibility of later experiments with rubidium and potassium.

Since the use of a 10-μ cell requires the detection of a shift which is 1/300th of the artificially-broadened linewidth, and since the shift increases by an order of magnitude in the small sample case, we had originally considered doing the experiment in a sample smaller than the wavelength of interest. Although such a cell can be constructed, problems of filling it with cesium vapor and of ascertaining that adsorbed atoms did not constitute the majority of atoms in our cell have caused us to concentrate on the "large" (10- to 1000-μ) cell case.

We will measure the shift between two cells as a function of density. In order to cope with the artificially-broadened line, we will measure the shift by making four different, simultaneous measurements as follows: One cell will be 10 μ long and the other will be 100 μ long; however their densities (temperatures) will be adjusted so that the absorption at the 1/e point on the low-frequency side of the line is the same for both cells. A temperature controller is presently being designed which will use the low-frequency-side absorption signals from the two cells to maintain the required temperature difference between the two cells to an accuracy of better than 0.1%. The difference in the high-frequency-side absorption signals from the two cells, if we assume a knowledge of the lineshape, will then give a measurement of the shift.

We are using a piezoelectrically-scanned, rather than a pressure-scanned, Fabry-Perot interferometer in order to make the measurements on both sides of the line simultaneously. Unlike a pressure-scanned device,[18,19] the free spectral range of a piezoelectrically-scanned device can be easily and predictably changed. It is therefore possible for the Fabry-Perots to transmit two narrow bands of frequencies at arbitrary points on each side of the line.

In the process of the experiment, white light from a tungsten-ribbon lamp will be collimated, divided into two beams, and directed into the two cesium cells. The light coming out of the two cells will be modulated at two different frequencies and then recombined into one beam. The beam will then be directed first into the two Fabry-Perot interferometers and then into the grating spectrometer. The spectrometer slit will be at a wide enough setting that radiation from both sides of the line will pass through. However, a 30° prism with its faces fully reflecting will be positioned at the exit slit in such a manner as to form essentially two slits, thereby directing the high-frequency radiation in one direction and the low-frequency radiation in another. Two photomultipliers will be set up to detect the resulting two beams, and phase-sensitive detection will be used to separate the long and short cell signals from each beam. The necessary four signals will therefore be available from one spectrometer assembly.

If we assume a lamp brightness of 0.3 W/cm^2-sr-Å and use the 1/2-m Jarrell-Ash grating spectrometer in the Laboratory, then the power available at the detector is 6×10^{-11} W. This corresponds to 3×10^8 photons at 8521 Å, from which, for the above selection of cell lengths, we wish to observe a change of 1% or 3×10^6 photons. We plan to detect this signal with an RCA 7102 photomultiplier with an S-1 photocathode, cooled by cold nitrogen gas to the vicinity of 100°K. A small, spherical, magnetically-scanned Fabry-Perot interferometer of limited luminosity, limited resolution, and fixed free spectral range is

now being tested, so that we may make preliminary measurements of the cesium lineshape before the arrival of the planar Fabry-Perots.

Program for the next interval: The Fabry-Perot interferometers and the microcells will be assembled and tested. We will test the temperature controller and construct the necessary ovens. We will then build the photomultiplier housing and make preliminary measurements of the lineshape. We will then add the phase-sensitive detection apparatus and attempt to observe the shift. Theoretical work will continue on the nature of the shift and on the effect of the hyperfine structure of cesium on the lineshape.

*This research was also supported by the Army Research Office under Contract DA-31-124-ARO-D-341 and by the Atomic Energy Commission.

(1) M. J. Stephen, J. Chem. Phys. 40, 669 (1964).

(2) U. Fano, Phys. Rev. 131, 259 (1963).

(3) G. P. Reck, H. Takebe, and C. A. Mead, Phys. Rev. 137, A683 (1965).

(4) R. H. Dicke, Phys. Rev. 93, 99 (1954).

(5) V. M. Fain, Soviet Phys. - JETP 36, 798 (1959).

(6) Stephen, op. cit., p. 669.

(7) R. H. Lehmberg, Phys. Rev. A2, 883 and 889 (1970).

(8) E. A. Power, Intermolecular Forces, ed., J. O. Hirschfelder (Interscience Publishers, New York, 1967) 12, p. 167.

(9) F. T. Arrechi and D. M. Kim, Opt. Comm. 2, 324 (1970).

(10) R. Friedberg and S. R. Hartmann, Opt. Comm. 2, 301 (1970).

(11) P. R. Berman and Willis E. Lamb, Jr., Phys. Rev. 187, 221 (1969).

(12) F. W. Byron and H. M. Foley, Phys. Rev. 134, A625 (1964).

(13) See Table III of Ref. 10. J. T. Manassah and H. M. Foley, Phys. Letters 31A, 265 (1970).

(14) H. G. Kuhn and E. L. Lewis, Polarization, Matière et Rayonnement (Presses Universitaires, Paris, 1969), p. 341.

(15) A. A. Abrikosov, L. P. Gorkov, and I. E. Dzyaloshinski, Methods of Quantum Field Theory in Statistical Physics (Prentice Hall Inc., Englewood Cliffs, N. J., 1963); J. T. Manassah, thesis, Columbia University (unpublished). We think that Eq. (33) of Ref. 3 wrongly omits the important nondiagonal (exchange) terms.

(16) Kuhn and Lewis, op. cit., p. 341.

(17) R. Chabbal, Rev. Opt. 37, 49 (1958).

(18) J. E. Mack, D. P. McNutt, F. L. Roesler, and R. Chabbal, Appl. Opt. 2, 873 (1963).

(19) H. G. Kuhn, E. L. Lewis, D. N. Starey, and J. M. Vaughn, Rev. Sci. Instr. 39, 86 (1968).

IV. MACROSCOPIC QUANTUM PHYSICS

A. QUANTIZED ROTATION OF SUPERFLUID HELIUM (R. W. Guernsey)

This experiment is designed to verify and measure the quantization of superfluid flow around the inside of a hollow ring. More precisely, the circulation κ should be quantized according to

$$\kappa = \oint \vec{v} \cdot \vec{dt} = n(h/m), \quad n = 0, \pm 1, \pm 2 \ldots,$$

where $\vec{v}$ is the local fluid velocity, and the line integral is taken around any closed path which encloses the center of the ring. Flows which satisfy this condition should persist indefinitely.

Our ring is fitted with a transverse partition containing a small hole. The geometry is such that when the ring is given angular velocity ω, the superfluid is forced to enter the circulation state with fluid velocity (far from the hole) closest to the ring velocity. As ω is increased, the fluid should jump to successively higher circulation states at regular intervals, $\Delta\omega = \hbar/mR^2$. The ring currently in use has a mean radius R = 0.654 cm, for which $\Delta\omega = 3.73 \times 10^{-4}$ sec^{-1} (5.14 revolutions per day).

The circulation jumps are detected by measuring the power dissipated in a momentary breakdown of superflow in the hole as the fluid system is forced into a new circulation state. Resolution of power changes as small as 10^{-18} W is achieved by attaching the ring to the bob of a high-Q torsion pendulum and measuring the power necessary to maintain a given oscillation amplitude. The angular velocity of the pendulum plus the steady rotation provided by the earth and a rotating table constitute the total ω of the ring. The torsion pendulum drives itself exactly on resonance by means of a feedback circuit. Typical regulation is $\Delta\omega = \pm 0.03$ revolutions per day (rpd). We hope that the quantum jumps may ultimately allow measure-

ment of any superimposed rotation to a precision of 0.01 rpd.

This apparatus was built at Stanford University over a period of two years. Preliminary data obtained there have been presented at the Twelfth International Conference on Low Temperature Physics, Kyoto, Japan on September 4 - 10, 1970, and are being published along with a more detailed description of the apparatus in the Proceedings of this conference. These first results, while noisy and in need of confirmation, seem to show circulation jumps at the expected intervals.

In late September, 1971, the unique parts of this apparatus were moved to the Columbia Radiation Laboratory. A survey of building vibrations showed a location in the basement of Pupin Hall to be sufficiently quiet for the experiment. The necessary cryogenic apparatus (i.e. an 8-in ID nitrogenless helium dewar and a large capacity helium-pumping system) and electronic equipment have been purchased and installed there. Minor modifications, tested prior to moving, have been incorporated into the apparatus in order to reduce the mechanical noise by a factor of ten. We expect to have clearer and more definitive results within the next few months, when the experiment should be operational again.

Program for the next interval: The circulation quantum interval will be measured, and the amount of dissipation associated with superflow breakdown in the hold will be determined. We intend to try minor variations of the ring geometry and hole size in order to find the maximum sensitivity to rotation.

B. VELOCITY-DEPENDENT OCCUPATION OF THE HELIUM-II SUPERFLUID STATE

(R. W. Guernsey, J. Kaplan)

The fraction of helium II in the superfluid state should depend on both the temperature of the liquid and the velocity v_s of the superfluid relative to the normal fluid. This latter dependence, which has not been measured, is probably important near the core of a superfluid vortex, in superflow through an orifice, and in other situations where large superfluid velocities are present. Knowledge of the superfluid density ρ_s as a function of v_s would give further insight into the physics of equilibrium (or metastable equilibrium) in helium II.

The feasibility of measuring $\rho_s(v_s)$ near the Lambda point has been evaluated. An analysis along lines proposed by Ginzburg and Pitaevskii[1] yields an estimated decrease in ρ_s of about 0.02% of the total fluid density ρ at the highest practical velocity ($v_s \sim 20$ cm/sec) and at an optimum temperature (2.14°K) near T_λ. It appears possible to build an apparatus capable of resolving changes in ρ_s/ρ of $\sim 10^{-5}$ by sensing changes in the resonant frequency of a high-Q torsion pendulum whose moment of inertia is partly determined by ρ_s. The variation in ρ_s velocities over a range of at least 5 to 20 cm/sec should then be measurable.

The helium will be confined to a narrow ring of radius R whose interior is divided into separate, well-defined circular channels about 0.2 μ in width. The temperature will be held constant (with a tolerance of $\pm 10^{-6}$°K) at a point in the range $T_\lambda - T$ from 10^{-2} to 10^{-1}°K, and it will be possible to rotate the ring at angular velocities of up to 30 rad/sec.

Let us suppose that the experiment begins with the ring and superfluid at rest. The ring is then brought gently to an angular velocity ω. If the superfluid remains at rest, then in the rest frame of the ring and normal fluid, it will have velocity $v_s = -R\omega$. For v_s sufficiently small, this will be a state of long-lived metastable equilibrium.[2] The limit v_c

depends on the channel size and the temperature. A typical value would be v_c = 23 cm/sec for a 0.2-μ channel at $T_\lambda - T = 0.04^\circ K$. As a result of the superfluid velocity relative to the walls and normal fluid, we expect to see a depletion of ρ_s and an equal increase in the normal fluid density ρ_n, such that the total fluid density, $\rho = \rho_n$, remains constant.[3]

The ring will be attached to the bob of a high-Q torsion pendulum whose peak angular velocity is a small fraction of ω. Only the normal fluid will be dragged with the walls of the ring, and thus only changes in its density will affect the resonant frequency of the pendulum. A change in this frequency will therefore indicate the change in ρ_n and, thus, the change in ρ_s.

Program for the next interval: We plan to begin work on the above apparatus. The principal experimental problems are:

a) Construction of the narrow channels needed inside the ring;

b) Refinement of temperature regulation to $\pm 10^{-6}{}^\circ K$;

c) Construction of the suspension and drive for rotation; and

d) Design of the system for measuring the resonant frequency of the pendulum.

(1) V. L. Ginzburg and L. P. Pitaevskii, Soviet Phys.-JETP 7, 858 (1958).

(2) J. S. Langer and J. D. Reppy, Prog. Low Temp. Physics 6, 1 (1970).

(3) E. Smith, R. Walton, H. V. Bohm, and J. D. Reppy, Phys. Rev. Letters 18, 637 (1967).

PERSONNEL

FACULTY

Director: S. R. Hartmann, Professor of Physics
H. M. Foley, Professor of Physics
P. Kusch, Professor of Physics
J. M. Luttinger, Professor of Physics
R. Novick, Professor of Physics
A. M. Sachs, Professor of Physics
I. I. Rabi, University Professor Emeritus
R. N. Zare, Professor of Chemistry
R. Friedberg, Associate Professor of Physics
W. Happer, Associate Professor of Physics
A. G. Redfield, Adjunct Professor of Physics
A. Lurio, Adjunct Assoc. Professor of Physics
P. Thaddeus, Adjunct Assoc. Professor of Physics
R. W. Guernsey, Assistant Professor of Physics
L. A. Levin, Assistant Professor of Physics

RESEARCH ASSOCIATES AND PHYSICISTS

Dr. T. Bergeman
Mr. M. J. Bernstein
Dr. M. Eminyan
Dr. K. German
Dr. R. Gupta
Dr. S. Hameed
Dr. M. R. Levitt
Dr. M. Matsuoka
Dr. D. Raskin
Dr. G. R. Tomasevich

VISITING RESEARCH SCIENTISTS*

Prof. D. Davids, New York University
Dr. R. deZafra, State University of New York at Stony Brook
Dr. J. T. Manassah, Princeton Institute for Advanced Study

*Not affiliated with the Columbia Radiation Laboratory

GRADUATE STUDENT RESEARCH ASSISTANTS

B. R. Bulos
S. Chandra
S. Chang
A. Flusberg
M. Friedlander
(RCA Fellowship)
Z. Friedlander
Patrick Hu
J. Kaplan
R. W. Leigh
P. F. Liao
N.-A. Lin
L. Lurie
W. Nagourney (IBM)
R. Nerf (NASA)
A. S.-T. Shih
S. Skwire
W. A. Stern
H. Y.-S. Tang
K. Tucker (NASA)
D. Weinflash
R. A. Weingarten

TECHNICAL RESEARCH ASSISTANTS

I. Beller
J. Gorham

PHYSICS DEPARTMENT ELECTRONICS ENGINEERING AND CONSTRUCTION SHOP

V. Guiragossian

PHYSICS DEPARTMENT MACHINE SHOP

J. Robertson

The facilities are available for the Columbia Radiation Laboratory

ADMINISTRATION

J. Gilbert

E. Dohman
B. A. Fubara
J. Rainey
F. Gambari

EDITOR

A. Owen